WAVE-INDUCED STRESS AND ITS EFFECTS ON CORAL REEF FISH SWIMMING PERFORMANCE AND ENERGETICS

Travis M. Marcoux

A Thesis submitted in partial satisfaction of the requirements
for the degree Master of Science

in

Marine Science

College of Natural and Computational Sciences

Hawai‘i Pacific University

Fall 2016

Honolulu, Hawaii

Advisory Committee:

Keith E. Korsmeyer, Chair
Chatham K. Callan
Eric W. Vetter

ABSTRACT

Using a novel wave-simulating apparatus, the Simulated Wave Motion Respirometer (SWMR), energetic costs were measured via intermittent-flow respirometry as fish swam through a regime of increasing wave frequencies and amplitudes. Oxygen consumption rates were measured for coral reef associated species that utilize different swimming modes. For all species examined, increases in wave intensity, as simulated by increases in frequency and amplitude of wave action, yielded higher metabolic rates (MR), however, there was no significant difference in net cost of swimming (NCOS; swimming MR - standard metabolic rate, SMR) among species. When examining the effect of frequency of oscillation on MR at similar average velocities, body and caudal fin (BCF) swimmers showed an increase in NCOS, while median and paired fin (MPF) swimmers did not, indicating that the cost of increasing wave frequency was higher for BCF swimmers than MPF swimmers. Increasing intensity of wave action altered swimming strategy for MPF swimmers, marked by frequent swimming in reverse for one half of the oscillation. This swimming strategy suggests that the cost of turning around every time the flow direction changes is less efficient than swimming in reverse despite an increase in fin-beat frequency (FBF). These results may help explain the observed relationships between morphology, swimming ability, habitat use, and the diverse swimming modes of coral reef fishes.

Hawai'i Pacific University

Wave Induced Stress and Its Effects on Coral Reef Fish Swimming Performance and Energetics

By

Travis M. Marcoux

September 12, 2016

This thesis is submitted in partial fulfillment of the requirements for the degree of Masters of Science in Marine Science at Hawai'i Pacific University. We the undersigned have examined this document and have found that it is complete and satisfactory in all respects, and all revisions required by the final examining committee have been made.

Author _____

Travis M. Marcoux

Committee Chair _____

Keith E. Korsmeyer, Ph. D

Committee Member _____

Chad Callan, Ph. D

Committee Member _____

Eric Vetter, Ph. D

Dean _____

Brenda Jensen PhD, Dean, College of Natural and Computational Sciences

Table of Contents

Acknowledgements

I would first like to thank my advisor, Dr. Keith Korsmeyer for taking me under his wing and guiding me to be a better scientist. I would also like to thank my committee members Dr. Eric Vetter and Dr. Chad Callan for all their support and guidance in the thesis process. Thank you also to HPU's statistics guru, Dr. David Hyrenbach for helping sort out statistics problems, and also to Dr. John Fleng Steffensen for allowing us to use the flume respirometer and helping us in creating a new flow design in his classic apparatus. A very special thank you to my girlfriend and rock, Stacia Goecke for putting up with me talking about fish swimming for two years and to my ~~~family for providing love and support from halfway around the world. ~~~

Chapter 1

Literature Review

1.1 Introduction

Throughout the course of evolution, abiotic and physical factors have played an integral role in species distributions and thereby limiting gene flow between spatially isolated populations of individuals (Dunson and Travis 1991). In coastal marine environments, wave stress is one of these factors that may limit the ability of an individual, and therefore, a population, to thrive under the constant ebb and flow of wave-induced action. This phenomenon is most prevalent on coral reef assemblages, where the shallow reefs are constantly exposed to the brunt of wave action, buffering the water flow before it reaches the beach (Moberg and Folke 1999). Coral reefs are also species rich habitats with abundant numbers of fishes competing for available resources (Moberg and Folke 1999). Along with high coral reef fish diversity there are multiple modes of swimming, the result of behavioral and morphological adaptations with abilities ranging from high maneuverability at low speeds to rapid bursts of linear acceleration (Fulton et al. 2013a; Pink and Fulton 2014). These diverse swimming modes will inherently demand a range of energetic investment from the fishes as they move through the water. Coping with wave stress is a potentially energetically expensive endeavor and any fish that has been adapted morphologically or physiologically to minimize energy expenditure will have an advantage in occupying areas of high wave action.

1.2 Wave Action

The dynamics of wave action begin as wind blowing across the ocean produces friction between the air and the surface of the water producing waves. Characterized as fluctuations of the sea surface away from equilibrium, each wave consists of a crest and trough. The wavelength is the distance measured between crests and the period is the amount of time it takes for a crest to travel one wavelength. It is common to categorize waves into three distinct groups: deep water waves, transitionary waves (or waves of transition), and shallow water waves (Constantin and Villari 2008; Constantin et al. 2008). In deep water waves, particle motion produced in the water column as a result of the surface wave are largely circular in motion and attenuate with increasing depth (Constantin et al. 2008). For deep water waves, the depth at which the circular motion is attenuated to less than 5% its original motion is ½ of the wavelength of the wave producing the wave action (Constantin et al. 2008).

As a wave travels toward the coast, the depth of the water column decreases, creating conformational changes to the water movement patterns. As the wave approaches the shore, the depth of the water column eventually decreases to below ½ the wavelength. At this point, the wave becomes a wave of transition and the movement of particles is compressed from its circular pattern into more elliptical trajectories (Constantin and Villari 2008). As the wave approaches the shoreline even further and depth decreases, the wave-induced action is reduced to the point of strictly longitudinal, or horizontal, movements (Constantin and Villari 2008). This effect is also called wave surge and is characterized as bi-directional, oscillatory flow, which is commonly experienced on shallow coral reefs. Another component of wave action in shallow water waves is a phenomenon called Stokes drift, which occurs more intensely when the amplitude (height) of the wave increases (Kenyon 1969). Stokes drift is the relative change in the position of a

hypothetical particle over a determined period of time in the direction of wave propagation and not due to the circular motion of wave-induced action (Stokes 1847; Craik 2005). This is due to the mean flow of the fluid and mostly occurs when waves are approaching shore. Shallow water waves, and wave surge, are the types of wave-driven action that would be expected near benthic environments on near-shore coral reef assemblages.

Shallow, near-shore coral reef assemblages are commonly exposed to incoming wave action, creating complex patterns of water motion as waves are forced to break or to continue to propagate across the reef flats. One of the main ecological functions of coral reef systems comes from its service as a physical structure for the incoming waves to dissipate large amounts of energy (Moberg and Folke 1999). Fringing and barrier reefs substantially buffer wave action, aiding in the creation of lagoons and the deposition of sediments which can lead to accretion of land and even the creation of entire islands (Stoddart 1973; Moberg and Folke 1999). This process is a consequence of waves breaking over the rising reef slope and the resulting complex mixing of different internal and external wave types across the reef flat (Kench and Brander 2006). Another factor contributing to the dissipation of wave energy is the effect of frictional forces between the incoming wave and the increased rugosity of the coral communities (Lowe et al. 2005). The dissipation of wave energy also allows for the development of favorable ecosystems for seagrass beds and mangrove forests; two biologically significant communities in tropical environments (Ogden and Gladfelter 1982).

The ability of coral reefs to buffer wave action differs greatly with the morphological characteristics of that reef including height, width, and inclination of the reef slope (Kench and Brander 2006). The maximum height reached by mature reefs occurs at the lowest level of the mean spring tide water mark. Here, the shallow edge of the reef slope would cause the formation

of breaking waves when tides reach their lowest levels (Kench and Brander 2006). Breaking waves on a shallow reef effectively release the incoming wave energy over the reef, stopping the propagation of energy reaching the shore (Denny 2006). As wave energy is dissipated, the horizontal motion of wave-induced action on the shallow coral flats is greatly reduced. It is also important to note that sea-level, including tidal fluctuations, may influence the ability of coral reefs to dissipate wave energy (Hearn 1999). When the water level is approaching low tide, the depth of the water column over the reef is decreased and breaking waves increase; the result being that coral reefs are more efficient buffers of wave energy at low tide (Kench and Brander 2006).

Wind direction and strength shape local wave conditions and dictate wave propagation over coral reef assemblages. Coral communities on the Great Barrier Reef that were more exposed to wind, and thus, wave-induced action, provided greater attenuation of wave energy over the reef crest (Kench and Brander 2006). Regardless of tidal height, these reefs were successful in buffering from 68% to 99.7% of incoming wave energy (Roberts et al. 1975; Gerritsen 1981; Lugo-Fernandez et al. 1998; Kench and Brander 2006). Compared with exposed reefs, those that were sheltered from high winds and experienced less wave stress showed lower dissipation of incoming wave energy, even exhibiting 0% attenuation at some sites (Kench and Brander 2006). This result is attributed to the lower elevation of the reef and the relationship between low wave heights relative to the increased depth of water the wave is moving through. In this environment, waves are typically not breaking and wave energy is allowed to travel along the reef flat with little resistance, creating the bi-directional, oscillatory flow present on shallow reefs.

For fishes, the constant oscillatory, bi-directional wave surge complicates swimming movements as they attempt to remain stationary in relation to a given point on the shallow reef. In order to station-hold against the bidirectional ebb and flow caused by wave action, fish constantly reorient themselves using visual and tactile cues to remain in one location, a process called rheotropism (Arnold 1974). Rheotaxis is a behavioral response to the direction of water currents, and in relation to the direction of the water flow, positive rheotaxis occurs when swimming into oncoming water currents. Conversely, when a fish is swimming with the current, it is called negative rheotaxis. These processes are mediated mostly by visual cues, utilizing the optimotor response to keep a specified object in the same visual position while the fish actively swims to maintain relative position to that object (Arnold 1974). While vision may be the main source of information for station-holding, the lateral line has been proven to also play a role in rheotaxis (Montgomery et al. 1997). The detection of water movement across the lateral line canal neuromasts may provide the individual with the current velocity and direction to be used in conjunction with visual cues to maximize efficiency of position holding, while minimizing effort needed to remain stationary (Montgomery et al. 1997). The process of constant reorientation in response to bidirectional wave surges on shallow reefs may increase the metabolic demand of the individual as it attempts to remain stationary against the incoming waves.

1.3 Swimming Modes

The extensive diversity of coral reef fishes includes a variety of body and fin shapes and modes of swimming, resulting in abilities ranging from high maneuverability at low speeds to rapid bursts of linear acceleration (Fulton et al. 2013a; Pink and Fulton 2014). According to

Fulton and Bellwood (2005), over 60% of represented species on the Great Barrier Reef swim by flapping the pectoral fins (labriform swimming, e.g., wrasses and surgeonfishes). The remaining 40% of species utilize various other swimming modes including balistiform (undulations or flapping of elongated dorsal and anal fins, e.g., triggerfishes) and body-and-caudal fin swimming (BCF, undulations of body and caudal fin).

1.3.1 Body and Caudal Fin Swimming

Body and caudal fin (BCF) swimming is characterized by axial undulatory movements of the posterior portion of the body and the caudal fin for propulsion. Within BCF swimming there is a spectrum of swimming types based on the proportion of the body used to generate the force needed for thrust. At one extreme is anguilliform swimming, observed in most eels, dogfish sharks, and other elongated fishes that use sinusoidal movements of the majority of their body (Kern and Koumoutsakos 2006). When viewed dorsally, anguilliform swimmers bend their bodies into anywhere from ½ to >1 sine wavelength. While they are an extreme example, they are not the most efficient swimmers as the large amplitude wavelength of their body creates large amounts of pressure drag (Müller et al. 2002; Kern and Koumoutsakos 2006). Towards the other end of the spectrum, subcarangiform and carangiform swimming uses undulations of just the posterior half of the body and caudal fin for propulsion. These modes of swimming are utilized by a wide range of BCF swimmers, but are named after the Carangidae family, which includes jacks (trevally) and scad.

Thrust in BCF swimmers is created by the sinusoidal movements of the fish as it undulates its body through the viscous water. Each body segment becomes a propulsive element

and increases the momentum of water moving posteriorly as it generates a force by lateral movement through the water (Sfakiotakis et al. 1999). As a result, there is a reaction force exerted by the water on the propulsion element that acts equally but opposing the body action. The reaction force is composed of a lateral element and a forward thrust element. While the thrust element is the force provided to propel the fish through the water, it is the lateral element of the water motion that results in a loss of energy as water is displaced laterally and not posteriorly (Sfakiotakis et al. 1999).

Body and caudal swimming is optimized in the thunniform swimmers, which includes the tunas, where both morphological and behavioral aspects contribute to the minimization of drag and maximization of thrust. This is accomplished by having a large bullet-shaped fusiform body that narrows down to a dorsoventrally compressed caudal peduncle, terminating in a tall lunate caudal fin (Webb 1984; Blake 2004). The large, high-mass, girth of the anterior body minimizes energy losses due to recoil of the body as it is moving laterally, while the narrow caudal peduncle shows local, large amplitude body movements and controls the caudal fin's angle of attack (Webb 1984; Blake 2004). While body movements in thunniform swimmers are restricted to <½ sine wavelength, these swimmers possess tendons that run anterior and posterior around the caudal peduncle to increase the working power of the large lunate caudal fin (Blake 2004). Thunniform swimmers have a plethora of characteristics to maximize thrust and minimize drag, and over the spectrum of BCF swimmers, those using smaller portions of their body for locomotion minimize drag and maximize thrust in the direction of movement.

1.3.2 Median and Paired Fin Swimming

With diversification and adaptation to novel environments, median and paired fin (MPF) swimming evolved in some groups of derived teleosts, allowing these fishes to move by oscillating or undulating their median (dorsal and anal) and paired (pectoral) fins while keeping their bodies rigid. Fin movements of MPF swimmers are aided largely by their soft, flexible fin rays, composed of lepidotrichia, making it easier to fine-tune small movements in tight quarters. Some species have also shown the ability to bend individual fin rays and have complex musculature that can rotate each fin ray independently (Sfakiotakis et al. 1999). One advantage of using median and paired fins as opposed to using the caudal fin for propulsion comes from the ability to move each fin independently, providing lift and thrust in any direction around the fish's center of mass (Webb 1984). This ability provides substantial maneuverability at low speeds and may provide an energetic advantage in highly complex environments, such as coral reefs. A wide range of body types exist for fishes that use MPF swimming, but Webb (1984) proposed that an optimal MPF swimmer would have a laterally-compressed, short, deep body with mid-lateral pectoral fin insertion, ventro-lateral pelvic fin insertion, soft-rayed and dorso-ventrally symmetrical dorsal and anal fins, and having reinforcement of the leading edge of all fins. MPF swimmers may reduce form drag, as compared with BCF swimmers, by keeping the body rigid and limiting the posterior lateral motion of the body (Webb 1984). Also evident at low speed is the efficiency of propulsion by median and paired fins when compared with BCF swimmers, whose efficiency declines rapidly below velocities of two body lengths per second (BL s^{-1}) (Webb 1984).

1.3.2.1 Labriform Swimming

Labriform swimming, named after the wrasse family Labridae, is a type of MPF swimming characterized by oscillations of the pectoral fins for locomotion and is the most common form used by coral reef fishes. With over 60% of fishes found on the reef using labriform swimming, this swimming strategy evolved separately among many groups of fishes (e.g. wrasses, surgeonfishes, and damselfishes) (Fulton and Bellwood 2005). In general, there are two extremes of pectoral fin movements that can be observed in labriform swimmers: rowing and flapping. Rowing strokes are those performed on the horizontal axis parallel to the direction of travel, while flapping strokes are mostly on the vertical plane but with fin ray movement also in the direction of travel (Walker and Westneat 2002a). These different fin movements work effectively under different conditions. From kinematic and dynamic simulations, Walker and Westneat (2002a) were able to determine that flapping is more mechanically efficient than rowing over the entire spectrum of swimming speeds, but rowing fins generate more thrust at low speeds. This trend has also been substantiated through fluid dynamics studies using 3-D based unsteady simulations to compute the forces generated by the pectoral fins (Ramamurti et al. 2002). This suggests that over the range of locomotor behaviors, rowing may be used for movements that require large amounts of thrust in a relatively short period of time, such as starting, stopping, and fast turns (Vogel 1994; Walker and Westneat 2002a). At high swimming speeds, however, flapping generates more thrust, an aspect taken advantage of by high speed labriform swimmers like the parrotfish (Korsmeyer et al. 2002). The rowing of the fins is also implicated in hovering by generating equal and opposite forces on power and recovery strokes in contrast to flapping labriform swimmers that must posturally reorient or completely lack the

ability to hover for more than a couple of fin strokes (Gerstner 1999; Korsmeyer et al. 2002; Walker and Westneat 2002b).

1.3.2.2 Balistiform Swimming

Another complex and less studied swimming type is that of balistiform swimming. Balistiform swimming, named for the Balistidae family of triggerfishes, utilizes synchronized movements of the elongated dorsal and anal fins for propulsion. While a single dorsal fin ray oscillating back and forth produces upward thrust (or lift), multiple fin-rays working together in a sinusoidal pattern connected by a membrane adds thrust posteriorly, creating a net movement parallel to the base of the fin (Sfakiotakis et al. 1999). Balistiform swimmers take advantage of this effect by having elongated symmetrical dorsal and anal fins arranged in a pattern of declination in the dorsal fin and inclination of the anal fin that converge upon the caudal fin. The result of this fin configuration is that maximum thrust is achieved posteriorly from the vector forces produced by both the dorsal and anal fins (Sfakiotakis et al. 1999). Compared with BCF swimmers, balistiform swimmers experience three times the amount of thrust in the direction of movement, which is aided by keeping their bodies rigid, reducing body drag and energy lost as a result of yawing motions (Lighthill and Blake 1990; Blake 2004).

The emergence of balistiform swimming sparked rapid changes in morphology in early triggerfishes despite slow species divergence times among ancestral species (Dornburg et al. 2011). With the appearance of a new swimming gait, ancestral triggerfish evolved new fin morphologies paired with different body shapes as they adapted to new ecological opportunities. As a result of the adaptive radiations of the balistiform swimmers, a pattern arose between fin

morphology and body shape, which allowed for specialization among and within the groups of triggerfishes. Analysis of phylogenetic relationships among ancestral triggerfishes showed that fin shape and body shape coevolved with certain body plans being more suited for either reef type or pelagic environments (Dornburg et al. 2011). Those fishes with elongated bodies are paired with rounder, stouter fins and are more commonly associated with coral reefs. This result suggests a swimming style that allows the fish to successfully maneuver in complex environments. On the opposite extreme, those fishes that are associated with pelagic environments have shorter, stouter, and more bulbous rostrums and possessed larger, sigmoidal-shaped, higher aspect-ratio fins (Dornburg et al. 2011).

1.4 Fin Aspect Ratio

Fin aspect ratio is the measure of the fin span relative to fin surface area, and higher values have been linked to greater efficiency of motion and reduced drag (Sambilay Jr 1990). To clearly illustrate the impact of high-aspect ratio fins on swimming performance, examples can be seen within each swimming style discussed thus far. Optimization of movement in BCF swimmers is seen in the thunniform swimmers that use a large high-aspect ratio lunate caudal fin for propulsion. In robotic experiments, RoboTuna has produced mean propulsive efficiencies of 91%, due to the relatively small amount of drag produced per unit of lift or thrust (Barrett et al. 1996). As compared with large, low-aspect ratio, paddle-shaped fins that may be useful for short bursts of high speed, the high aspect-ratio, lunate caudal fin produces less drag because of the narrow, differentiated fin lobes that create sharp edges for eddys to be concentrated, and therefore is mechanically efficient at both relatively high speeds and during continuous swimming. In labriform swimmers, the difference between fishes that primarily use drag-based

propulsion and those that use lift-based propulsion is mostly due to the shape of the fin and its aspect ratio. Those using drag-based propulsion are typically reef associated fishes that take advantage of their large, low aspect-ratio pectoral fin to more effectively maneuver and navigate complex reef environments at low speeds (Walker and Westneat 2000). Other reef specialists like the parrotfishes flap their high fin aspect-ratio pectoral fins utilizing lift-based propulsion to sustain relatively high speeds for extended periods of time at the cost of poorer maneuverability at lower speeds (Korsmeyer et al. 2002). This strategy makes lift-based propulsors with high fin aspect-ratio more suited to the pelagic environment.

1.5 Waves and Swimming Mode

The relationships among swimming mode, fin aspect-ratio, and wave exposure have been fully explored and developed from studies at Lizard Island on the Great Barrier Reef. Early studies explored the idea that wave-driven action as a result of wave exposure could affect species distribution on the reef. Fulton et al. (2001) observed that among labriform swimmers, species with low aspect-ratio fins that mainly utilized drag-based propulsion were more prevalent in areas with the lowest wave exposures, while those species with high fin aspect-ratios were much more abundant in high wave exposure areas. Species distributions of labriform swimming fishes on the reef at Lizard Island were observed to be a function of the ability of the individual to cope with wave-induced action over high- and low-wave exposed conditions (Fulton et al. 2001; Fulton et al. 2005).

Further research performed by Fulton and Bellwood (2005) sought to quantify this relationship over a much larger scale, involving many families of fishes using multiple

swimming modes. Using Lizard Island again as a study location, four experimental study sites were selected to represent a spectrum of wind exposures, and thus, wave exposures around the perimeter of the island. Those sites were classified as exposed (exposed to direct wind influence), oblique (located at an angle to the incoming wind), lagoonal, and sheltered (no direct wind influence). In order to categorize fish distribution as a function of wave exposure, the researchers measured the wave-induced flows at each location. When analyzed, the speed of water movement was consistent with wind exposure, with the highest flow at the exposed site, and lowest at the sheltered (exposed= 38.3 cm s^{-1}, oblique= 24.4 cm s^{-1}, lagoonal= 17.1 cm s^{-1}, and sheltered= 6.2 cm s^{-1}). Species distribution was determined through visual censuses at each site, categorizing each fish to the species level, and ultimately including 156 species across seven families. The vast majority of fishes observed on the reef were labriform swimmers (over 60% of fishes). Even though labriform swimmers were the most abundant on the reef, as velocity increases, the proportion of labriform fishes also increases, and the proportion of both pectoral/caudal and BCF swimmers significantly declines. This pattern suggests that labriform swimmers are the most efficient swimmers around Lizard Island and the lift-based mechanism of propulsion at high speeds provide an advantage in areas of high wave exposure (Fulton and Bellwood 2005).

In Hawai‘i, protection from waves was determined to be the most important mechanism in shaping coral reef communities, even more so than structural complexity and coral reef rugosity (Dollar 1982; Friedlander and Parrish 1998b; Friedlander et al. 2003). Species richness and diversity were found to be highest in locations of moderate wave exposure, with lowest fish biomass in areas of direct exposure and highest fish biomass in areas sheltered from the majority of wave action (Friedlander and Parrish 1998a; Friedlander et al. 2003). Fish biomass, species

diversity, and species richness were also negatively correlated to surf height (Friedlander and Parrish 1998a).

From these results, and others, Langerhans (2008) developed a model predicting the phenotypic characteristics of fishes living in varying levels and types of water flows. Achieving some success, Langerhans describes the need for further analysis of body stiffness, muscle structure, and unsteady swimming performance to further explore the accuracy of his model. More interestingly, recent findings support behavioral adaptations to changing water velocities. Fish exposed to high water flow velocities as a result of wave action more actively orient themselves directly into the incoming waves as a means of rheotaxis, more than in sheltered environments (Heatwole and Fulton 2013). Also, as wave exposure increased, most high aspect-ratio labriform swimmers did not alter swimming behavior, while other non-labriform swimmers recruited additional fins for stabilization, indicating the effectiveness of high fin aspect-ratio in higher velocity environments (Heatwole and Fulton 2013). While this trend is easily seen among species, it has also been described within a species. Spiny Chromis (*Acanthochromis polyacanthus*) individuals living in high wave-exposure environments have more tapered fins with high aspect-ratios, compared with individuals living in sheltered environments (Fulton et al. 2013b).

1.6 Energetics and Metabolism

Increased activity due to station-holding and rheotactic behavior in oscillatory water flow is expected to be an energetically demanding process that requires recruitment of many muscle groups to control the fins during movement. In order to sustain prolonged swimming and

constant reorientation, a stable oxygen supply to the muscles must be maintained to ensure proper function of the muscle groups. In the body, oxygen is required for aerobic cellular respiration to generate ATP. Acting as the terminal electron receptor for the electron transport chain, oxygen plays an integral role in oxidative phosphorylation, where ATP is produced and used in metabolic processes. In short, oxygen supply is the determining factor for sustained ATP production for metabolic processes such as muscle activity and digestion. It is because of this marked relationship between oxygen and metabolic processes that we are able to relate oxygen consumption rates to activity levels in fish. This process is called respirometry.

Most respirometry protocols for coral reef fishes involve individuals placed within a closed vessel system with a simple flow circuit to measure oxygen consumption rates. The system consists of an enclosed recirculation loop submerged within a larger bath of open flow-through, aerated sea water. Recirculation of water through the submerged loop is achieved by propeller or pump driven action to generate desired flow (Steffensen et al. 1984; Korsmeyer et al. 2002; Clark et al. 2013; Fulton et al. 2013a; Roche et al. 2014). In the past, measurements of oxygen consumption rates have been recorded via a polarographic oxygen probe housed in a thermostated cuvette (Korsmeyer et al. 2002), but these types of probes require constant, even flow and need to be calibrated several times a day to ensure accurate results. Recent studies have switched to the more stable and flow insensitive, fiber-optic oxygen sensors (Svendsen et al. 2010; Fulton et al. 2013a; Roche et al. 2014).

Intermittent-flow respirometry is used to reduce the confounding factors affecting oxygen consumption rates in a closed vessel for prolonged periods of time. The procedure for intermittent flow consists of three phases: a closed period, a flushing period, and a mixing period. The closed period is the phase where water is recirculated within the respirometer and

recording of oxygen consumption rates takes place. The flushing period occurs after the recording period to flush out the oxygen deficient water and pump in new, oxygenated water from the water bath into the respirometry chamber. This phase of flushing is also required to remove the potential accumulation of nitrogenous excretory wastes, carbon dioxide and other end products of respiration, which all affect the oxygen consumption rates of the individual (Steffensen 1989). The mixing phase is added between the flushing and recording phase to ensure complete mixing and adequate response time for the oxygen sensor prior to recording the oxygen decline. The amount of time used in each phase varies for each study but typical periods of full cycles range from 10-15 minutes, with the closed phase (5-7 minutes) roughly equaling the combination of a flushing phase (4-6 minutes) plus a shorter mixing phase (1-2 minutes) (Korsmeyer et al. 2002; Svendsen et al. 2010; Fulton et al. 2013a; Roche et al. 2014).

Measuring oxygen consumption rates in the empty respirometer before and after the subject fish is introduced can account for background levels of microbial respiration in the water and respirometry system (Steffensen 1989; Korsmeyer et al. 2002). The background levels of oxygen consumption can then be subtracted from values of oxygen consumption (M_{O2}) measured with the fish. Growth of bacteria and other microorganisms can be reduced through the use of UV sterilizers (Roche et al. 2014). Microbial M_{O2} is a greater problem if the fish is not size appropriate for the volume of the respirometer. If the subject individual is too small for the respirometer, the measurements of fish M_{O2} will be minimal relative to background M_{O2} (Steffensen 1989).

1.6.1 Determination of Metabolic Rates and Swimming Performance

Oxygen consumption rates (M_{O2}) are calculated from the slope of the linear regression of oxygen concentration decline over time for each recording cycle, described as follows:

$$\dot{M}_{O2} = sV_{resp}.$$

In this equation, s is the slope in oxygen content per unit time, and V_{resp} is the volume of the respirometer minus the volume of the fish. Prior to running experimental procedures, and after a fasting period, it is essential to place the subject individual in the apparatus for a prolonged period of time, typically overnight, to calculate the oxygen consumption rate of the individual while at rest (Korsmeyer et al. 2002). This measure is called the standard metabolic rate (SMR) and is the lowest metabolic rate that the individual can sustain. Using SMR as a benchmark level, increases in oxygen consumption rates, and thus metabolic energy demands, can be measured as swimming activity is increased in the respirometer.

In respirometry experiments to measure swimming costs, the velocity of the water flow through the experimental chamber (e.g., a swim tunnel or flume) is increased to induce swimming at higher speeds. A number of swimming benchmarks can be measured as swimming speed increases. As speed increases, most labriform and balistiform swimmers need to recruit additional muscle groups and as a consequence, they change their locomotory gait to ensure sustained movement in the water flow (Korsmeyer et al. 2002; Fulton and Bellwood 2005; Svendsen et al. 2010). The velocity at which this change of locomotory mode occurs is called the gait transition velocity (Korsmeyer et al. 2002; Svendsen et al. 2010). Swimming velocities are typically increased past the point of gait transition to find that individual's critical swimming speed (U_{crit}). Critical swimming speed is the maximum speed that the individual can sustain

swimming and trials are usually terminated when the subject cannot maintain position and is pushed against the back grid of the chamber for an extended period of time (Roche et al. 2014).

The relationship between speed and M_{O2} can be described based on a hydrodynamics-based power function (Wu 1977; Videler 1993):

$$M_{O2}=a+bU^{C},$$

where a is the standard metabolic rate (SMR), *U* is the swimming speed, *b* is the linear coefficient, and *c* is the slope of the log-log regression of the metabolic increment (MO2–a) as a function of swimming speed (Korsmeyer et al. 2002; Roche et al. 2014). Another important aspect of metabolism that can be determined from respirometry experiments is the cost of transport (COT), or the amount of oxygen consumed per unit mass per unit distance. Using the relationship between COT and swimming speed (typically a U-shaped trend), the optimum swimming speed (U_{opt}) for that individual can be determined as the swimming velocity where COT is minimized (Korsmeyer et al. 2002).

The difference between the maximum metabolic rate and the standard metabolic rate describes the aerobic scope of that individual fish. Aerobic scope is a measure of the ability of a fish to perform prolonged periods of energetically expensive activity at a level above that of the standard metabolic rate. Thus, aerobic scope is often used as a proxy for fitness or performance of fish in different environmental conditions (Clark et al. 2013). In swimming respirometry experiments of active swimmers, like many coral reef fishes, aerobic scope can be used to measure how well fish are able to deal with higher velocity flow and may ultimately determine the habitat in which they are able to live. An extreme example of this is the Blue-lined Wrasse *Stethojulis bandanensis*, which is able to sustain a 22-fold increase in metabolic rate from rest,

and whose U_{opt} is 70% faster than other fishes of similar size (7.7 body lengths s^{-1} vs 2.0-4.5 body lengths s^{-1}) (Fulton et al. 2013a). These results suggest that the Blue-lined Wrasse are a more efficient swimmer than the high-speed specialist, thunniform swimmers, and have metabolic abilities that rival that of endothermic birds and mammals (Fulton et al. 2013a).

1.7 Recent Research on Coral Reef Fishes and Swimming Energetics under Unsteady Flows

In the previous example of *S. bandanensis*' broad aerobic scope, the researchers were able to attribute the relative efficiency of swimming to the labriform mode utilized by that species. *S. bandanensis* is able to achieve its efficiency as a result of using its high aspect-ratio pectoral fins, achieving forward thrust and lift during both the up-stroke and the down-stroke (Fulton et al. 2013a). *S. bandanensis* also kept the body rigid while oscillating the pectoral fins around the center of mass, thus reducing large amounts of drag produced by the lateral motions of BCF swimming. As a result of their swimming abilities, these fish (and others utilizing similar methods) can be found in large numbers in environments that experience extremely variable water flows and are often exposed to high wave activity (Fulton et al. 2013a).

The marked relationship between oxygen consumption and swimming activity has been extensively researched and understood that as physical activity increases, so does the oxygen demand, and thus the metabolic activity of the fish is a function of the intensity of physical activity that fish is performing (Pettersson and Hedenström 2000; Brown et al. 2004). Recent studies have begun to explore the effects of variable, or unsteady, flow on the swimming performance and metabolic rates of fishes exposed to wave-induced water motion. Roche et al. (2014) investigated the effect of low-amplitude and high-amplitude changes in flow velocity in

one direction on oxygen consumption rate (M_{O2}), critical swimming speed (U_{crit}), and fin beat frequency of the labriform swimmer *Cymatogaster aggregata,* or Shiner Surfperch. Using intermittent-flow respirometry to measure oxygen consumption rates, the researchers placed individuals of *C. aggregata* in varying unidirectional velocities, with frequencies of high-amplitude (1.0 body length s^{-1}) and low-amplitude (0.5 body lengths s^{-1}) fluctuation over a period of 5 seconds (0.2 Hz). This procedure was intended to imitate the effects of wave-induced action on reefs with high and low exposure to waves, but in a unidirectional fashion. Compared with both steady and low amplitude variations in flow, during high amplitude fluctuations *C. aggregata* showed higher energetic costs (25.3% increase in M_{O2}), a decrease in critical swimming speed (U_{crit}), and increased fin-beat frequency (Roche et al. 2014). This study indicates that when these fish are exposed to intensely varying water flow (i.e. more wave-induced action), there is a general decrease in swimming performance and an increase in metabolic rate.

The impacts of wave driven action were further explored in a study by Binning and Roche (2013) of another labriform swimmer, *Acanthochromis polyacanthus,* the Spiny Chromis, collected from areas of differing wave-exposures. In this study, the authors hypothesized that the varying levels of wave exposure would influence adaptive phenotypic plasticity, causing individuals of the same species to respond differently to their respective environments. Individuals of *A. polyacanthus* captured from areas of high wave-exposure were found to have higher maximum metabolic rates, higher critical swimming speeds (33% increase in U_{crit}), and a significantly higher fin aspect ratio, when compared with fish from at low and moderate wave exposure habitat (Binning et al. 2013). Furthermore, the individuals from high wave-exposure areas had a broader aerobic scope, indicating the ability to better sustain prolonged periods of

energetically demanding aerobic activity (Binning et al. 2013). Taken together, results from both studies indicate that adaptive changes, such as increased fin aspect ratio and aerobic scope, have developed to help fishes that are exposed to high wave action cope with the energetic demands related to wave-driven action and the unsteady flow velocities associated with it.

These studies are of great value, as predictions of relative metabolic costs can be made in regard to living in habitats from low wave-exposure to high wave-exposure. However, there is a sizeable gap in the research with regards to energetic costs of swimming in the wave surge of bi-directional, oscillatory water flow, which would be much closer to the conditions coral reef fishes are exposed to on the reef. Also, the bulk of the observations over the past 15 years have been collected on or directly adjacent to Lizard Island, an island along the Great Barrier Reef off the coast of Australia. We do not know if the same patterns of species distribution will be seen on other reefs across the world where species assemblages may differ.

While 60% of coral reef fish use labriform swimming as their locomotor strategy, some studies show that the balistiform swimming mode, utilized by triggerfish and filefish, may be more energetically efficient (Korsmeyer et al. 2002). Korsmeyer et al. (2002) conducted swim respirometry experiments to measure M_{O2}, U_{crit}, gait transition velocity, and COT for both the balistiform swimming Lagoon Triggerfish, *Rhinecanthus aculeatus,* and the labriform swimming Schlegel's Parrotfish, *Scarus schlegeli.* That study found that while gait transition occurred at much lower velocities in the triggerfish, the COT and total oxygen consumption rate of *R. aculeatus* during MPF swimming was significantly lower than that of *S. schlegeli*, at low swimming speeds. The gait transition in *R. aculeatus* describes the change from balistiform swimming to a form of BCF swimming, and for speeds from ~25 cm s^{-1} to ~45 cm s^{-1}, can still be described as more efficient than MPF swimming in the parrotfish. It is only when flow

velocities approach 45 cm s^{-1} and higher that parrotfish MPF swimming becomes more efficient per unit distance traveled. This suggests that triggerfishes may be more effective swimmers at low speeds and at maneuvering than the parrotfish, while the parrotfish can better sustain high speed swimming activities. This study only examined steady, straight swimming, and how these abilities translate to the unsteady, rapidly fluctuating flows in a wave-swept environment is an important area for further study to understand the distributions and habitat use of coral reef fishes.

1.8 References

Arnold GP (1974) Rheotropism in Fishes. Biological Reviews 49:515-576

Barrett D, Grosenbaugh M, Triantafyllou M (1996) The optimal control of a flexible hull robotic undersea vehicle propelled by an oscillating foil. Autonomous Underwater Vehicle Technology, 1996 AUV'96, Proceedings of the 1996 Symposium on:1-9

Binning S, Roche D, Fulton C (2013) Localised intraspecific variation in the swimming phenotype of a coral reef fish across different wave exposures. Oecologia 174:623-630

Blake RW (2004) Fish functional design and swimming performance. Journal of Fish Biology 65:1193-1222

Brown JH, Gillooly JF, Allen AP, Savage VM, West GB (2004) Toward a Metabolic Theory of Ecology. Ecology 85:1771-1789

Constantin A, Villari G (2008) Particle trajectories in linear water waves. Journal of Mathematical Fluid Mechanics 10:1-18

Constantin A, Ehrnström M, Villari G (2008) Particle trajectories in linear deep-water waves. Nonlinear Analysis: Real World Applications 9:1336-1344

Craik AD (2005) George Gabriel Stokes on water wave theory. Annu Rev Fluid Mech 37:23-42

Denny MW (2006) Ocean waves, nearshore ecology, and natural selection. Aquatic Ecology 40:439-461

Dollar S (1982) Wave stress and coral community structure in Hawaii. Coral Reefs 1:71-81

Dornburg A, Sidlauskas B, Santini F, Sorenson L, Near TJ, Alfaro ME (2011) The influence of an innovative locomotor strategy on the phenotypic diversification of triggerfish (Family: Balistidae). Evolution 65:1912-1926

Dunson WA, Travis J (1991) The Role of Abiotic Factors in Community Organization. The American Naturalist 138:1067-1091

Friedlander AM, Parrish JD (1998a) Temporal dynamics of fish communities on an exposed shoreline in Hawaii. Environmental Biology of Fishes 53:1-18

Friedlander AM, Parrish JD (1998b) Habitat characteristics affecting fish assemblages on a Hawaiian coral reef. Journal of Experimental Marine Biology and Ecology 224:1-30

Friedlander AM, Brown EK, Jokiel PL, Smith WR, Rodgers KS (2003) Effects of habitat, wave exposure, and marine protected area status on coral reef fish assemblages in the Hawaiian archipelago. Coral Reefs 22:291-305

Fulton C, Bellwood D, Wainwright P (2001) The relationship between swimming ability and habitat use in wrasses (Labridae). Marine Biology 139:25-33

Fulton C, Bellwood D, Wainwright P (2005) Wave energy and swimming performance shape coral reef fish assemblages. Proceedings of the Royal Society B: Biological Sciences 272:827-832

Fulton CJ, Bellwood DR (2005) Wave-induced water motion and the functional implications for coral reef fish assemblages. Limnology & Oceanography 50:255-264

Fulton CJ, Johansen JL, Steffensen JF (2013a) Energetic Extremes in Aquatic Locomotion by Coral Reef Fishes. Plos One 8:6

Fulton CJ, Binning SA, Wainwright PC, Bellwood DR (2013b) Wave-induced abiotic stress shapes phenotypic diversity in a coral reef fish across a geographical cline. Coral Reefs 32:685-689

Gerritsen F (1981) Wave attenuation and wave set-up on a coastal reef. University of Trondheim

Gerstner CL (1999) Maneuverability of four species of coral-reef fish that differ in body and pectoral-fin morphology. Canadian Journal of Zoology 77:1102-1110
Hearn CJ (1999) Wave-breaking hydrodynamics within coral reef systems and the effect of changing relative sea level. Journal of Geophysical Research: Oceans 104:30007-30019
Heatwole SJ, Fulton CJ (2013) Behavioural flexibility in reef fishes responding to a rapidly changing wave environment. Marine Biology 160:677-689
Kench PS, Brander RW (2006) Wave Processes on Coral Reef Flats: Implications for Reef Geomorphology Using Australian Case Studies. Journal of Coastal Research 22:209-223
Kenyon KE (1969) Stokes drift for random gravity waves. Journal of Geophysical Research 74:6991-6994
Kern S, Koumoutsakos P (2006) Simulations of optimized anguilliform swimming. Journal of Experimental Biology 209:4841-4857
Korsmeyer KE, Steffensen JF, Herskin J (2002) Energetics of median and paired fin swimming, body and caudal fin swimming, and gait transition in parrotfish (Scarus schlegeli) and triggerfish (Rhinecanthus aculeatus). The Journal Of Experimental Biology 205:1253-1263
Langerhans RB (2008) Predictability of phenotypic differentiation across flow regimes in fishes. Integrative and Comparative Biology 48:750-768
Lighthill J, Blake R (1990) Biofluiddynamics of balistiform and gymnotiform locomotion. Part 1. Biological background, and analysis by elongated-body theory. Journal of Fluid Mechanics 212:183-207
Lowe RJ, Falter JL, Bandet MD, Pawlak G, Atkinson MJ, Monismith SG, Koseff JR (2005) Spectral wave dissipation over a barrier reef. Journal of Geophysical Research: Oceans (1978–2012) 110
Lugo-Fernandez A, Roberts H, Wiseman Jr W, Carter B (1998) Water level and currents of tidal and infragravity periods at Tague Reef, St. Croix (USVI). Coral Reefs 17:343-349
Moberg F, Folke C (1999) Ecological goods and services of coral reef ecosystems. Ecological Economics 29:215-233
Montgomery JC, Baker CF, Carton AG (1997) The lateral line can mediate rheotaxis in fish. Nature 389:960-963
Müller UK, Stamhuis EJ, Videler JJ (2002) Riding the Waves: the Role of the Body Wave in Undulatory Fish Swimming. Integrative and Comparative Biology 42:981-987
Ogden JC, Gladfelter EH (1982) Coral reefs, seagrass beds and mangroves: their interaction in the coastal zones of the Caribbean: report. Workshop on Coral Reefs, Seagrass Beds and Mangroves: their Interaction in the Coastal Zones of the Caribbean(23-30 May 1982: St Croix, Virgin Islands, US)
Pettersson LB, Hedenström A (2000) Energetics, cost reduction and functional consequences of fish morphology. Proceedings of the Royal Society of London Series B: Biological Sciences 267:759-764
Pink JR, Fulton CJ (2014) Right tools for the task: intraspecific modality in the swimming behaviour of coral reef fishes [electronic resource]. Marine biology 161:1103-1111
Ramamurti R, Sandberg WC, Löhner R, Walker JA, Westneat MW (2002) Fluid dynamics of flapping aquatic flight in the bird wrasse: three-dimensional unsteady computations with fin deformation. The Journal Of Experimental Biology 205:2997-3008
Roberts HH, Murray SP, Suhayda JN (1975) Physical processes in fringing reef system. Journal of Marine Research 33:233-260

Roche DG, Taylor MK, Binning SA, Johansen JL, Domenici P, Steffensen JF (2014) Unsteady flow affects swimming energetics in a labriform fish (Cymatogaster aggregata). Journal of Experimental Biology 217:414-422
Sfakiotakis M, Lane DM, Davies JBC (1999) Review of fish swimming modes for aquatic locomotion. Oceanic Engineering, IEEE Journal of 24:237-252
Steffensen JF (1989) Some errors in respirometry of aquatic breathers: how to avoid and correct for them. Fish Physiology and Biochemistry 6:49-59
Steffensen JF, Johansen K, Bushnell PG (1984) An automated swimming respirometer. Comparative Biochemistry and Physiology Part A: Physiology 79:437-440
Stoddart D (1973) Coral reefs of the Indian Ocean. Biology and geology of coral reefs 1:51-92
Stokes GG (1847) On the theory of oscillatory waves. Trans Cambridge Philos Soc 8:441-473
Svendsen JC, Tudorache C, Jordan AD, Steffensen JF, Aarestrup K, Domenici P (2010) Partition of aerobic and anaerobic swimming costs related to gait transitions in a labriform swimmer. Journal of Experimental Biology 213:2177-2183
Videler JJ (1993) Fish swimming. Springer
Vogel S (1994) Life in moving fluids: the physical biology of flow. Princeton University Press
Walker JA, Westneat MW (2000) Mechanical performance of aquatic rowing and flying. Proceedings of the Royal Society of London Series B: Biological Sciences 267:1875-1881
Walker JA, Westneat MW (2002a) Kinematics, Dynamics, and Energetics of Rowing and Flapping Propulsion in Fishes. Integrative & Comparative Biology 42:1032
Walker JA, Westneat MW (2002b) Performance limits of labriform propulsion and correlates with fin shape and motion. Journal of Experimental Biology 205:177-187
Webb PW (1984) Body Form, Locomotion and Foraging in Aquatic Vertebrates. American Zoologist 24:107-120
Wu TY (1977) Introduction to the scaling of aquatic animal locomotion. DTIC Document

Chapter 2

Wave-Induced Stress and Its Effects on Coral Reef Fish Swimming Performance and Energetics

Abstract

Using a novel wave-simulating apparatus, the Simulated Wave Motion Respirometer (SWMR), energetic costs were measured via intermittent-flow respirometry as fish swam through a regime of increasing wave frequencies and amplitudes. Oxygen consumption rates were measured for coral reef associated species that utilize a wide variety of swimming modes. For all species examined, increases in wave intensity, as simulated by increases in frequency and amplitude of wave action, yielded higher metabolic rates (MR), however, there was no significant difference in net cost of swimming (NCOS; swimming MR - standard metabolic rate, SMR) among species. When examining the effect of frequency of oscillation on MR at similar average velocities, body and caudal fin (BCF) swimmers showed an increase in NCOS, while median and paired fin (MPF) swimmers did not, indicating that the cost of increasing wave frequency was higher for BCF swimmers than MPF swimmers. Increasing intensity of wave action was met with changes in swimming strategy for MPF swimmers, marked by frequent swimming in reverse for one half of the oscillation. This swimming strategy suggests that the cost of turning around every time the flow direction changes is less efficient than swimming in reverse despite an increase in fin-beat frequency (FBF). These results may help explain the observed relationships between morphology, swimming ability, habitat use, and the diverse swimming modes of coral reef fishes.

2.1 Introduction

In coastal habitats, wave-induced water motions result in complex flow characteristics that strongly influence fish community composition (Denny and Gaylord 2010). Wave-driven flow regimes are particularly prevalent on fringing and barrier reefs, which are exposed to incoming waves, reducing wave energy before it reaches the coastline (Moberg and Folke 1999). Dealing with water motions caused by wave stress is potentially energetically expensive for fishes, and those that are behaviorally, morphologically, or physiologically adapted to minimize energy expenditure will have a selective advantage in occupying areas of increased flow (Fulton et al. 2013b).

With increasing sea surface temperatures and anthropogenic CO_2 levels associated with global climate change, coral reef ecosystems are at risk, including coral reef fishes (Hoegh-Guldberg et al. 2007). The loss of corals on fringing reefs will have a profound effect on shallow coral reef ecosystems, including the loss of structural habitat for coral reef fish and invertebrate species, and a substantial increase in wave action inshore (Friedlander and Parrish 1998b; Sheppard et al. 2005; Hoegh-Guldberg et al. 2007). The intensification of inshore wave action may alter typical behaviors of reef-associated fishes (Moberg and Folke 1999; Sheppard et al. 2005). If some fishes are unable to cope with increased wave action, it may cause a shift in locations of appropriate habitat, altering fish distributions and reef dynamics (Friedlander and Parrish 1998a). By examining the relationship between metabolic rate and the intensity of swimming in wave-driven flow, the capabilities and responses of fish to wave exposure can be further understood and lead to predictions of future species distributions in the wild under different climate change scenarios.

Coral reef fishes display a diversity of body and fin shapes and modes of swimming, resulting in abilities ranging from high maneuverability at low speeds to rapid bursts of linear acceleration (Fulton et al. 2013b; Pink and Fulton 2014). According to Fulton and Bellwood (2005), over 60% of species on the Great Barrier Reef swim using the pectoral fins (labriform swimming; e.g., wrasses and surgeonfishes), a type of median and paired fin (MPF) swimming. The remaining 40% of species utilize various other swimming modes, including balistiform (undulations or flapping of elongated dorsal and anal fins; e.g., triggerfishes; also a MPF swimming type) and body-and-caudal fin swimming (BCF, undulations of body and caudal fin).

Previous studies on habitat specializations of MPF swimmers have shown that fin morphology and energetic efficiency influence habitat choice (Fulton et al. 2001; Fulton and Bellwood 2005; Fulton et al. 2005). For labriform swimmers, fishes with more mechanically efficient, high aspect-ratio fins were more likely to inhabit areas of higher wave exposure, while areas sheltered from wave action were dominated by species using drag-based swimming (rowing of fins) and low aspect-ratio fins (Fulton et al. 2001; Fulton et al. 2005). This relationship has not been explored in balistiform swimming, a swimming type with numerous reef-specialist species. This style of locomotion, named for the triggerfish family Balistidae, uses undulations or oscillations of the elongated dorsal and anal fins while keeping the body rigid, thus minimizing body drag and yawing motion, and making the fish highly maneuverable (Blake 2004; Dornburg et al. 2011). In addition, studies have shown highly efficient locomotion of triggerfish swimming in steady flow conditions (Korsmeyer et al. 2002; Loofbourrow 2009).

Many studies have examined the energetics of steady, straight-line swimming in fishes (Steffensen et al. 1984; Korsmeyer et al. 2002; Svendsen et al. 2010; Fulton et al. 2013a), however, no studies have investigated energetics in unsteady, oscillatory flows, that are typically

found on wave-swept reefs. As offshore waves travel inshore and water depth decreases over shallow reefs, the circular, wave-induced water movement is compressed into a predominantly longitudinal, or horizontal, motion known as wave surge, characterized by bi-directional, oscillatory water flow (Constantin and Villari 2008). Fishes that occupy these shallow coral reefs must cope with constant changes in water flow in order to maintain position on the reef. Recently, Roche et al. (2014) examined swimming performance in unsteady velocities of unidirectional flow, but this scenario does not represent the bi-directional water movement seen in shallow coastal environments. There is a gap in our understanding of the energetic costs of swimming in bi-directional wave action, more typical of flow patterns on the reef, and how fishes with various swimming modes respond.

Using a novel intermittent-flow respirometry apparatus, the Simulated Wave Motion Respirometer (SWMR), this study aims to explore the relationship between metabolic rate and bi-directional, oscillatory, wave-induced action by swimming fishes through an increasing regime of simulated wave surge intensities. By examining multiple species across a range of swimming modes and body morphologies, I intend to discern which characteristics or behavioral strategies may provide a selective advantage in occupying areas of increased wave-driven action.

2.2 Materials and Methods

2.2.1 Fish Acquisition

Species were selected to cover a variety of swimming modes and morphologies of swimming fins. Within the MPF swimmers, species were selected with a range of fin aspect ratios, to determine how individuals of different swimming strategies were affected by wave action. A total of 30 individuals were tested from eight different species (Table 2.1). Body-caudal fin (BCF) swimmers included the Hawaiian Flagtail, or Āholehole, (*Kuhlia xenura* (Jordan and Gilbert, 1882) and *Kuhlia sandvicensis* (Steindachner, 1898)) and the Flathead Gray Mullet (*Mugil cephalus* Linneaus, 1758). Since distinguishing between *Kuhlia xenura* and *Kuhlia sandvicensis* was uncertain at the sizes used for this study, the species will be referred to as the complex, *Kuhlia* spp. Labriform swimmers included the Black-spot Sergeant (*Abudefduf sordidus* (Forsskål, 1775)), Clown Anemonefish (*Amphiprion ocellaris* Cuvier, 1830), and the Goldring Surgeonfish, or Kole (*Ctenochaetus strigosus* (Bennett, 1828)). Balistiform swimmers included the Lagoon Triggerfish, or Humuhumunukunukuapua‘a, (*Rhinecanthus aculeatus* (Linneaus, 1758)), and the Bursa Triggerfish (*Sufflamen bursa* (Bloch and Schneider, 1801)). One species of ostraciiform swimmer was also tested, the Spotted Boxfish (*Ostracion meleagris* Shaw, 1796).

Subjects were obtained either through wholesale aquarium fish retailers or collected from near-shore Oahu by permit, held in flow-through seawater tanks (25 - 28°C, 30-32 ppt, 12:12 light-dark photoperiod) at the Oceanic Institute of Hawai‘i Pacific University, and fed daily with commercial marine fish food pellets and chopped frozen squid. Fish were acclimated in laboratory conditions for at least two weeks before testing.

2.2.2 Simulated Wave Motion Respirometer

Oxygen consumption rates were measured through computerized, intermittent-flow respirometry (Steffensen et al. 1984). In order to measure metabolic rates during oscillatory wave action, the Simulated Wave Motion Respirometer, or SWMR, was developed to make measurements under repeatable, unsteady, bidirectional swimming (Figure 2.1). Rather than use a propeller or piston driven flow channel to create oscillatory water flows, the SWMR shifts the frame of reference to the surrounding water mass (rather than the seafloor), and utilizes the optomotor response to prompt a rheotactic response to induce oscillatory swimming in relatively still water within the respirometer. Compared with steady, uni-directional swimming in a traditional swim flume, the SWMR better replicates station-holding swimming against a bidirectional wave-surge, more typical of behaviors on the reef, and requires changes in swimming direction to maintain a relative position.

The SWMR respirometer (volume = 3.15 L) was submerged in a flow-through seawater bath (110 L) to maintain consistent temperature (26 ± 2°C). A closed recirculation loop of tubing with a submersible pump circulated water through the fish chamber and past the optical dissolved oxygen sensor and conductivity probe for continuous measurement of oxygen content, temperature, and salinity. A second, computer-actuated, submersible pump was used to initiate the flushing phase of the intermittent-flow respirometry cycle and pump aerated seawater from the surrounding tank water through the respirometer. The probes were connected to an Orion 5-Star Portable pH/ORP/ISE/DO/Conductivity Multimeter (Thermo Fisher Scientific Inc., Waltham, MA) that automatically corrects dissolved oxygen content for the temperature and salinity of the water. Output from the multimeter was sent to a computer for continuous recording (0.2 Hz) via LabView 2014 (National Instruments Inc., Austin, TX). Water in the

surrounding tank was pumped through an ultraviolet sterilizer (SmartUV Lite, Emperor Aquatics, Inc.) to reduce background levels of microbial respiration. A titanium aquarium grounding probe (TAAM, Inc.) was used to reduce electromagnetic noise generated by the UV sterilizer that could interfere with the conductivity probe.

Oscillatory swimming movements were induced by placing the fish in a 15 cm long swimming shuttle that traveled back and forth inside a 50 cm long, clear acrylic respirometry tube (8.9 cm inside diameter). The inside swimming section was colored with black and white vertical bars, intended to elicit the optomotor response and swimming to remain stationary relative to the bar pattern. This swimming shuttle was coupled with magnets to an external partial sleeve that traveled back and forth using a scotch yoke mechanism to convert rotational motion to linear oscillation.

Wave frequency was measured by recording the time required for one complete rotation of the scotch yoke mechanism (one total oscillation or wave period) using a stopwatch. Frequency was measured as:

$$\text{Frequency} = \frac{1}{\text{Time for one full oscillation}}$$

Amplitude was determined by adjusting the length of the radius of the scotch yoke mechanism to a displacement equal to 1.0, 1.5, and 2.0 body lengths (BL) of the subject fish.

2.2.3 Validation of the SWMR relative wave motion

Prior to running any experimental procedures in the SWMR, validation studies were conducted to ensure that the relative water velocities in the respirometer matched the intended

velocities of motion and that large-scale turbulence was not generated by the shuttle movements. This procedure and supporting data can be found in Appendix 1: Validation of the SWMR relative wave motion.

2.2.4 Experimental Procedure

Before conducting each experiment, oxygen consumption rates were recorded for 1 h to determine the initial background level of microbial oxygen consumption in the SWMR apparatus without a subject. Each measurement cycle was 12 min in duration, with a 4 min open, flushing phase, a 1 min closed, mixing phase, and a 7 min, closed recirculation phase during which the decline in oxygen content was measured.

Subjects were fasted for 36 h prior to testing to prevent elevated metabolic rates associated with digestion. Each subject was measured for total body length (BL) and mass, and then placed into the SWMR and allowed to acclimate overnight for at least 18 h. During this period, oxygen consumption rate was recorded to determine the standard metabolic rate (SMR), a measurement of the lowest sustainable metabolic rate of the fish when at rest. The next morning, the fish were run through an exercise regime of increasing amplitudes of oscillatory movement over 10 s, 5 s, and 3.3 s wave periods (frequencies of 0.1, 0.2, and 0.3 Hz, respectively). The total length of the fish determined the amplitudes of displacement at which the experiments were run. With a maximum amplitude of the SWMR set at 15 cm, the aim was to test fish under 7.5 cm in total length to achieve amplitudes of 1.0 BL, 1.5 BL, and 2.0 BL at each frequency, while remaining within the limits of the SWMR. Subjects were run in cycles of increasing intensity, with oxygen consumption measured over two respirometry cycles at each intensity. Following the exercise regime, the SWMR motion was stopped and oxygen

consumption rates were measured for two cycles at rest. The fish was then removed from the SWMR and returned to their individual tank. A second blank procedure was then run to determine background levels of microbial oxygen consumption post-experiment which were used to correct the metabolic rates.

2.2.5 Swimming Kinematics

To further examine the relationship between wave driven action and swimming performance, two kinematic parameters were examined: fin beat frequency (FBF) and percent turning. Video recordings (GoPro Hero 3+ Black; 720p, 120 fps) of the lateral view were made by mounting the camera to follow the oscillatory motions of the shuttle within the respirometer. Fin beat frequency was measured for the pectoral fins of *A. ocellaris* and *C. strigosus* from a 1 min video recording captured during each 7 min measuring phase. Due to the translucence of the swimming fins and lack of sufficient video resolution, fin beat frequency could not be analyzed for other species.

Videos were edited to a 30 s video clip corrected for lens aberrations ("fish eye") using GoPro Studio software and imported in Logger Pro data collection software program (Vernier Software and Technology) for analysis. FBF was calculated as the time required for one full fin beat, starting from the onset of the first detectable fin deflection. For each swimming intensity, FBF was calculated over at least 3 full wave oscillations and separately analyzed for each half of the oscillation, separating out the effect of some fishes swimming backwards during one half of the cycle. Mean FBF and standard deviation were calculated for each individual fish (for swimming forward and in reverse separately) within each intensity and averaged together to represent the mean variation at that combination of frequency and amplitude. To analyze changes

in FBF over time during half the cycle, FBFs were binned together into short time bins (~10) over each half cycle at each frequency to allow for direct comparisons at the same relative time point within the cycle (0.6 s bins at 0.1 Hz, 0.3 s at 0.2 Hz, and 0.2 s bins at 0.3 Hz frequency). FBF for each time bin was calculated separately for individual fish within that intensity (each swimming direction done separately) and averaged together to get a mean FBF and standard deviation for each time bin at each intensity. Also from the video recordings, the percent turning was quantified as the number of times the individual turned around relative to the number of changes in direction by the SWMR shuttle over a 1 min period during each respirometry cycle.

2.2.6 Data Analysis

Oxygen consumption rates were calculated from the decline in oxygen content during each 7 min closed recirculating phase of the intermittent-flow respirometry cycle. Metabolic rate (MO_2) was calculated from the slope of a linear regression fit to the decrease in oxygen content over time using the formula:

$$M_{O2}=s*V_{resp},$$

where s equals the slope of the best-fit linear regression and V_{resp} equals the volume of the respirometer. Metabolic rates were corrected for background oxygen consumption rates assuming a linear change between the two background measurement runs before and after experimental measurements.

Standard metabolic rates were calculated from a frequency histogram of M_{O2} measured overnight, excluding the initial acclimation period (6 h) after placing the fish in the respirometer. Two normal curves were fit to the frequency histogram to separate the lower SMR distribution of M_{O2} from the higher M_{O2} values due to spontaneous activity (Steffensen et al. 1994). Net cost of swimming (NCOS) was calculated as the measured oxygen consumption rate at each swimming

intensity minus the SMR, making the net cost of swimming the increase in metabolic rate due to swimming activity of that individual at each intensity. For each individual, total metabolic rate and net cost of swimming (NCOS) were averaged for both cycles run at each swimming intensity. Any cycles where atypical swimming patterns were recorded (e.g., resting on the bottom, erratic movements, biting at the walls), were excluded from analysis.

Before conducting statistical analyses, the relationship between total standard metabolic rate and body mass was examined to correct mass-scaling effects. Swimming metabolic rates, standard metabolic rates, and NCOS were adjusted to a common mass of 10 g using the following equation:

$$MR_{10} = MR_m \times \left(\frac{10}{mass}\right)^{b-1},$$

where *b* is the mass-scaling exponent determined empirically from SMR measurements. The resulting metabolic rates are referred to as swimming MR_{10} (mass adjusted swimming metabolic rate), SMR_{10} (mass adjusted standard metabolic rate), and $NCOS_{10}$ (mass adjusted net cost of swimming).

The average swimming velocity for each combination of wave frequency and amplitude was calculated as the mean absolute velocity through one complete wave cycle, using the equation:

$$\text{Average Velocity} = 4 \times \text{Amplitude} \times \text{Frequency}$$

2.2.7 Statistical Analyses

Statistical analyses were restricted to four main species with a sample size greater or equal to 5, which included *Kuhlia* spp. (*n*=5), *A. ocellaris* (*n*=5), *C. strigosus* (*n*=6), and *S. bursa* (*n*=5). Data from the lowest frequency (0.1 Hz) were not included in the statistical analysis due to erratic swimming of all *C. strigosus* individuals. One *C. strigosus* individual was also discarded due to erratic swimming at the 0.2 Hz frequency. Similarly, the lowest two intensities (0.1 Hz frequency, 1 BL amplitude and 0.1 Hz frequency, 1.5 BL amplitude) were also discarded when analyzing fin-beat frequency for *C. strigosus*. Insufficient data were collected for statistics to be run on the following species: *M. cephalus* (*n*=3), *A. sordidus* (*n*=1), *O. meleagris* (*n=2*), and *R. aculeatus* (*n*=3). However, descriptive analyses of these species were included in this study as comparison to the species used in the main analyses.

In order to examine the effect of amplitude and frequency on the metabolic rate (net cost of swimming, $NCOS_{10}$) among species, a three-way, repeated measures analysis of variance (ANOVA) was conducted using the following species: *Kuhlia* spp*., A. ocellaris, C. strigosus,* and *S. bursa*. A one-way ANOVA was conducted to examine differences in standard metabolic rate among the aforementioned species.

To examine the effect of frequency on $NCOS_{10}$ at similar average velocities within species, NCOS and average velocity were log-transformed to linearize the relationship (Korsmeyer et al., 2002). Then the difference between each NCOS measurement and average NCOS was calculated for each individual, as a way to account for repeated-measures, prior to conducting one-way analysis of covariance (ANCOVA). By comparing each fish to its own mean log $NCOS_{10}$, this removes the effect of the repeated measures design, and allows for the ANCOVA analysis to be run. The ANCOVAs were conducted on this log difference in NCOS

from the mean, at the 0.2 and 0.3 Hz frequencies, with log average velocity as a covariate for each species. P-values for significance were used assuming sphericity unless Mauchly's Test of Sphericity revealed violations of assumption of sphericity. In those instances, the Greenhouse-Geisser correction was used.

To examine the effect of amplitude and frequency on mean fin-beat frequency, a three-way repeated measures ANOVA was conducted on *A. ocellaris* swimming forward and *C. strigosus* swimming forward and in reverse. A two-way repeated measures ANOVA was used to compare the effect of time and direction of swimming (forward, reverse) on fin-beat frequency for the species *C. strigosus.* Significance level for this study was $p<0.05$ and all statistical test were conducted with SPSS (IBM, v.22).

2.3 Results

Due to some species having low sample size, only data from species with $n \geq 5$ were used in statistical analyses, consisting of four species. These four species (*Kuhlia* spp*., Amphiprion ocellaris, Ctenochaetus strigosus,* and *Sufflamen bursa*) were the four main species analyzed, while data from the other four species (*Mugil cephalus*, *Abudefduf sordidus*, *Ostracion meleagris*, and *Rhinecanthus aculeatus*) are provided to give further context to trends seen in the data.

2.3.1 Standard Metabolic Rate

Before conducting analyses, the relationship between body mass and total SMR was examined to correct for any differences in MR due to differences in mass. This was done for all species combined (Fig. 2.2) and separately for the four main species analyzed (Fig. 2.3). The common scaling exponent (*b*) for all species was found to be 0.667 (Fig. 2.2), while the common scaling factor for the four main species was found to be 0.895 (Fig. 2.3). To correct for the small mass differences among individuals, the overall scaling exponent of 0.895 was used to normalize all values to a common mass of 10 g for *Kuhlia* spp.*, A. ocellaris, C. strigosus,* and *S. bursa* (Table 2.2).

Standard metabolic rates from overnight measurements (SMR) showed a wide range of MR at rest for each species examined. For the four main species analyzed, one significant difference was identified, (ANOVA, $F(3, 16)= 3.43$, $p=0.043$), indicating that *C. strigosus* had a significantly higher SMR than *S. bursa* (post hoc Tukey HSD $p = 0.028$) (Fig. 2.4, Table 2.2). Standard metabolic rate for the other four species examined ranged from 80 mg O_2 kg^{-1} h^{-1} (*O. meleagris*) to 200 mg O_2 kg^{-1} h^{-1} (*M. cephalus*) (Fig. 2.5).

2.3.2 Swimming Metabolic Rate

In general, metabolic rates during oscillatory swimming increased with increases in wave amplitude and frequency (Figs. 2.4 and 2.5, left columns), and also with the average swimming velocity at each wave intensity (mean absolute velocity over a single wave cycle) (Figs. 2.4 and 2.5, right columns). To correct for differences among species in SMR (i.e., metabolic rate at zero swimming activity), the net cost of swimming (NCOS = swimming MR – SMR), was calculated

for each swimming intensity. This NCOS represents the metabolic increment above rest, due to swimming activity. *Kuhlia* spp. showed the lowest and most consistent increases as wave intensity increased, while *S. bursa* and *A. ocellaris* showed the greatest increases and the most variable differences between frequencies at each amplitude (Fig. 2.6). Although only a single individual was tested, *A. sordidus* showed the smallest overall increases in total metabolic rate and net cost of swimming, closely followed by *O. meleagris* (n=2) (Figs. 2.5 and 2.7). Total mean metabolic rate for each species showed much more variability at the highest wave intensities, ranging from 200 mg O_2 kg^{-1} h^{-1} (*A. sordidus*) to nearly 600 mg O_2 kg^{-1} h^{-1} (*M. cephalus*) (Fig. 2.5).

For the four main species analyzed, both wave frequency and amplitude were found to have a significant effect on net cost of swimming, $NCOS_{10}$ ($F(1, 16)= 64.33$, $p<0.001$; $F(2, 32)= 63.22$, $p<0.001$; respectively, Fig. 2.6). Also, there was a significant interaction effect between the frequency and amplitude of wave motion on $NCOS_{10}$ ($F(3, 16)= 5.14$, $p=0.012$), indicating that $NCOS_{10}$ responded differently to increases in amplitude at the different frequencies. In general, $NCOS_{10}$ increased greater with amplitude at higher frequencies of oscillation (Fig. 2.6). There was, however, no significant difference in $NCOS_{10}$ between any of the four species ($F(3, 16)= 1.97$, $p= 0.159$) (Fig. 2.6).

The effect of the frequency of direction change on swimming costs was examined by comparing $NCOS_{10}$ at different frequencies, but amplitudes that resulted in similar average swimming velocities (Fig. 2.6 and Fig. 2.7, right column). In comparing $NCOS_{10}$ as a function of average velocity at both 0.2 and 0.3 Hz wave frequency, *Kuhlia* spp. showed significant increases in $NCOS_{10}$ at 0.3 Hz (Fig. 2.6, right column; Fig. 2.8A). The rates of increase in $NCOS_{10}$ with average velocity were similar between 0.2 and 0.3 Hz oscillation in three of the

four species [ANCOVA homogeneity of slopes, *Kuhlia* spp.- $F(1, 26)= 0.66$, $p= 0.42$; *A. ocellaris* $F(1, 26)= 0.06$, $p= 0.82$; *S. bursa*- $F(1, 25)= 1.39$, $p= 0.25$), Fig. 2.8], but not for *C. strigosus* ($F(1, 31)= 4.32$, $p= 0.046$; Fig. 2.8C). For the three species showing homogeneity of regression slopes, the covariate, log average velocity, was significantly related to the difference from the mean log $NCOS_{10}$ (*Kuhlia* spp.- $F(1,27)= 33.93$, $p< 0.001$; *A. ocellaris*- $F(1, 27)= 57.69$, $p< 0.001$; *S. bursa*- $F(1, 26)= 42.19$, $p< 0.001$). For *Kuhlia* spp., however, there was also a significant effect of frequency on $NCOS_{10}$ at similar average velocities, ($F(1, 27)= 9.00$, $p= 0.048$), indicating higher net swimming costs due to the increases in frequency of direction change, regardless of average swimming velocity. *A. ocellaris* showed a slight, but not significant, increase in average NCOS with frequency $F(1, 27)= 3.22$, $p= 0.084$, and *C. strigosus* and *S. bursa* showed similar NCOS at both frequencies, at the same average swimming velocity ($F(1, 20)= 0.66$, $p= 0.43$; $F(1, 26)= 2.078$, $p= 0.16$, respectively)

2.3.3 Changing Swimming Direction

With a change in the direction of movement with each wave cycle, all fish species were observed to anticipate the direction changes after a short period of time, but some fish turned around to maintain forward swimming, while others would swim backwards in one direction and forwards in the other (i.e., no turning). *Kuhlia* spp. and *A. ocellaris* showed the highest percent turning over all amplitudes and frequencies, turning at least 75% of the time, and near 100% of the time at the highest frequency (Fig. 2.9). The two other species, *C. strigosus* and *S. bursa* would usually swim backwards in one direction, with the highest percent turning occurring at the highest swimming intensity only 55% of the time (Fig. 2.9). *C. strigosus* turned the least at every intensity compared with all other species. Percent turning for *S. bursa* increased as amplitude

increased within every frequency and showed the highest percent turning at the highest frequency (Fig. 2.9).

In order to examine the relationship between fish turning and $NCOS_{10}$, the residuals from the three-way repeated measures ANOVA were plotted against the percent turning observed for each fish (results not shown). No noticeable correlation existed between the residuals of the $NCOS_{10}$ ANOVA and percent turning.

2.3.4 Pectoral Fin-Beat Frequency

A. ocellaris swam using a combination of the pectoral fins and body-caudal fin undulations, while *C. strigosus* used the pectoral fins almost exclusively. Only pectoral fin beat frequencies (FBF) could be reliably measured from the video recordings. The effect of frequency and amplitude on mean FBF was examined for *A. ocellaris* swimming forward and for *C. strigosus* swimming both forwards and in reverse (Fig. 2.10). Both amplitude and frequency had a significant effect on FBF (Three-way repeated measures ANOVA, $F(2, 24)= 4.54$, $p<0.001$; $F(1, 12)= 6.15$, $p<0.001$, respectively) and FBF was significantly different among the three species/directions,($F(2, 12)= 6.36$, $p =0.001$). Pairwise comparisons revealed that *C. strigosus* FBF swimming forward was significantly lower than both *C. strigosus* swimming in reverse and *A. ocellaris* swimming forward ($p=0.002$, $p=0.002$, respectively) (Fig. 2.10). Interestingly, *C. strigosus* FBF swimming in reverse and *A. ocellaris* FBF were very similar (not significantly different, $p=1.000$).

Pectoral fin-beat frequency for *A. ocellaris* ranged from 2 beats s^{-1} to 5.5 beats s^{-1} as swimming intensity increased and remained relatively stable throughout each wave cycle (Fig.

2.11). At all intensities analyzed for *C. strigosus*, and for both swimming forwards and in reverse, there was a significant effect of time within the cycle on fin-beat frequency ($p<0.05$, Fig. 2.12). While swimming both forward and in reverse, a common trend was an elevated fin-beat frequency at the beginning of the cycle (during rapid acceleration as velocity was increasing), following a decrease (as velocity was decreasing), then an abrupt increase nearing the end of the cycle (prior to direction change) (Fig. 2.12).

For the *C. strigosus*, the direction of swimming had a significant effect on fin-beat frequency, with higher FBF when swimming backwards at all intensities except for the lowest, 0.1 Hz frequency, 2 BL amplitude intensity. At the two highest intensities, 0.3 Hz frequency and 1.5 and 2 BL amplitude, there was a significant interaction effect between direction of swimming and time, $F(5, 20)= 3.124$, $p=0.030$, and $F(4, 16)= 4.28$, $p= 0.015$, respectively. This indicates that at these intensities, swimming forward and in reverse affected fin-beat frequency differently over time. At 0.3 Hz frequency, 1.5 BL amplitude (Fig. 2.12, row C, middle panel), while swimming forward at the onset of the cycle, there is an initial increase in fin-beat frequency, followed by a decrease as velocity increases. This is in contrast with swimming in reverse, where fin-beat frequency initially is elevated and remains high until velocity begins to decrease. A similar trend is seen at the next highest intensity (0.3 Hz & 2.0 BL, Fig. 2.12, row C, last panel).

2.4 Discussion

For fishes living in coastal, wave-swept areas, many behavioral strategies exist to cope with increases in wave action depending on the fishes' ecological niche, including seeking refuge, drifting/swimming with the wave motion, or moving to an area of lower wave action (Friedlander and Parrish 1998a; Friedlander et al. 2003; Depczynski and Bellwood 2005; Fulton

and Bellwood 2005; Fulton et al. 2005; Santin and Willis 2007; Heatwole and Fulton 2013). This study was the first of its kind, designed to examine the energetic costs for fishes attempting to remain in position above the ocean floor (i.e., station-holding) with increases in bi-directional, oscillatory, wave-driven water motion. The metabolic rate of fishes swimming in this oscillatory pattern were found to increase as both frequency and amplitude of wave action increased, indicating higher metabolic costs as wave action increases (Figs. 2.6 and 2.7). In this study, we were able to achieve similar frequency of oscillation, but lower amplitude, of a typical trade-wind driven wave set in Hawaii (0.11 Hz and 2 m wave height; NPS Geologic Resources Division 2009). Compared with other reefs, the wave intensities in this study reached average velocities and frequency of oscillation similar to sheltered and lagoonal habitats on the Great Barrier Reef (6.2 to 17.1 cm s-1, and 0.06 to 0.66 Hz; Fulton and Bellwood 2005). The increase in metabolic rate as wave action increases is further supported by a study on the swimming costs of Shiner Surfperch during unsteady flow compared with steady flow (Roche et al. 2014). Compared with straight-line swimming, Roche et al. (2014) found that swimming in uni-directional, high-amplitude unsteady flow increased energetic costs by 25.3%, suggesting that estimates of MR in steady flow underestimate the energetic costs of fishes swimming in unsteady conditions.

Interestingly, in the present study there were no significant differences in overall increases in MR between the species tested (Figs. 2.6 and 2.7). Total swimming MR may be higher in some species due to differences in mass and in the standard, or resting, metabolic rates (SMR, Figs. 2.4 and 2.5), but after adjusting for mass-scaling and removing SMR, increases in MR with swimming (net cost of swimming, NCOS) were similar. However, it is important to

note that not all fishes attempt to maintain a constant position in the water column with wave action.

The fact that there were no significant differences in NCOS between species is surprising given previous research investigating the effect of body morphology and swimming mode on energetic costs of swimming. Previous studies of MPF specialist swimmers suggest that high maneuverability coupled with metabolic efficiency at higher water velocities should make MPF swimmers like balistiform and labriform swimmers more efficient at station-holding, especially as wave action increases (Blake 1978; Drucker and Lauder 2000; Walker and Westneat 2000; Korsmeyer et al. 2002; Blake 2004; Webb and Weihs 2015). Specifically, the balistiform swimmers were expected to show lower swimming MR due to a highly adapted morphology toward low speed maneuverability and its ability to achieve prolonged, high-speed swimming (up to 4.1 BL s^{-1} in *R. aculeatus;* Blake 1978; Korsmeyer et al. 2002). These swimmers benefit from utilizing sinusoidal displacement of elongated dorsal and anal fins that is estimated to create three-times the thrust in the direction of movement compared with BCF swimmers, and by keeping a rigid body to minimize body drag and reduce energy lost as a result of yawing motions (Lighthill and Blake 1990; Sfakiotakis et al. 1999; Blake 2004). These specializations, however, did not result in obvious differences in swimming MR for the balistids (*S. bursa* and *R. aculeatus*) compared with the other species in this study (Figs. 2.4-2.7).

Despite having a small sample size (n=2), the closely related tetraodontiform, *O. meleagris* (osctraciiform swimmer) showed some of the smallest increases in swimming MR. Lower swimming MR of this species may be due to recruitment of individual fins to provide minor swimming corrections, rather than large body movements, and they were observed to drift with the flow substantially more than the balistids. This type of multi-propulsor swimming mode

has been shown to be as energetically efficient as similar sized BCF swimmers in straight-line swimming, and capable of reaching speeds up to 6 BL s^{-1} (Gordon et al. 2000; Van Wassenbergh et al. 2015). In Hawai‘i, these fishes can be found closely associated with reefs, feeding on benthic invertebrates, and able to negotiate complex reef structures due to the stability and maneuverability provided by course-correcting median and paired fins, combined with a caudal fin utilized as a rudder (Hobson 1974; Walker 2000; Hove et al. 2001; Van Wassenbergh et al. 2015).

Also contrasting with previous studies, the BCF swimmer *Kuhlia* spp. showed the lowest and most consistent increases in swimming MR across all amplitudes and frequencies (Fig. 2.6). Previous studies suggest that BCF swimmers are more specialized for unidirectional movements, providing higher power output for greater acceleration and cruising at high speeds, in contrast with unsteady flow where fishes with greater maneuverability should outperform those with efficient straight-line swimming (Webb 1984; Korsmeyer et al. 2002; Blake 2004). However, because of their low MR in the face of increasing wave action, *Kuhlia* spp. may be more adapted to a wider range of flow regimes, and not restricted to areas of low wave exposure. In Hawai’i, these species are commonly found across a wide range of coastal habitats around the entire island, including coral reefs, sandy beaches, and stream mouth estuaries, all of which represent differing flow regimes from high to low energy wave exposure (Randall and Randall 2001).

Although there was no significant difference in overall NCOS among species, different swimming strategies and changing costs were found within species in response to increases in frequency of oscillation. From studies of straight-line swimming, we know that as swimming velocity increases, energetic costs rise following a power relationship (Korsmeyer et al. 2002). However, in unsteady, bidirectional flow, fish can be subjected to increasing frequency of

oscillation while still swimming at the same average velocity. Different combinations of frequency and amplitudes can produce similar average velocities, but as frequency increases, the fish is forced to cope with frequent flow direction changes inducing shifts in behavior. At higher frequencies, smaller amplitudes result in similar swimming velocities, but more turns are required to deal with the increased number of flow direction changes. For BCF swimmers, increasing frequency at similar average velocities appears to increase the cost of swimming more substantially than it does for MPF swimmers. The BCF swimmer *Kuhlia* spp. showed significantly higher NCOS at 0.3 Hz compared with 0.2 Hz oscillation, over the same average velocities (Fig. 2.8). This result is not unexpected, given the fact that more frequent turning at similar average velocities should increase the energetic cost of swimming. In contrast, the MPF swimmers (*C. strigosus* and *S. bursa*) showed no significant change in costs of swimming, which is surprising because this suggests that the cost of changing direction does not increase for MPF swimmers as wave frequency increases. Most importantly, this suggests that the cost of turning is greatest for *Kuhlia* spp. and may reflect the difference in swimming mode (BCF vs. MPF). Supporting this notion is the fact that *A. ocellaris* (a combination BCF/pectoral fin swimmer) also showed a slightly higher, on average, (but not significantly higher, $p = 0.084$) NCOS at 0.3 Hz compared to 0.2 Hz oscillation. For the strict MPF swimmers (*S. bursa* and *C. strigosus*), there is considerable overlap in NCOS at the higher frequency but same average velocity, which suggests a very low cost of changing direction. The difference in metabolic responses may be due to the MPF swimming mode or may also be affected by whether the fish turned around with every shuttle direction change (versus swimming in reverse in one direction) (Fig. 2.9).

Unlike *Kuhlia* spp., the two MPF swimmers *C. strigosus* and *S. bursa* were frequently observed to swim backwards with a flow direction change, rather than turn completely around.

For the labriform swimmer *C. strigosus*, the percent turning paired with changes in FBF may show that swimming in reverse is a mechanism for coping with increasing frequency of water flow change. While there is little research on fish swimming in reverse, Flammang and Lauder (2016) described fin kinematics of reverse swimming in the Blue-gill Sunfish (*Lepomis macrochirus*) as an orchestrated movement of multiple fins, individually recruited to counteract instability of yawing around the center of mass of the fish. *L. macrochirus* must recruit not only the pectoral fins, but the dorsal and anal fins along with the caudal fin to produce thrust and simultaneously counteract small instabilities using the same fins. While this study did not investigate the costs of swimming backwards, it could be hypothesized that the increased recruitment of muscle activity would increase metabolic rate, allocating more resources toward fin movement than while swimming forward, which is a much more stable endeavor (Tudorache et al. 2009). Further supporting this hypothesis, *C. strigosus* was found to have a significantly higher FBF while swimming in reverse over most intensities compared with swimming forward, indicating that more fin-beats were required to cover the same distance (Fig. 2.12). Even so, *C. strigosus* did not show significantly higher MR compared with all other species, suggesting that swimming in reverse (despite higher FBF and greater instability) may be more energetically efficient than turning around every time flow direction changes. Lending to its behavioral flexibility, *C. strigosus* is another closely reef-associated species, and can be found navigating structurally complex reefs, grazing on diatoms and detritus that have been deposited in sediments accumulated over rocks and dead coral (Hobson 1974).

This relationship may also be true for the balistiform swimmer *S. bursa* which was observed to swim in reverse more often than not, further supporting the idea that MPF swimmers may need to employ behavioral changes to cope with increases in wave-driven action (Fig. 2.9).

Like *C. strigosus*, *S. bursa* can be found navigating close to the reef, but *S. bursa* prefer foraging the ocean floor for invertebrates (mainly echinoids), and resting in crevices in the coral structures at night (Hobson 1974). Station-holding behavior may be necessary while this species forages the ocean floor, facilitating the behavior of swimming in reverse while attempting to locate food and also while taking advantage of refugia within the reef structure.

The BCF swimmers *Kuhlia* spp. and *A. ocellaris* were observed to turn with each direction change in order to swim forward a vast majority of the time (always over 75%), suggesting they are less able to swim in reverse, or it may be less efficient for these species. It may be possible for BCF swimming fishes to swim in reverse using the pectoral fins, such as species with larger, low aspect-ratio fins similar to *A. ocellaris* (Appendix 3). However, having an elongated body and posterior shifting of the fish's center of mass may complicate stability issues compared with the deeper bodied *C. strigosus,* whose center of mass is more centrally located (Weihs 2002; Claverie and Wainwright 2014; Webb and Weihs 2015; Flammang and Lauder 2016). In addition, swimming in reverse may be more complicated for BCF swimming species with longer, thinner pectoral fins (high aspect-ratio), similar to *Kuhlia* spp., that are not capable of generating sufficient thrust to propel movement in reverse (Flammang and Lauder 2016). For these fish, swimming backwards may be limited, or generated using whole body undulations, theoretically increasing metabolic demands greatly (Flammang and Lauder 2016).

While the SWMR was designed to examine the metabolic costs of fishes forced to swim in an oscillatory wave pattern in essentially still water, a comparison test was conducted between this apparatus and a Steffensen-type recirculating flume respirometer for *C. strigosus* (Appendix 2). In this comparison, the swimming section was much larger in the flume respirometer, giving the fish more freedom of movement, but eliminating the ability to measure oxygen consumption

rates (too small of a fish in a large water volume for reliable respirometry; Svendsen et al. 2016). Measurements of FBF, coupled with personal observations showed that the individual used more physical space swimming in the flume respirometer, drifting with the oscillatory flow, and had a lower FBF especially as frequency and amplitude increased. However, *C. strigosus* was observed to swim in reverse with a direction change in both apparatuses, eliminating the possibility that a low percent turning was an artefact of swimming in the SWMR.

One obvious area for future research would be a direct comparison of similar species swimming in both straight-line swimming in a traditional flume with bi-directional, oscillatory wave-motion swimming. This comparison would reveal the differences in swimming cost related just to the acceleration/deceleration cycle and direction changes required in wave flows. This study only examined the metabolic costs of swimming in bi-directional oscillatory flow, similar to what is commonly experienced on the reef. One unexpected result was the difference in swimming behaviors, such as swimming in reverse, and this study was not designed to separate the metabolic costs of swimming in reverse versus swimming forward. While there was no correlation of frequency of turning and NCOS across individuals, there was a relatively small dataset for this analysis to be conducted. Future studies might examine the effect of swimming in reverse versus swimming forward on fin-beat frequency and ultimately oxygen consumption rates.

2.5 Conclusions

As intensity of wave-action increases in both frequency and amplitude, fishes attempting to station-hold are subject to substantial increases in MR, although overall increases do not seem to differ significantly among species. However, when examining metabolic costs as a function of increasing frequency at similar average velocities, BCF swimmers seem to incur greater NCOS than MPF swimmers. These differences in MR may be due to differences in the efficiency of each swimming mode (BCF versus MPF) as frequency increases, or may reflect differences in swimming capability and behavioral flexibility of MPF swimmers. While it may be more efficient for BCF swimmers to turn around with every flow direction change, MPF swimmers may have greater flexibility in adapting their swimming style to avoid the high cost of re-orienting themselves into the direction of flow.

2.6 References

Blake R (1978) On balistiform locomotion. Journal of the Marine Biological Association of the United Kingdom 58:73-80

Blake RW (2004) Fish functional design and swimming performance. Journal of Fish Biology 65:1193-1222

Claverie T, Wainwright PC (2014) A morphospace for reef fishes: elongation is the dominant axis of body shape evolution. PloS one 9:e112732

Constantin A, Villari G (2008) Particle trajectories in linear water waves. Journal of Mathematical Fluid Mechanics 10:1-18

Denny MW, Gaylord B (2010) Marine ecomechanics. Annual Review of Marine Science 2:89-114

Depczynski M, Bellwood DR (2005) Wave energy and spatial variability in community structure of small cryptic coral reef fishes. Marine Ecology Progress Series 303:283-293

Dornburg A, Sidlauskas B, Santini F, Sorenson L, Near TJ, Alfaro ME (2011) The influence of an innovative locomotor strategy on the phenotypic diversification of triggerfish (Family: Balistidae). Evolution 65:1912-1926

Drucker EG, Lauder GV (2000) A hydrodynamic analysis of fish swimming speed: wake structure and locomotor force in slow and fast labriform swimmers. Journal of Experimental Biology 203:2379-2393

Flammang BE, Lauder GV (2016) Functional morphology and hydrodynamics of backward swimming in bluegill sunfish, Lepomis macrochirus. Zoology

Friedlander A, Brown E, Jokiel P, Smith W, Rodgers K (2003) Effects of habitat, wave exposure, and marine protected area status on coral reef fish assemblages in the Hawaiian archipelago. Coral Reefs 22:291-305

Friedlander AM, Parrish JD (1998a) Temporal dynamics of fish communities on an exposed shoreline in Hawaii. Environmental Biology of Fishes 53:1-18

Friedlander AM, Parrish JD (1998b) Habitat characteristics affecting fish assemblages on a Hawaiian coral reef. Journal of Experimental Marine Biology and Ecology 224:1-30

Fulton C, Bellwood D, Wainwright P (2001) The relationship between swimming ability and habitat use in wrasses (Labridae). Marine Biology 139:25-33

Fulton C, Bellwood D, Wainwright P (2005) Wave energy and swimming performance shape coral reef fish assemblages. Proceedings of the Royal Society B: Biological Sciences 272:827-832

Fulton CJ, Bellwood DR (2005) Wave-induced water motion and the functional implications for coral reef fish assemblages. Limnology & Oceanography 50:255-264

Fulton CJ, Johansen JL, Steffensen JF (2013a) Energetic Extremes in Aquatic Locomotion by Coral Reef Fishes. Plos One 8:6

Fulton CJ, Binning SA, Wainwright PC, Bellwood DR (2013b) Wave-induced abiotic stress shapes phenotypic diversity in a coral reef fish across a geographical cline. Coral Reefs 32:685-689

Heatwole SJ, Fulton CJ (2013) Behavioural flexibility in reef fishes responding to a rapidly changing wave environment. Marine Biology 160:677-689

Hobson ES (1974) Feeding relationships of teleostean fishes on coral reefs in Kona, Hawaii. Fish Bull 72:915-1031

Hoegh-Guldberg O, Mumby P, Hooten A, Steneck R, Greenfield P, Gomez E, Harvell C, Sale P, Edwards A, Caldeira K (2007) Coral reefs under rapid climate change and ocean acidification. science 318:1737-1742

Hove JR, O'Bryan LM, Gordon MS, Webb PW, Weihs D (2001) Boxfishes (Teleostei: Ostraciidae) as a model system for fishes swimming with many fins: kinematics. Journal of Experimental Biology 204:1459-1471

Korsmeyer KE, Steffensen JF, Herskin J (2002) Energetics of median and paired fin swimming, body and caudal fin swimming, and gait transition in parrotfish (Scarus schlegeli) and triggerfish (Rhinecanthus aculeatus). The Journal Of Experimental Biology 205:1253-1263

Lighthill J, Blake R (1990) Biofluiddynamics of balistiform and gymnotiform locomotion. Part 1. Biological background, and analysis by elongated-body theory. Journal of Fluid Mechanics 212:183-207

Loofbourrow, H. (2009). Hydrodynamics of Balistiform swimming in the Picasso Triggerfish, Rhinecanthus aculeatus (T). University of British Columbia. Retrieved from https://open.library.ubc.ca/cIRcle/collections/24/items/1.0066913 (Original work published 2009)

Malcolm S. Gordon, Jay R. Hove, Paul W. Webb, Daniel Weihs (2000) Boxfishes as Unusually Well-Controlled Autonomous Underwater Vehicles. Physiological and Biochemical Zoology 73:663-671

Moberg F, Folke C (1999) Ecological goods and services of coral reef ecosystems. Ecological Economics 29:215-233

NPS Geologic Resources Division (2009) Coastal Hazard Analysis Report. 105 p

Pink JR, Fulton CJ (2014) Right tools for the task: intraspecific modality in the swimming behaviour of coral reef fishes [electronic resource]. Marine biology 161:1103-1111

Randall JE, Randall HA (2001) Review of the fishes of the genus Kuhlia (Perciformes: Kuhliidae) of the Central Pacific. Pacific Science 55:227-256

Roche DG, Taylor MK, Binning SA, Johansen JL, Domenici P, Steffensen JF (2014) Unsteady flow affects swimming energetics in a labriform fish (Cymatogaster aggregata). Journal of Experimental Biology 217:414-422

Santin S, Willis TJ (2007) Direct versus indirect effects of wave exposure as a structuring force on temperate cryptobenthic fish assemblages. Marine Biology 151:1683-1694

Sfakiotakis M, Lane DM, Davies JBC (1999) Review of fish swimming modes for aquatic locomotion. Oceanic Engineering, IEEE Journal of 24:237-252

Sheppard C, Dixon DJ, Gourlay M, Sheppard A, Payet R (2005) Coral mortality increases wave energy reaching shores protected by reef flats: examples from the Seychelles. Estuarine, Coastal and Shelf Science 64:223-234

Steffensen JF, Johansen K, Bushnell PG (1984) An automated swimming respirometer. Comparative Biochemistry and Physiology Part A: Physiology 79:437-440

Steffensen JF, Bushnell PG, Schurmann H (1994) Oxygen consumption in four species of teleosts from Greenland: no evidence of metabolic cold adaptation. Polar Biology 14:49-54

Svendsen JC, Tudorache C, Jordan AD, Steffensen JF, Aarestrup K, Domenici P (2010) Partition of aerobic and anaerobic swimming costs related to gait transitions in a labriform swimmer. Journal of Experimental Biology 213:2177-2183

Svendsen M, Bushnell P, Christensen E, Steffensen J (2016) Sources of variation in oxygen consumption of aquatic animals demonstrated by simulated constant oxygen consumption and respirometers of different sizes. Journal of fish biology 88:51-64
Van Wassenbergh S, van Manen K, Marcroft TA, Alfaro ME, Stamhuis EJ (2015) Boxfish swimming paradox resolved: forces by the flow of water around the body promote manoeuvrability. Journal of The Royal Society Interface 12:20141146
Walker JA (2000) Does a rigid body limit maneuverability? Journal of Experimental Biology 203:3391-3396
Walker JA, Westneat MW (2000) Mechanical performance of aquatic rowing and flying. Proceedings of the Royal Society of London Series B: Biological Sciences 267:1875-1881
Webb PW (1984) Body Form, Locomotion and Foraging in Aquatic Vertebrates. American Zoologist 24:107-120
Webb PW, Weihs D (2015) Stability versus maneuvering: challenges for stability during swimming by fishes. Integrative and comparative biology 55:753-764
Weihs D (2002) Stability Versus Maneuverability in Aquatic Locomotion. Integrative and Comparative Biology 42:127-134

2.7 Figures and Tables

Table 2.1. *Sample size, mass and length (mean ± S.D.) for all fish species in this study, organized by predominate swimming mode (Body-Caudal Fin, BCF, swimmers, and Median-Paired Fin, MPF, swimmers: Labriform, Balistiform, and Ostraciiform).*

Swimming Mode and Species	Common Name	Number of Individuals	Mass (g)	Total Length (cm)	Hawaiian Name
Body-and-Caudal Fin Swimmers					
Kuhlia spp.	Hawaiian Flagtail	5	5.5 ± 2.0	7.4 ± 0.9	āholehole
Mugil cephalus	Flathead Grey Mullet	3	3.5 ± 0.3	7.2 ± 0.3	ama‘ama
Labriform Swimmers					
Abudefduf sordidus	Black-Spot Sergeant	1	6.5	7.0	kūpīpī
Amphiprion ocellaris	Clown Anemonefish	5	5.3 ± 0.7	6.5 ± 0.3	N/A
Ctenochaetus strigosus	Goldring Surgeonfish	6	8.9 ± 0.8	7.5 ± 0.4	kole
Balistiform Swimmers					
Rhinecanthus aculeatus	Lagoon Triggerfish	3	9.4 ± 1.6	7.0 ± 0.4	humuhumunukunukuapua‘a
Sufflamen bursa	Lei Triggerfish	5	9.2 ± 2.5	7.4 ± 0.4	humuhumu lei
Osctraciiform Swimmers					
Ostracion meleagris	Spotted Boxfish	2	15 ± 1	7.9 ± 0.2	moa

***Table 2.2**. Total and mass-specific standard metabolic rates (SMR, mean ± S.D.) for main species studied. SMR_{10} values are mass-specific SMR adjusted to a common mass of 10 g using a mass scaling exponent of 0.895.*

Species	Total SMR (mg O_2 h^{-1})	Mass-specific SMR (mg O_2 kg^{-1} h^{-1})	SMR_{10} (mg O_2 kg^{-1} h^{-1})
Amphiprion ocellaris	0.764 ± 0.210	144.1 ± 36.9	134.7 ± 34.4
Ctenochaetus strigosus	1.64 ± 0.386	181.9 ± 28.9	179.8 ± 29.8
Sufflamen bursa	0.956 ± 0.241	107.5 ± 30.4	105.9 ± 28.9
Kuhlia spp.	0.929 ± 0.658	157.8 ± 48.4	148.5 ± 51.0

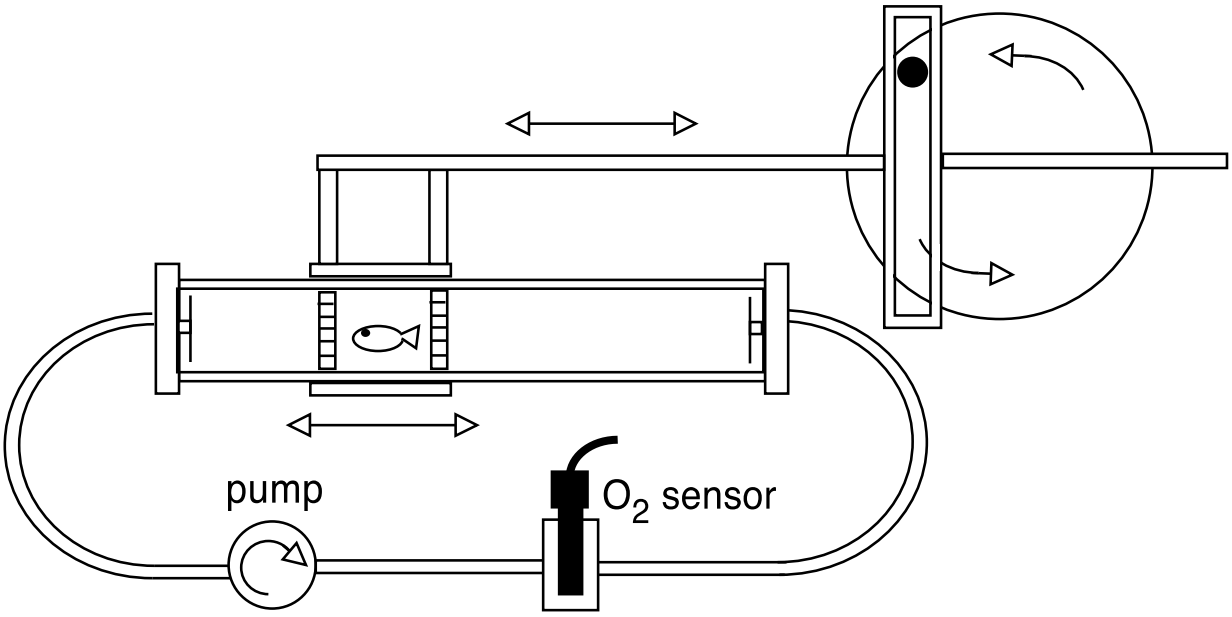

Figure 2.1. Schematic of the simulated wave motion respirometer (SWMR). The apparatus uses a scotch yoke mechanism to convert rotational motion into linear oscillation, with sinusoidal displacement and velocity over time. A partial sleeve, surrounding a long (50 cm), cylindrical (8.9 cm I.D.) clear acrylic respirometry tube, is coupled to internal PVC rings by magnets, creating a 15 cm long swimming section that travels back and forth within the respirometer. The external sleeve is marked with black & white vertical bars to elicit the optomotor response and induce swimming within the moving section. By changing the rotational speed and radius of the circular motion, the wave frequency and amplitude, respectively, can be altered. Water within the respirometer tube is circulated past an optical dissolved oxygen sensor for measurement of oxygen consumption rate. A second computer-actuated pump (not shown) periodically flushes the respirometer with clean oxygenated water from a surrounding water bath (Korsmeyer, unpublished).

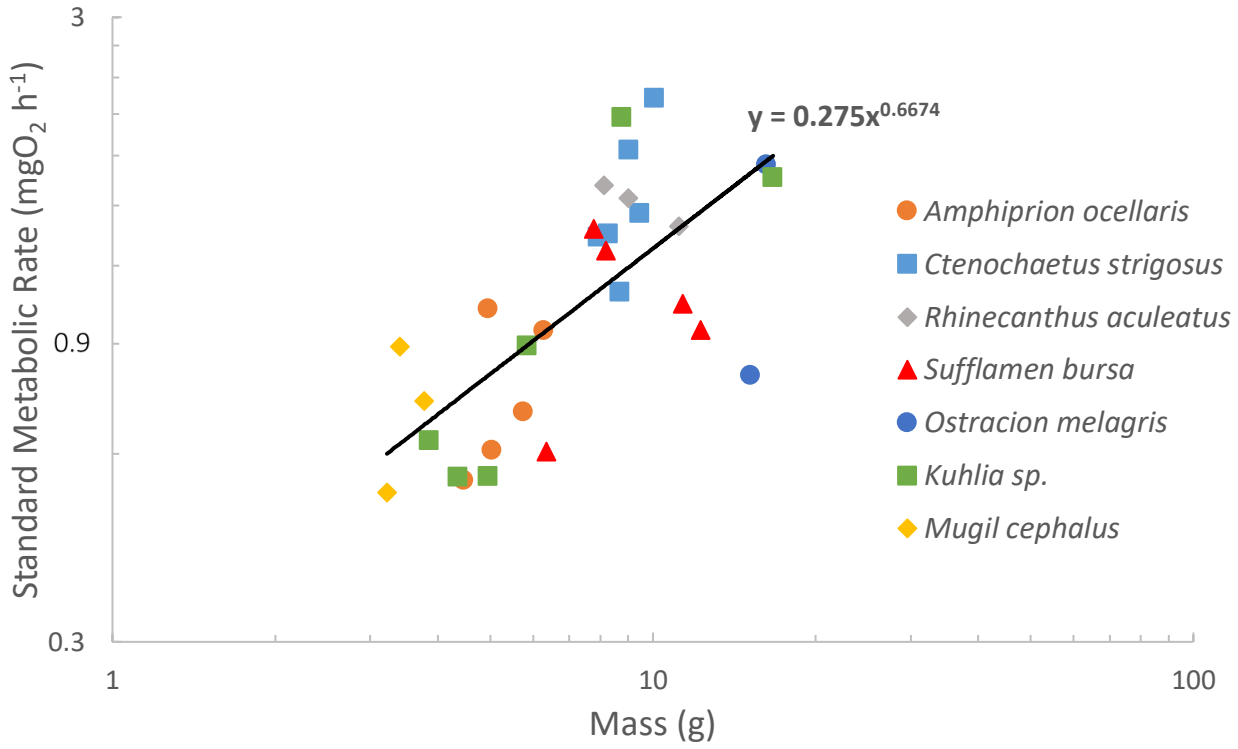

Figure 2.2. Total standard metabolic rate (SMR, mg O_2 h^{-1}) as a function of mass (g) for all species tested in the SWMR apparatus plotted on a log-log scale. The regression line includes all species. The common scaling exponent for these species was 0.667.

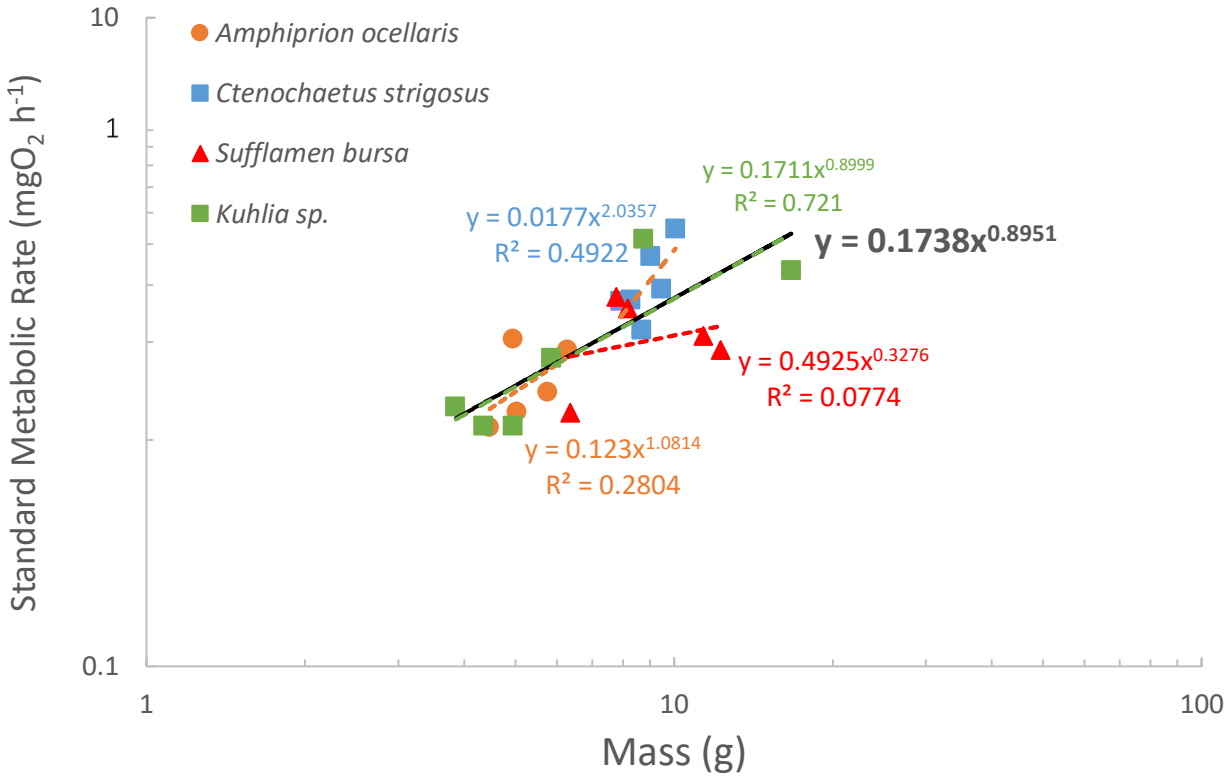

Figure 2.3. Total standard metabolic rate (SMR, mg O_2 h^{-1}) as a function of body mass (g) for four species of fish tested in the SWMR apparatus plotted on a log-log scale. Colored regression lines are for individual species and the black fitted line is for all four species combined. The common scaling exponent for all four species was 0.895.

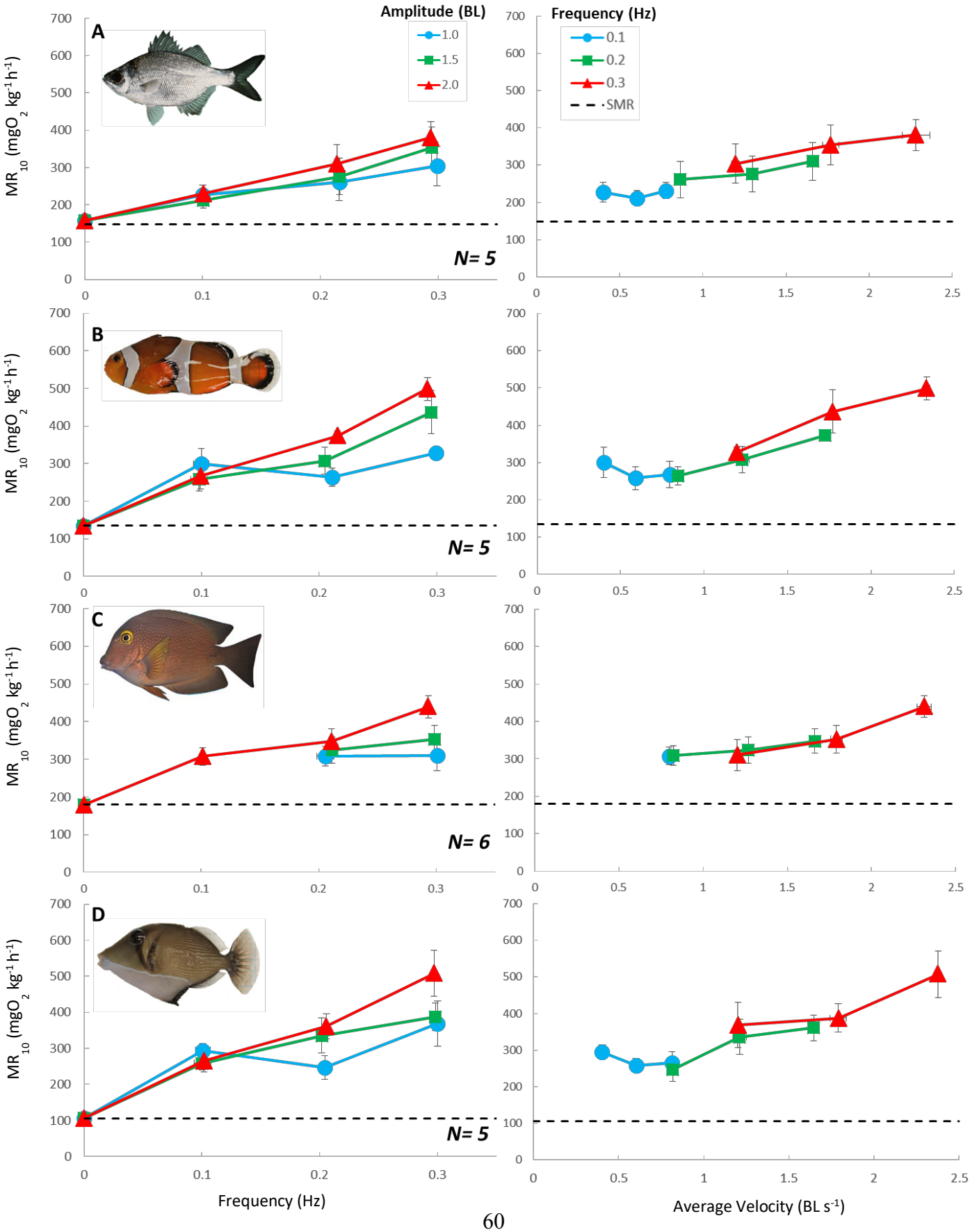
Amplitude (BL)
1.0
1.5
2.0
Frequency (Hz)
0.1
0.2
0.3
SMR
A
B
C
D
N= 5
N= 5
N= 6
N= 5
MR10 (mgO2 kg-1 h-1)
Frequency (Hz)
Average Velocity (BL s-1)

Figure 2.4. Metabolic rate (mean ± S.E.) as a function of wave frequency (Hz) at 3 different wave amplitudes (reported relative to fish body length, BL) (**left column**), and as a function of average swimming velocity (BL s^{-1}) at the three frequencies (**right column**), during oscillatory swimming. Metabolic rates were normalized to a common fish mass of 10 g (MR_{10}). **A.)** *Kuhlia* spp. (mean TL= 7.4 cm, mean mass= 5.5 g) **B.)** *Amphiprion ocellaris* (mean TL= 6.5 cm, mean mass= 5.3 g) **C.)** *Ctenochaetus strigosus* (mean TL= 7.5 cm, mean mass= 8.9 g) and **D.)** *Sufflamen bursa* (mean TL= 7.4 cm, mean mass= 9.2 g). Standard metabolic rate is indicated by the dashed line. Average swimming velocity was calculated as the average absolute velocity over one wave cycle. No data exists for *C. strigosus* (**C**) at the two lowest intensities (frequency 0.1 Hz, 1 BL amplitude and frequency 0.1 Hz, 1.5 BL amplitude) due to erratic swimming of all individuals of the species.

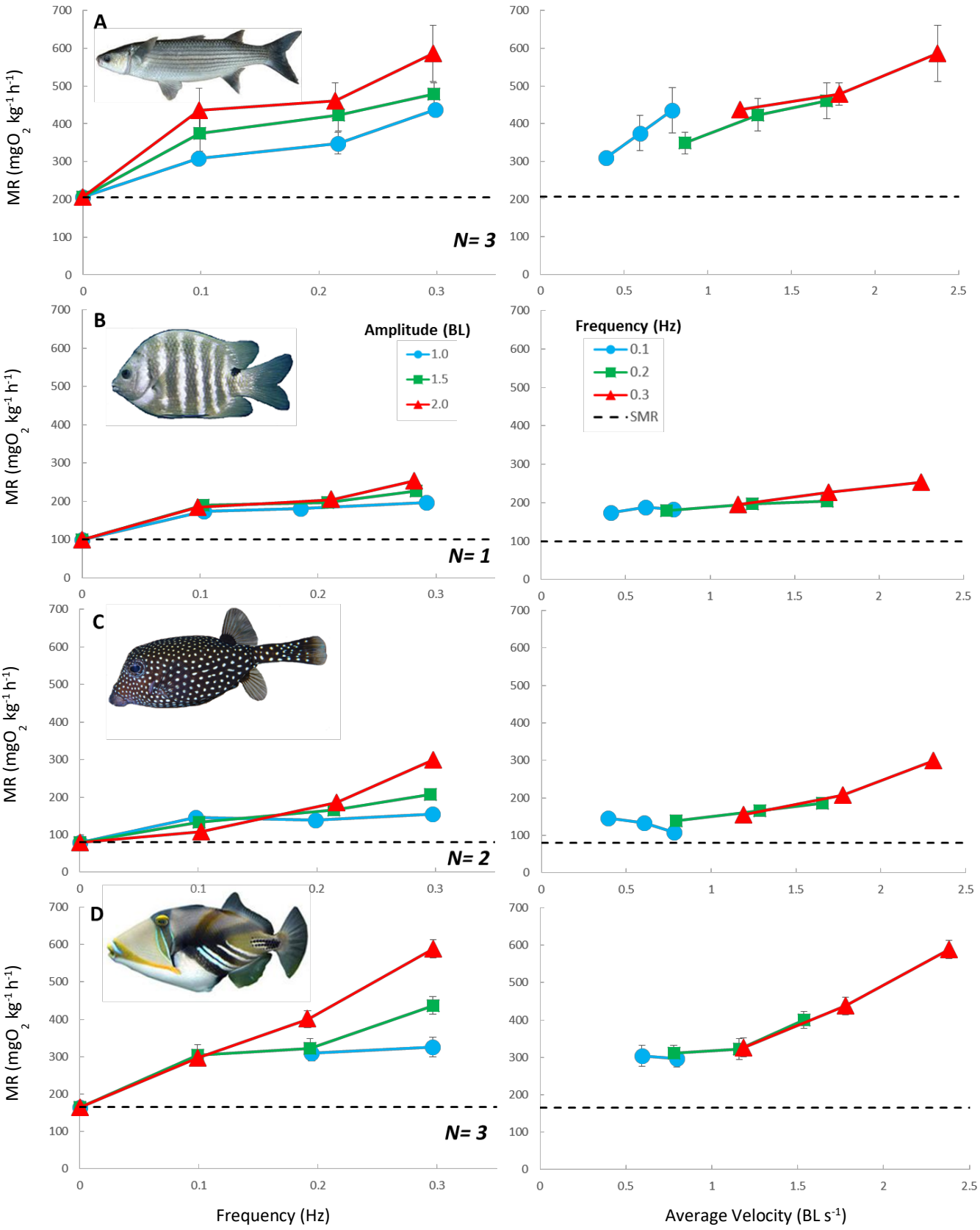
A
B
C
D
N= 3
N= 1
N= 2
N= 3
Amplitude (BL)
1.0
1.5
2.0
Frequency (Hz)
0.1
0.2
0.3
SMR
MR (mgO2 kg-1 h-1)
Frequency (Hz)
Average Velocity (BL s-1)

Figure 2.5. Metabolic rate (mean ± S.E.) as a function of wave frequency (Hz) at 3 different wave amplitudes (reported relative to fish body length, BL) (**left column**), and as a function of average swimming velocity (BL s^{-1}) at the three frequencies (**right column**), during oscillatory swimming. **A.)** *Mugil cephalus* (mean TL= 7.2 cm, mean mass= 3.5 g) **B.)** *Abudefduf sordidus* (TL= 7.0 cm, mass= 6.5 g) **C.)** *Ostracion meleagris* (mean TL= 7.9 cm, mean mass= 15.7 g) and **D.)** *Rhinecanthus aculeatus* (mean TL= 7.0 cm, mean mass= 9.4 g). Standard metabolic rate is indicated by the dashed line. Average swimming velocity was calculated as the average absolute velocity over one wave cycle.

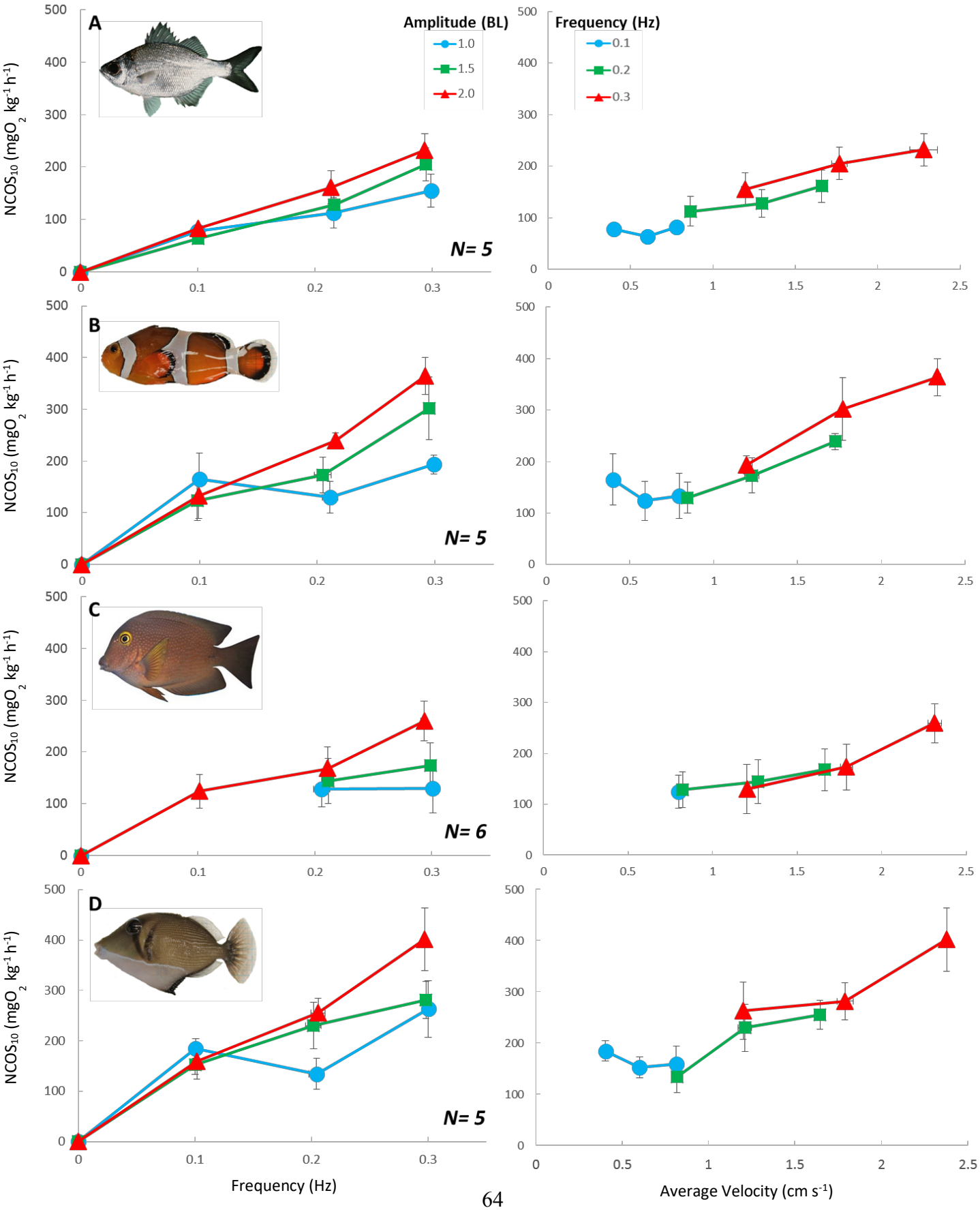
A
B
C
D
Amplitude (BL)
1.0
1.5
2.0
Frequency (Hz)
0.1
0.2
0.3
N= 5
N= 5
N= 6
N= 5
NCOS10 (mgO2 kg-1 h-1)
Frequency (Hz)
Average Velocity (cm s-1)

Figure 2.6. Net cost of swimming normalized to a common mass of 10 g fish ($NCOS_{10}$, mean ± S.E.) as a function of wave frequency (Hz) at 3 different wave amplitudes (reported relative to fish body length, BL) (**left column**), and as a function of average swimming velocity (BL s^{-1}) at the three frequencies, during oscillatory swimming (**right column**) for **A.)** *Kuhlia* spp. (mean TL= 7.4 cm, mean mass= 5.5 g) **B.)** *Amphiprion ocellaris* (mean TL= 6.5 cm, mean mass= 5.3 g) **C.)** *Ctenochaetus strigosus* (mean TL= 7.5 cm, mean mass= 8.9 g) and **D.)** *Sufflamen bursa* (mean TL= 7.4 cm, mean mass= 9.2 g). NCOS was calculated by subtracting SMR from swimming MR. Average swimming velocity was calculated as the average absolute velocity over one wave cycle. No data exists for *C. strigosus* (**C**) at the two lowest intensities (frequency 0.1 Hz, 1 BL amplitude and frequency 0.1 Hz, 1.5 BL amplitude) due to erratic swimming of all individuals of the species.

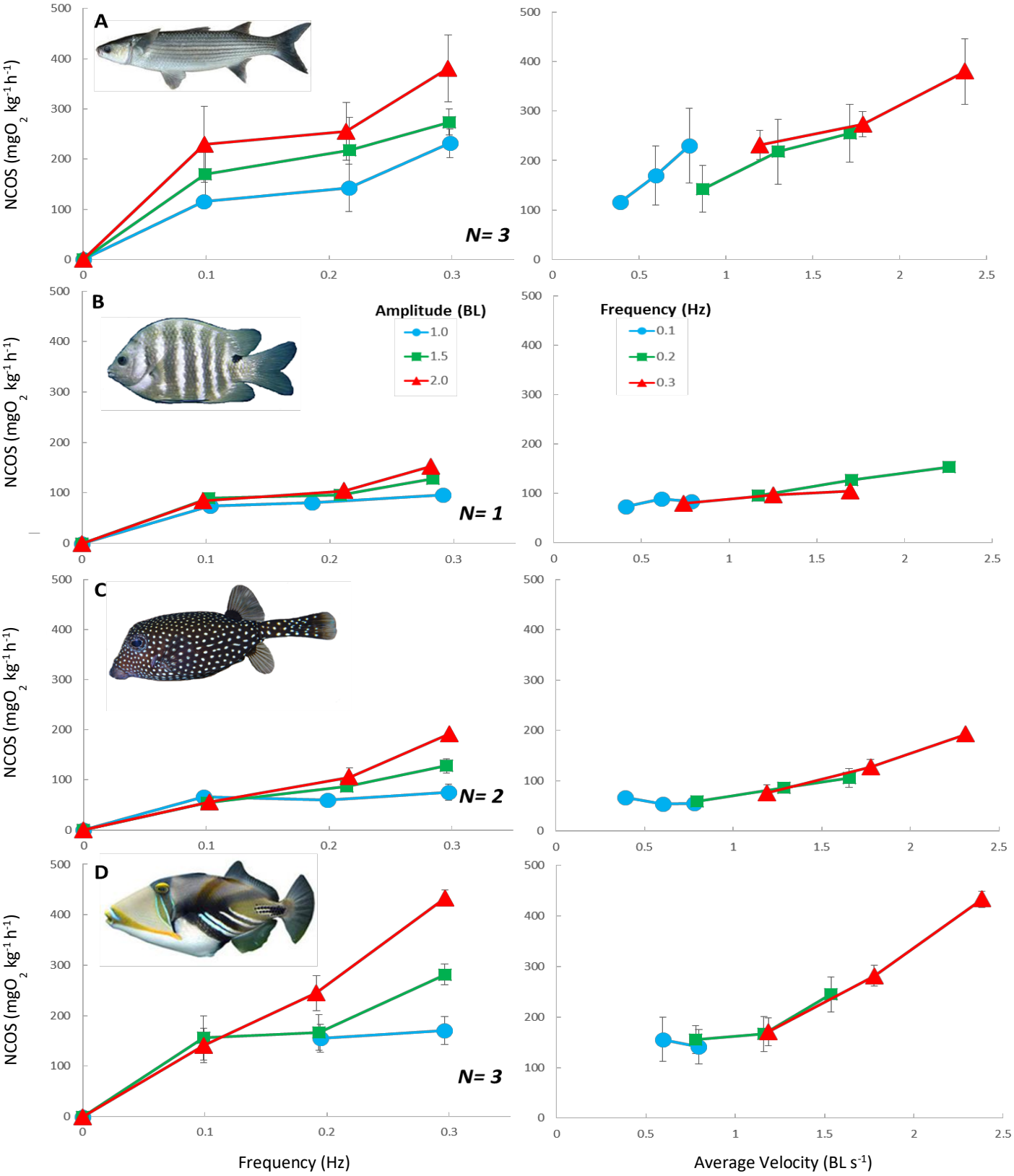
A
B
C
D
N= 3
N= 1
N= 2
N= 3
Amplitude (BL)
1.0
1.5
2.0
Frequency (Hz)
0.1
0.2
0.3
NCOS (mgO2 kg-1 h-1)
Frequency (Hz)
Average Velocity (BL s-1)

Figure 2.7. Net cost of swimming (NCOS, mean ± S.E.) as a function of wave frequency (Hz) at 3 different wave amplitudes (reported relative to fish body length, BL) (**left column**), and as a function of average swimming velocity (BL s^{-1}) at the three frequencies (**right column**), during oscillatory swimming for **A.)** *Mugil cephalus* (mean TL= 7.2 cm, mean mass= 3.5 g) **B.)** *Abudefduf sordidus* (TL= 7.0 cm, mass= 6.5 g) **C.)** *Ostracion meleagris* (mean TL= 7.9 cm, mean mass= 15.7 g) and **D.)** *Rhinecanthus aculeatus* (mean TL= 7.0 cm, mean mass= 9.4 g). NCOS was calculated by subtracting SMR from swimming MR. Average swimming velocity was calculated as the average absolute velocity over one wave cycle.

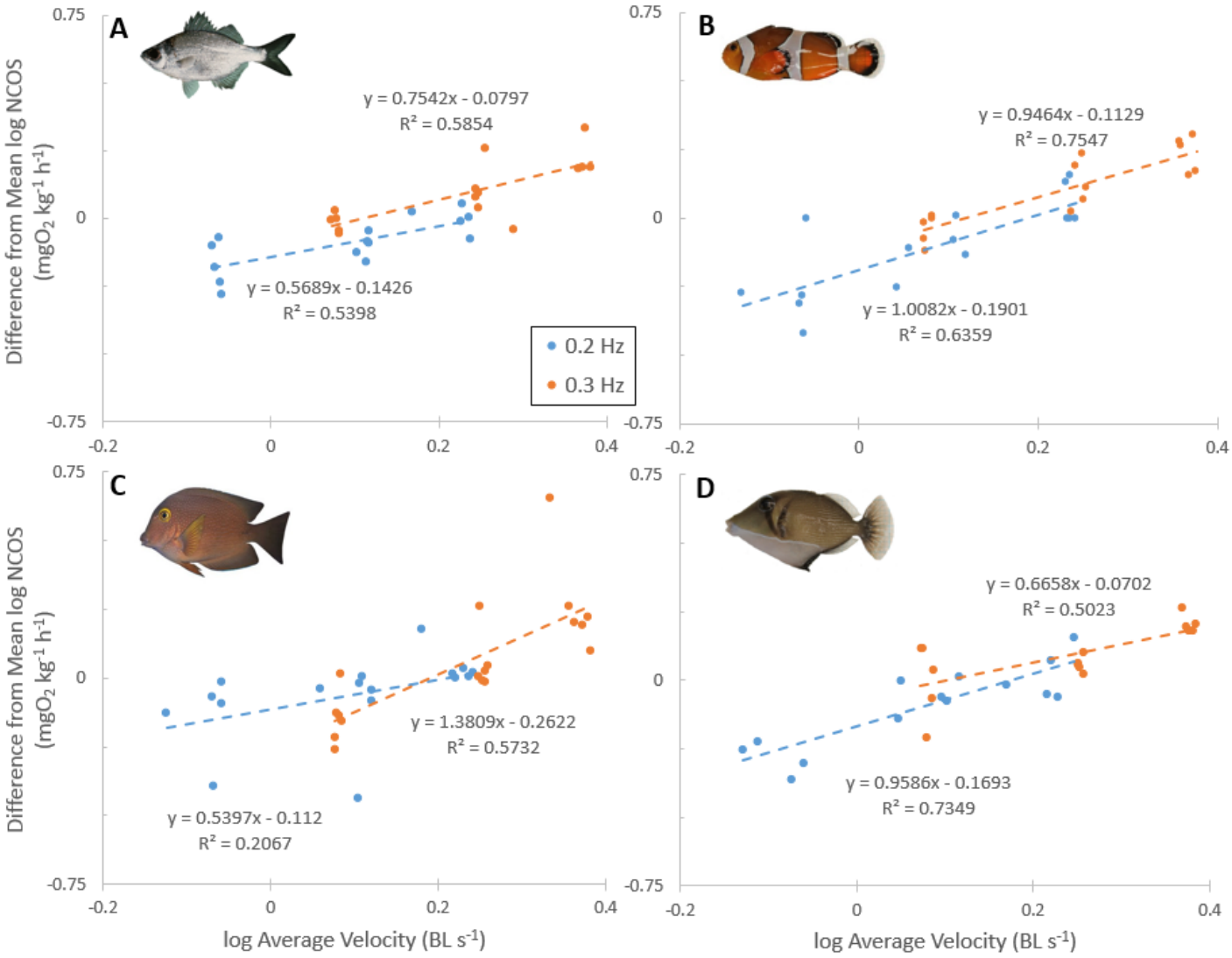

Figure 2.8. Difference from average net cost of swimming (NCOS) as a function of average velocity (reported relative to body length, BL per second, BL s^{-1}) at two frequencies of oscillatory swimming (0.2 and 0.3 Hz). Values are log transformed to linearize relationship. **A.)** *Kuhlia* spp. (mean TL= 7.4 cm, mean mass= 5.5 g, *n*= 5) **B.)** *Amphiprion ocellaris* (mean TL= 6.5 cm, mean mass= 5.3 g, *n*= 5) **C.)** *Ctenochaetus strigosus* (mean TL= 7.5 cm, mean mass= 8.9 g, *n*=5) and **D.)** *Sufflamen bursa* (mean TL= 7.4 cm, mean mass= 9.2 g, *n*= 5). Difference from mean log NCOS were calculated as the difference from the mean log NCOS for each individual fish. Dashed lines indicate regressions corresponding to each frequency. ANCOVA revealed that only *Kuhlia* spp. had significantly different elevations in NCOS with frequency ($F(1, 27)= 9.00$, $p= 0.048$).

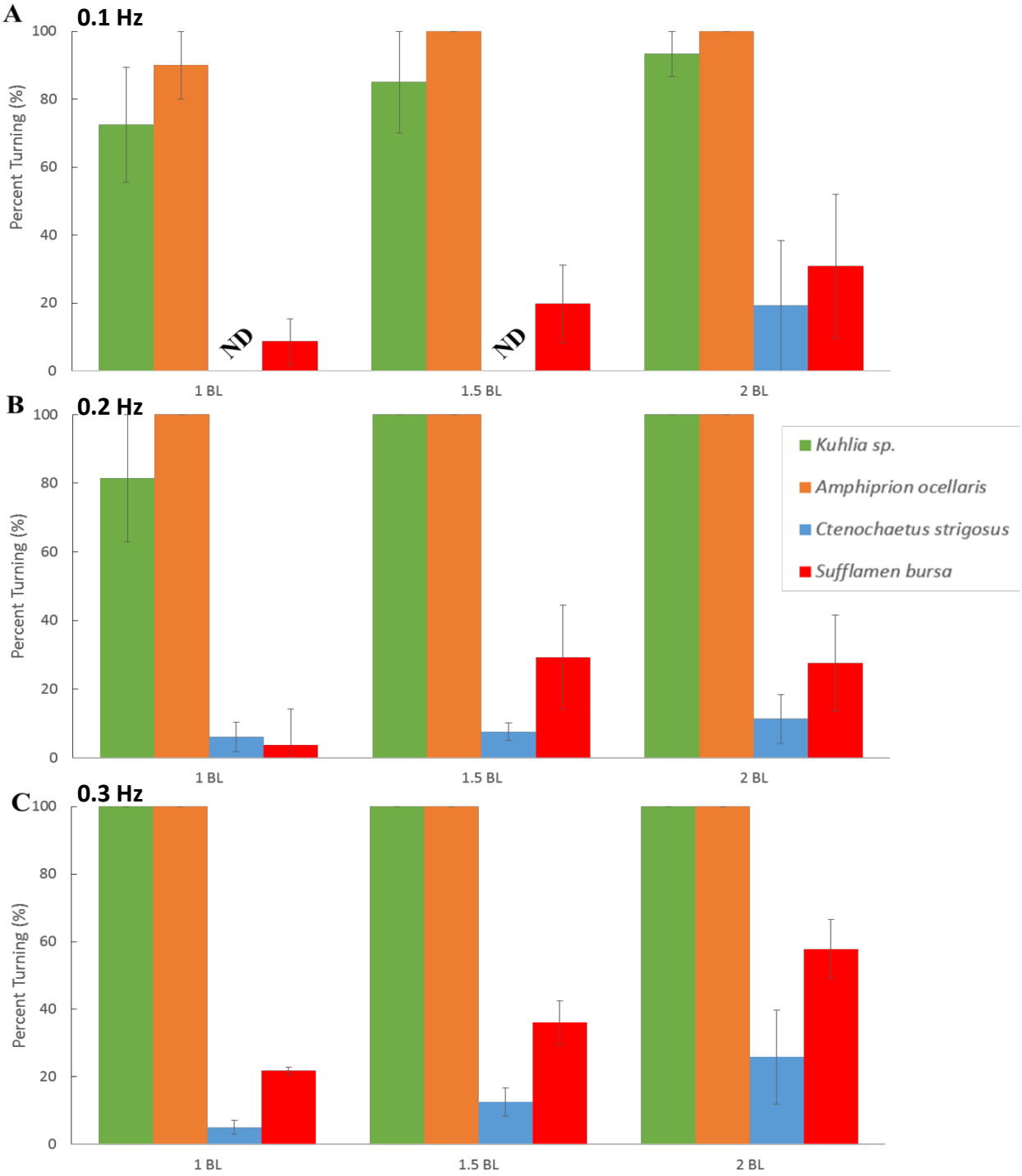

Figure 2.9. Percent turning (mean ± S.E.) as a function of amplitude (reported relative to fish body length, BL) at three frequencies, 0.1 Hz (**A**), 0.2 Hz (**B**), and 0.3 Hz (**C**), during oscillatory swimming. Percent turning was quantified as the number of times the individual turned around relative to the total number of direction changes by the SWMR. **ND** indicates data points for which no data exists due to erratic swimming.

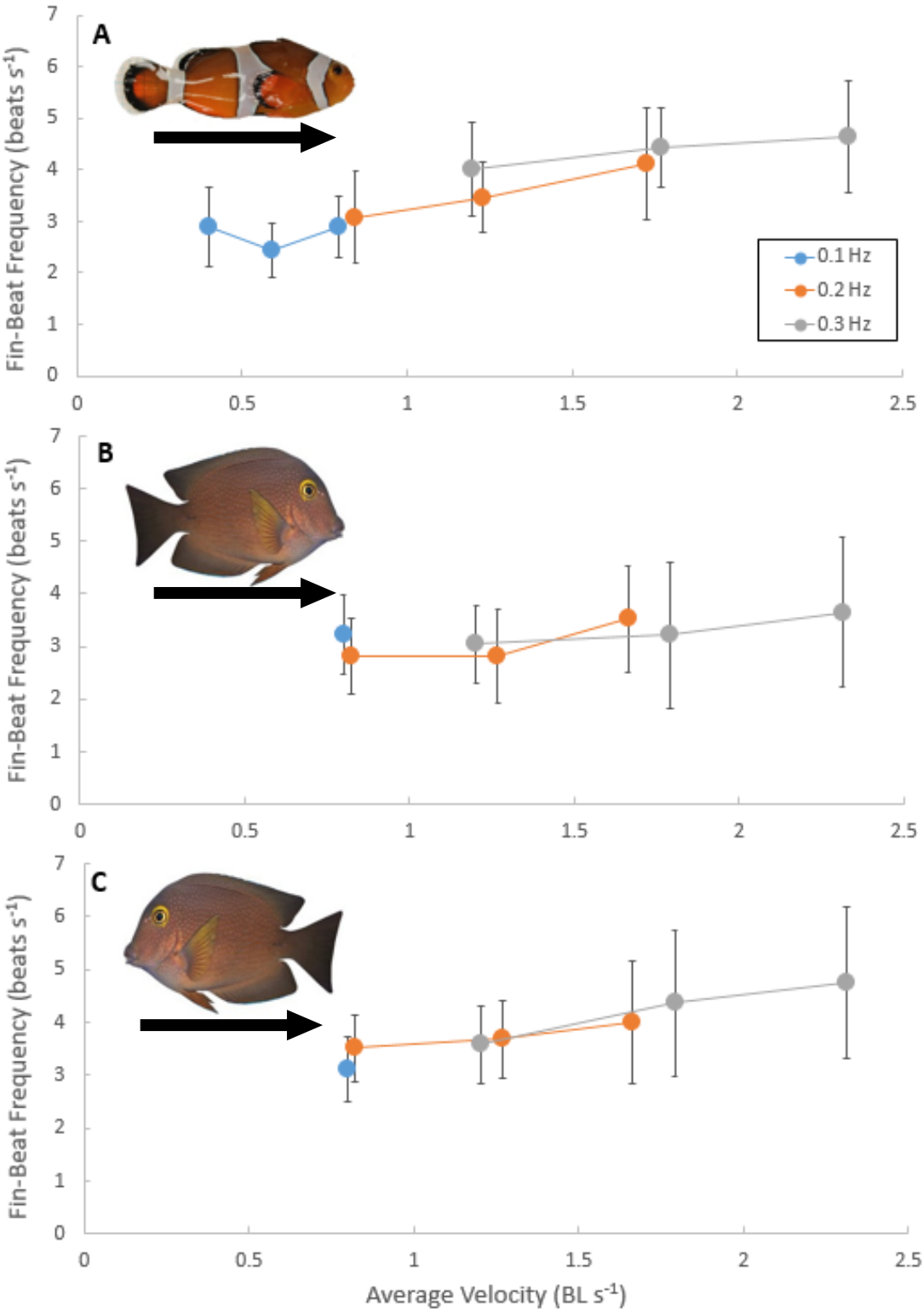

Figure 2.10. Average pectoral fin-beat frequency (beats s^{-1}) as a function of average swimming velocity during oscillatory swimming (reported relative to fish body length per second, BL s^{-1}) at

three frequencies of oscillation for **A.)** *Amphiprion ocellaris* swimming forward, **B.)** *Ctenochaetus strigosus* swimming forward, and **C.)** *C. strigosus* swimming in reverse. Error bars are the average of the standard deviations from each individual, to represent changes in variability of FPF during oscillatory swimming. No data exist at the two lowest average velocities for the 0.1 Hz frequency for *C. strigosus* due to erratic swimming of all individuals at these intensities.

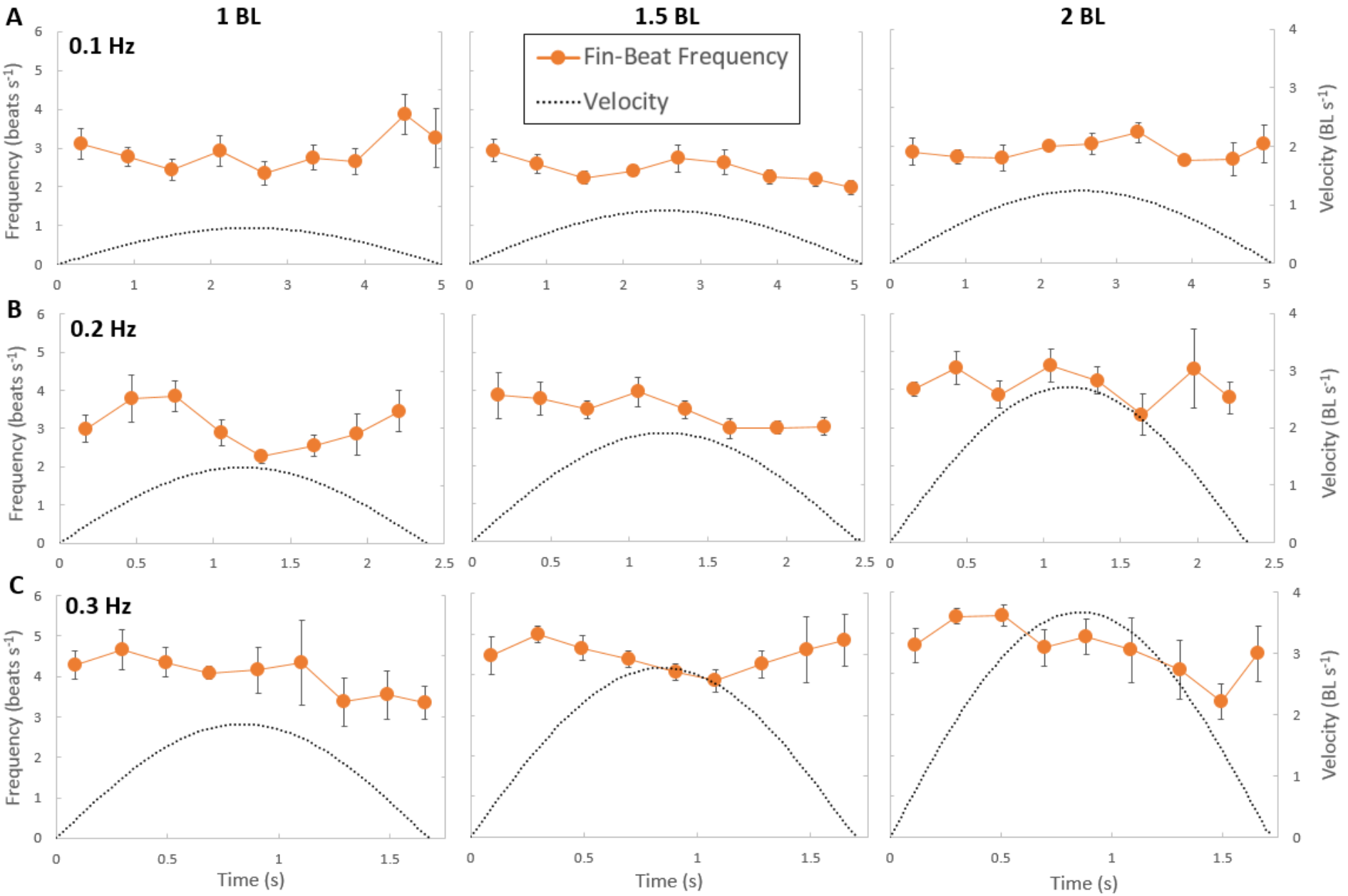
A
1 BL
1.5 BL
2 BL
0.1 Hz
Fin-Beat Frequency
Velocity
B
0.2 Hz
C
0.3 Hz
Frequency (beats s-1)
Velocity (BL s-1)
Time (s)

Figure 2.11. Fin-beat frequency (mean ± S.E.) as a function of time during one half cycle of oscillatory swimming for the Clown Anemonefish (*Amphiprion ocellaris*). Amplitude of displacement (reported relative to fish body length, BL) increases from 1 BL (**left column**), to 1.5 BL (**center column**), to 2 BL displacement (mean maximum displacement= 1.94 BL) (**right column**). Wave frequency increases from **A.)** 0.1 Hz, to **B.)** 0.2 Hz, to **C.)** 0.3 Hz. The dotted line indicates the instantaneous velocity (BL s^{-1}) of the shuttle moving in the SWMR apparatus.

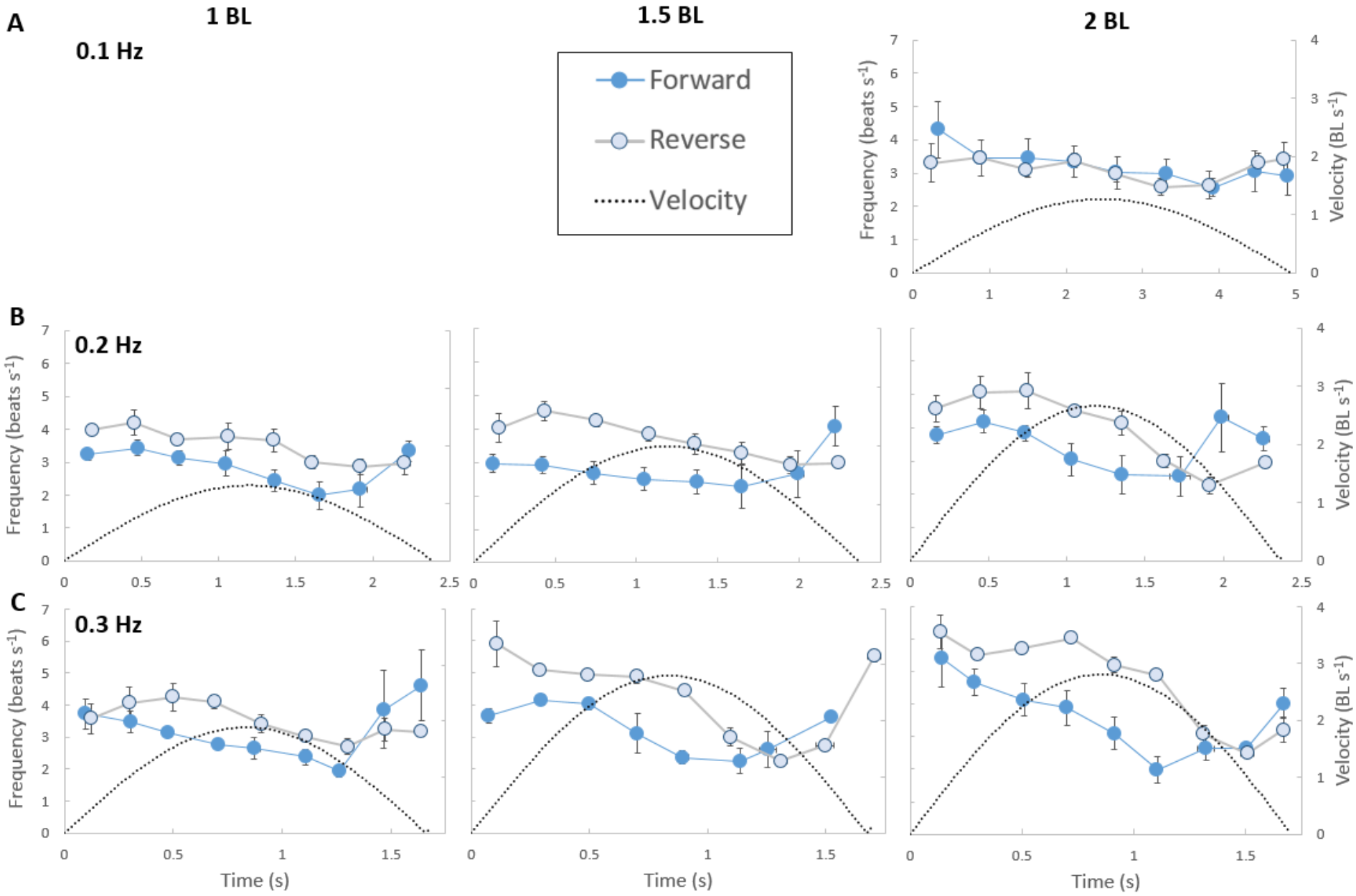
A
1 BL
1.5 BL
2 BL
0.1 Hz
Forward
Reverse
Velocity
Frequency (beats s-1)
Velocity (BL s-1)
B
0.2 Hz
C
0.3 Hz
Time (s)

Figure 2.12. Fin-beat frequency (mean ± S.E.) as a function of time during one half cycle of oscillatory swimming for the Goldring Surgeonfish (*Ctenochaetus strigosus*), for both forward swimming (dark blue) and swimming in reverse (light blue). Amplitude of displacement (reported relative to fish body length, BL) increase from 1 BL (**left column**), to 1.5 BL (**center column**), to 2 BL displacement (mean maximum displacement= 1.975 BL) (**right column**). Wave frequency increases from **A.)** 0.1 Hz to **B.)** 0.2 Hz, to **C.)** 0.3 Hz. The dotted line indicates the instantaneous velocity (BL s^{-1}) of the shuttle moving in the SWMR apparatus. All intensities for swimming forwards and in reverse showed a significant effect of time within the cycle (0.1 Hz, 2 BL- $F(7, 21)= 3.00$, $p= 0.024$; 0.2 Hz, 1 BL- $F(6, 18)= 4.37$, $p= 0.007$; 0.2 Hz, 1.5 BL- $F(5, 20)= 2.76$, $p= 0.013$; 0.2 Hz, 2 BL- $F(4, 16)= 7.80$, $p= 0.001$; 0.3 Hz, 1 BL- $F(5, 20)= 4.49$, $p= 0.007$; 0.3 Hz, 1.5 BL- $F(5, 20)= 9.72$, $p= 0.000$; 0.3 Hz, 2 BL- $F(4, 16)= 19.34$, $p= 0.000$). Direction of swimming had a significant effect on FBF at all intensities except for panel **A** (0.2 Hz, 1 BL- $F(1, 3)= 10.91$, $p= 0.046$; 0.2 Hz, 1.5 BL- $F(1, 4)= 17.91$, $p= 0.013$; 0.2 Hz, 2 BL- $F(1, 4)= 754.78$, $p= 0.002$; 0.3 Hz, 1 BL- $F(1, 4)= 9.99$, $p= 0.034$; 0.3 Hz, 1.5 BL- $F(1, 4)= 35.51$, $p= 0.004$; 0.3 Hz, 2 BL- $F(1, 4)= 22.71$, $p= 0.009$).

Appendix 1

Validation of the SWMR relative wave motion

Prior to running any experimental procedures in the SWMR, validation studies were conducted to ensure that flow in the respirometer was primarily laminar and relative water velocities matched the intended velocities of motion. Intended velocity was calculated from the equation:

$$\text{Intended velocity} = (\text{Max. velocity} * \sin(2\pi * \text{frequency} * \text{time}) + \pi)$$

Where:

$$\text{Maximum velocity} = \frac{2\pi * \text{amplitude}}{\text{period}}$$

To validate actual relative water velocity, the SWMR was filled with freshwater to which 0.08 g of neutrally-buoyant red fluorescent polyethylene microspheres (Cospheric, density = 1.005 g cc^{-1}, 212-215 μm diameter) were added. A sheet of green light was then projected downward along the center of the respirometry vessel via a 50 mW 523 nm laser with cylindrical lens to illuminate and induce fluorescence in the microspheres within a narrow, 1 mm wide sheet. The SWMR was then run through a series of movement cycles with increasing periods and amplitudes to simulate conditions in which experimental procedures would be run for a fish with a total length of 7.5 cm. One-minute digital video segments (1280 x 720 resolution at 120 fps) were taken during each cycle with a GoPro camera (GoPro Hero 3+ Black) that had been attached to a moving arm of the SWMR to record relative movement within the shuttle as it moved back and forth within the respirometry vessel. Video segments were then imported to GoPro Studio software (Version 2.5.4) to remove fish eye effects and converted to 20 second clips. The video segments were then imported to imaging software (Virtualdub 1.10.4) and

converted to image sequences to be analyzed through the particle tracking software MtrackJ (Version 1.5.0). Manual tracking of individual particles over at least three frames were used to calculate average relative particle velocities, and particle velocities in both the x (horizontal) and y (vertical) axes to insure that flow was laminar and matched intended velocities, the results of which can be seen in the following figures (A1.1-A1.9).

A1.1 Figures

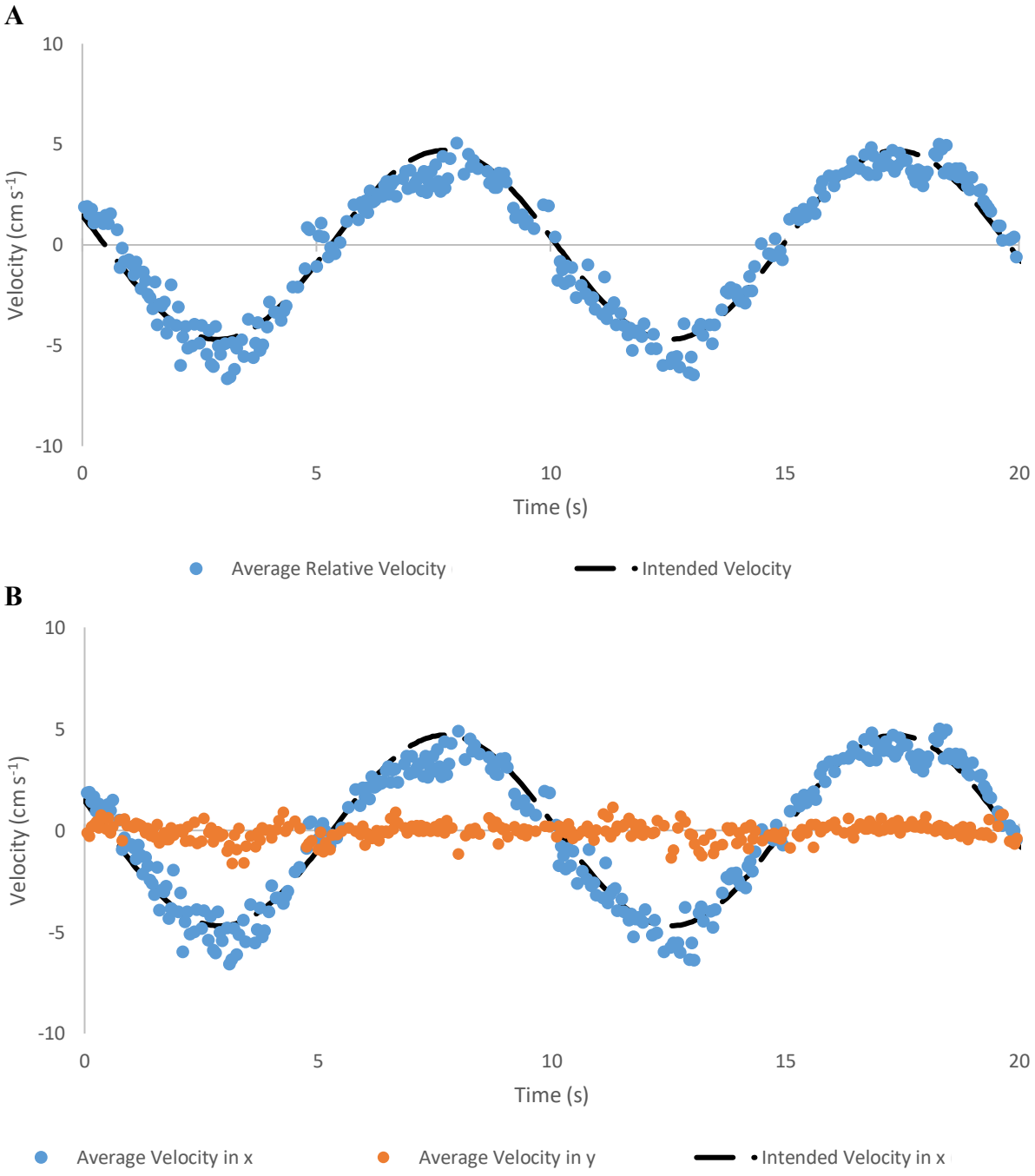

Figure A1.1. Average A.) relative velocity and B.) velocity in the x and y direction over a 20 second period of movement within the Simulated Wave Motion Respirometer (SWMR) at an amplitude of 7.5 cm and 0.1 Hz frequency. Velocities were calculated using particle tracking software (MTrackJ) where individual particles were manually tracked over a period of at least three frames. Each point represents the average velocity of a particle tracked over three particle tracking runs at the same amplitude and frequency. Intended velocities were calculated using the formula described in further detail in the previous SWMR Validation section.

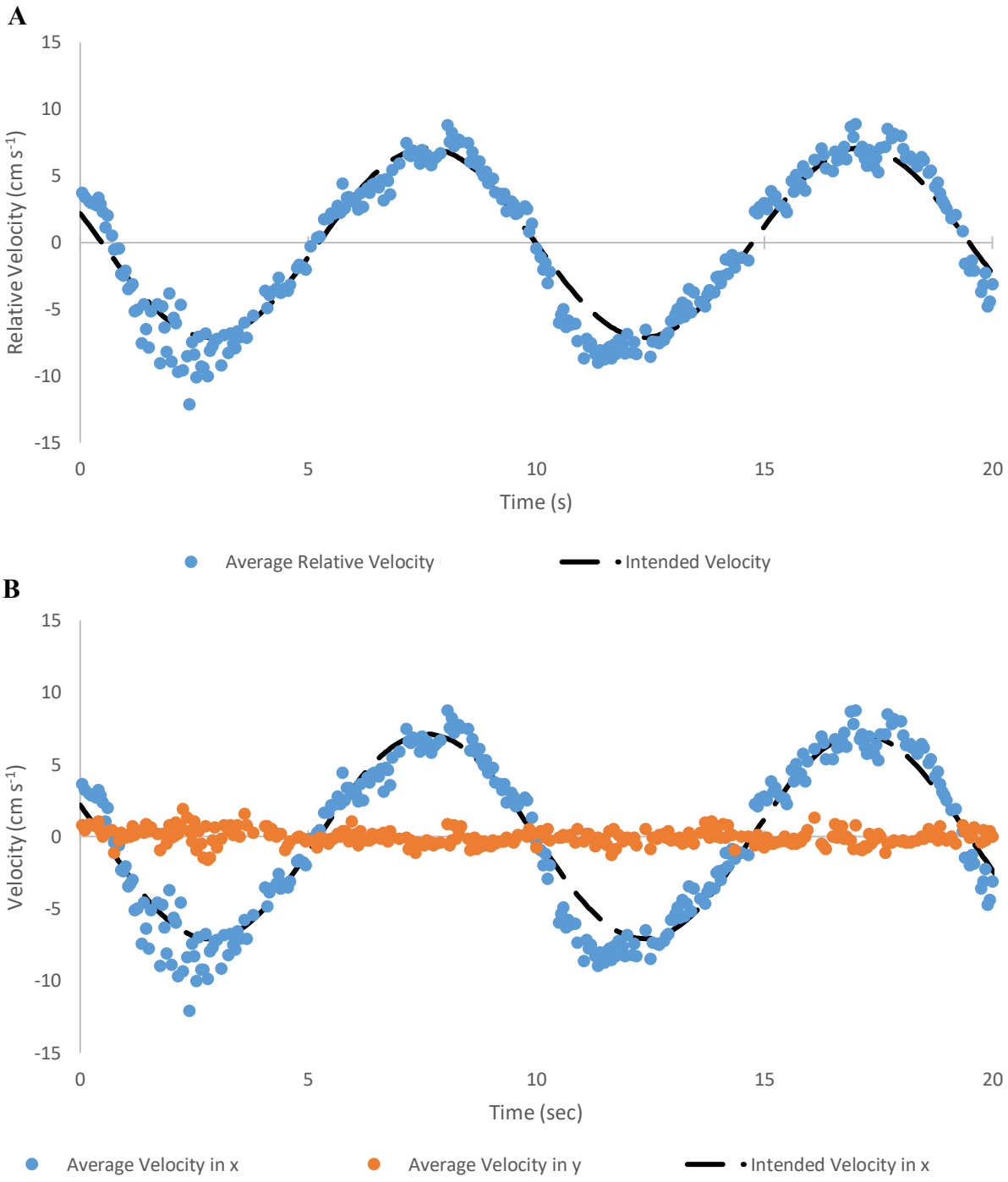

Figure A1.2. Average A.) relative velocity and B.) velocity in the x and y direction over a 20 second period of movement within the Simulated Wave Motion Respirometer (SWMR) at an amplitude of 11.3 cm and 0.1 Hz frequency. Velocities were calculated using particle tracking software (MTrackJ) where individual particles were manually tracked over a period of at least three frames. Each point represents the average velocity of a particle tracked over three particle tracking runs at the same amplitude and frequency. Intended velocities were calculated using the formula described in further detail in the previous SWMR Validation section.

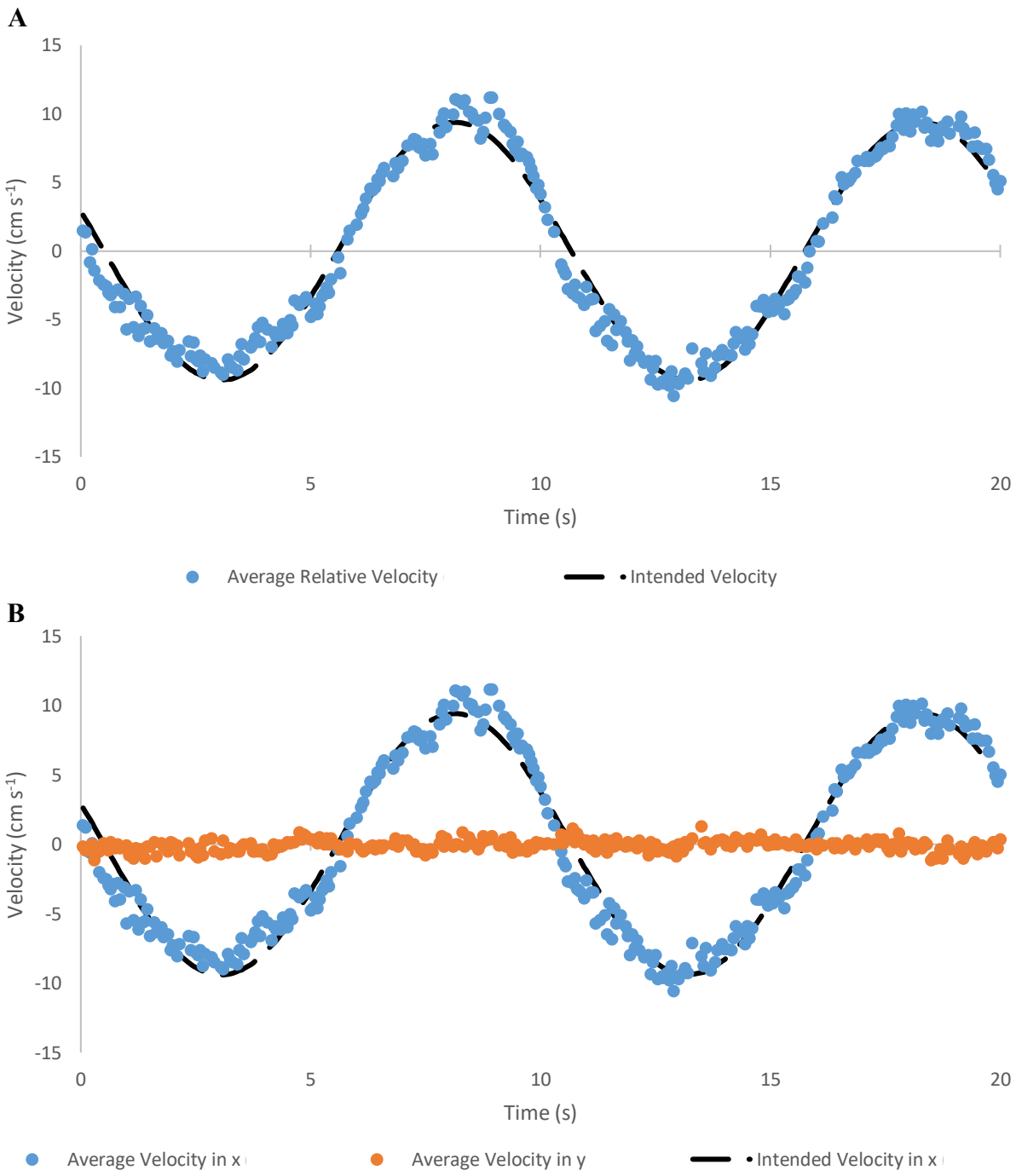

Figure A1.3. Average A.) relative velocity and B.) velocity in the x and y direction over a 20 second period of movement within the Simulated Wave Motion Respirometer (SWMR) at an amplitude of 15 cm and 0.1 Hz frequency. Velocities were calculated using particle tracking software (MTrackJ) where individual particles were manually tracked over a period of at least three frames. Each point represents the average velocity of a particle tracked over three particle tracking runs at the same amplitude and frequency. Intended velocities were calculated using the formula described in further detail in the previous SWMR Validation section.

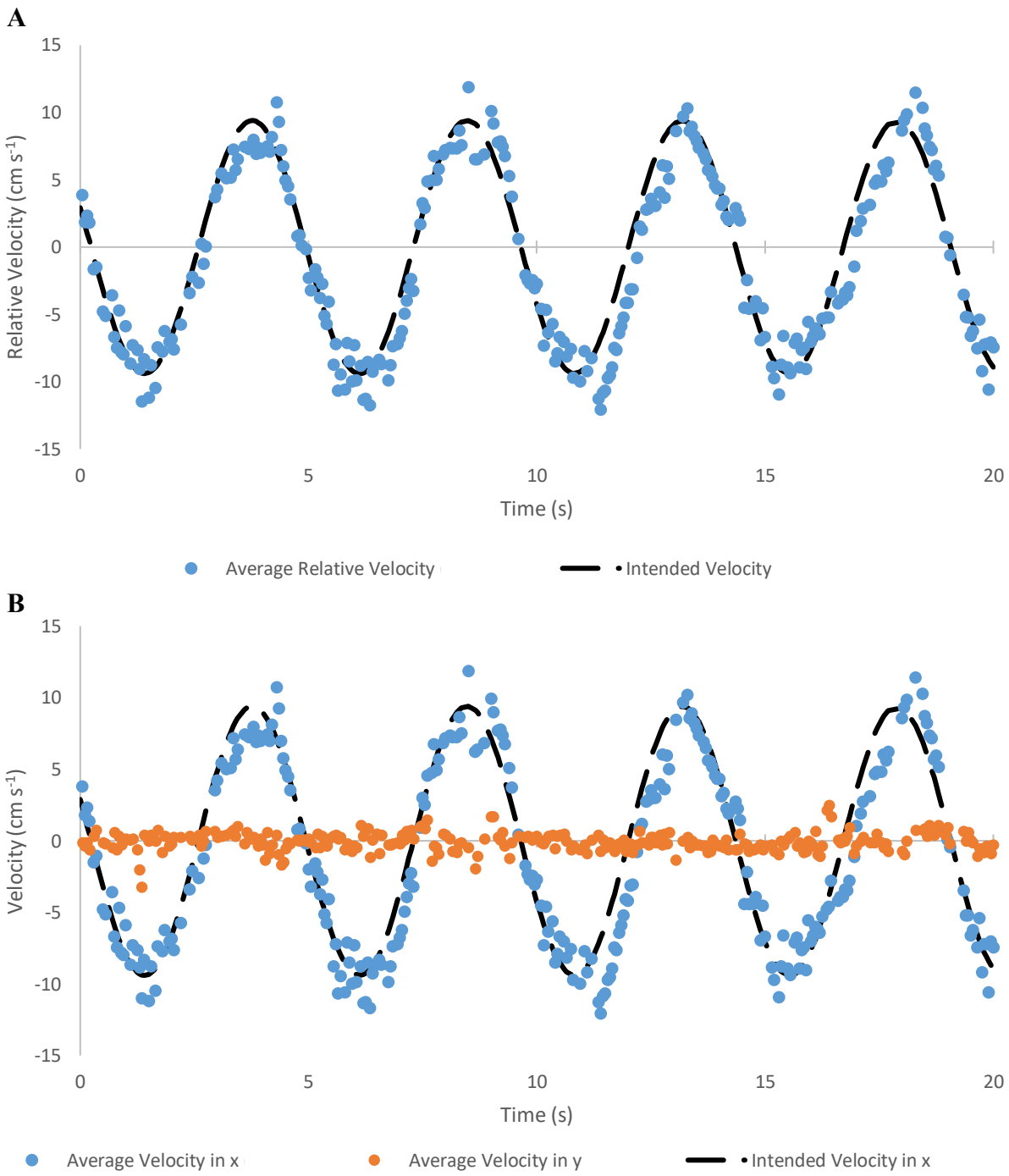

Figure A1.4. Average A.) relative velocity and B.) velocity in the x and y direction over a 20 second period of movement within the Simulated Wave Motion Respirometer (SWMR) at an amplitude of 7.5 cm and 0.2 Hz frequency. Velocities were calculated using particle tracking software (MTrackJ) where individual particles were manually tracked over a period of at least three frames. Each point represents the average velocity of a particle tracked over three particle tracking runs at the same amplitude and frequency. Intended velocities were calculated using the formula described in further detail in the previous SWMR Validation section.

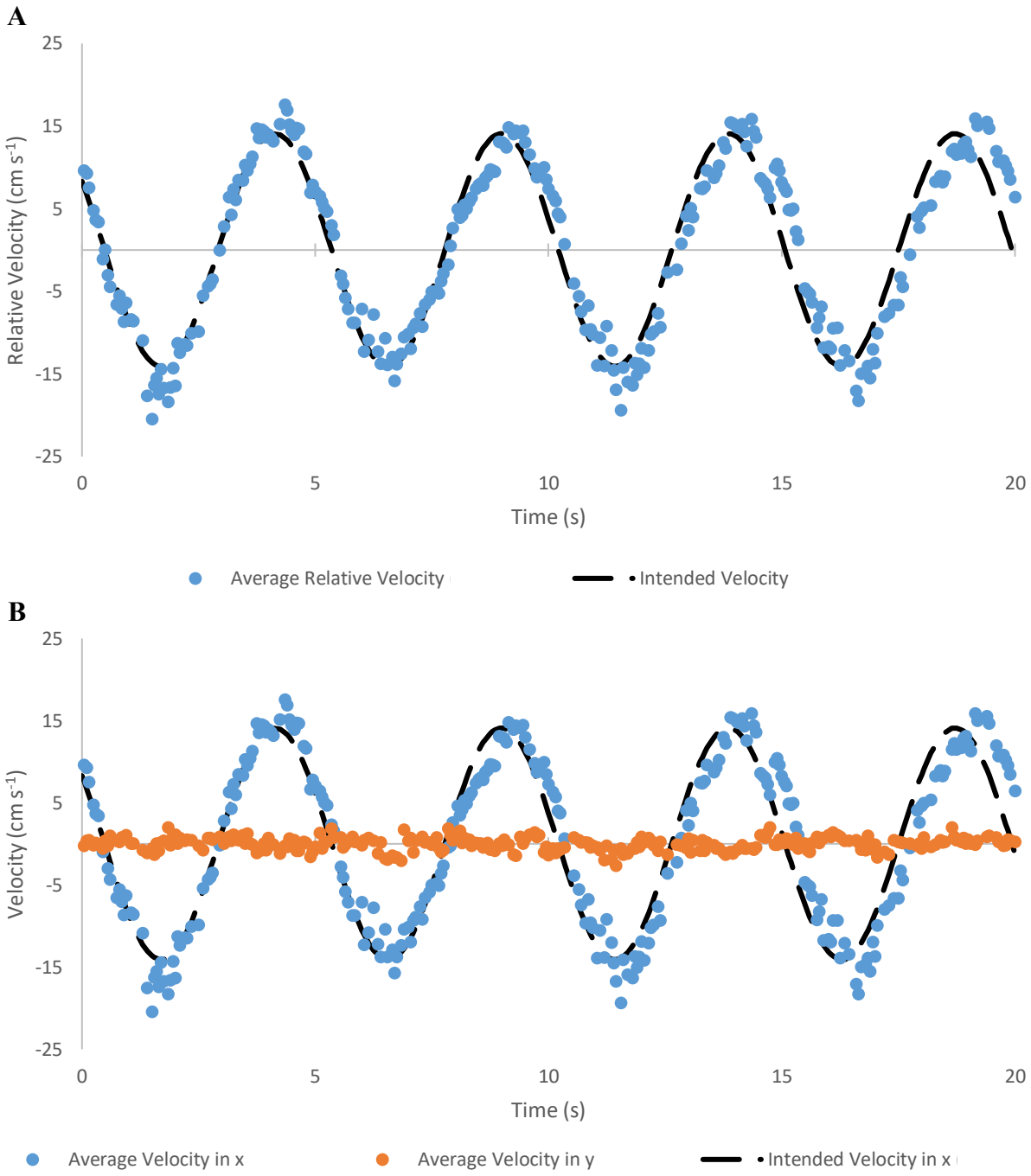

Figure A1.5. Average A.) relative velocity and B.) velocity in the x and y direction over a 20 second period of movement within the Simulated Wave Motion Respirometer (SWMR) at an amplitude of 11.3 cm and 0.2 Hz frequency. Velocities were calculated using particle tracking software (MTrackJ) where individual particles were manually tracked over a period of at least three frames. Each point represents the average velocity of a particle tracked over three particle tracking runs at the same amplitude and frequency. Intended velocities were calculated using the formula described in further detail in the previous SWMR Validation section.

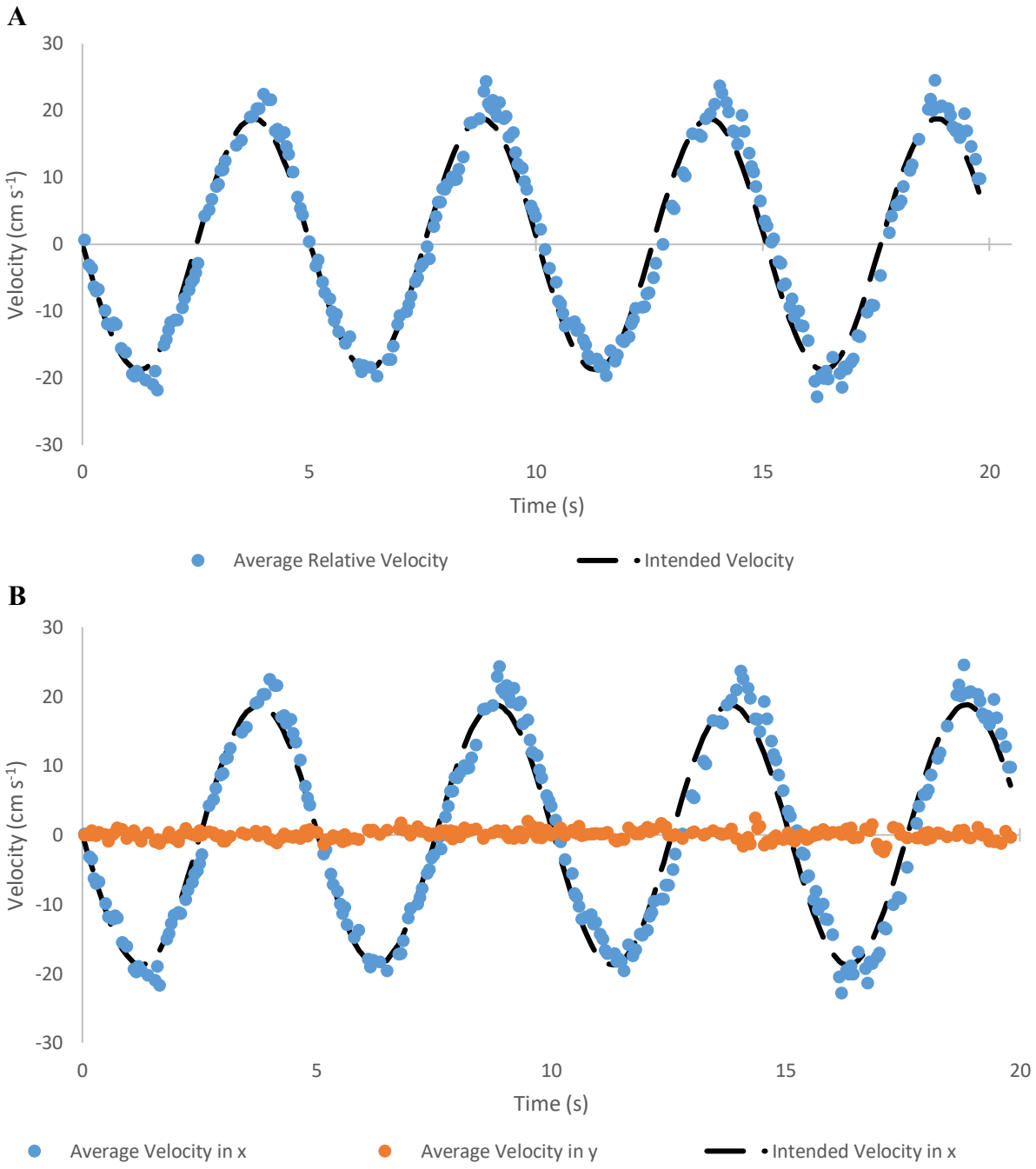

Figure A1.6. Average A.) relative velocity and B.) velocity in the x and y direction over a 20 second period of movement within the Simulated Wave Motion Respirometer (SWMR) at an amplitude of 15 cm and 0.2 Hz frequency. Velocities were calculated using particle tracking software (MTrackJ) where individual particles were manually tracked over a period of at least three frames. Each point represents the average velocity of a particle tracked over three particle tracking runs at the same amplitude and frequency. Intended velocities were calculated using the formula described in further detail in the previous SWMR Validation section.

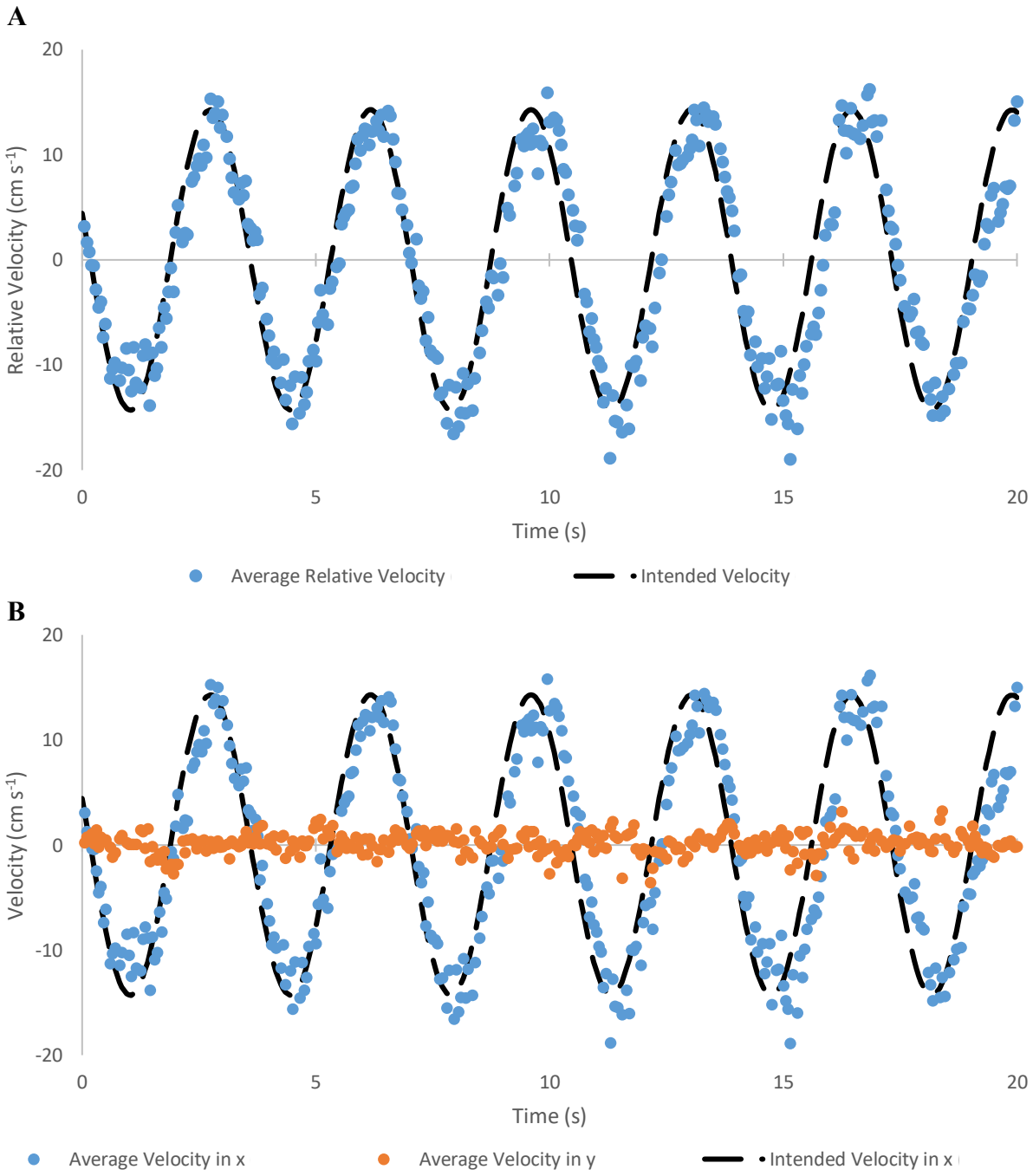

Figure A1.7. Average A.) relative velocity and B.) velocity in the x and y direction over a 20 second period of movement within the Simulated Wave Motion Respirometer (SWMR) at an amplitude of 7.5 cm and 0.3 Hz frequency. Velocities were calculated using particle tracking software (MTrackJ) where individual particles were manually tracked over a period of at least three frames. Each point represents the average velocity of a particle tracked over at least two particle tracking runs at the same amplitude and frequency. Intended velocities were calculated using the formula described in further detail in the previous SWMR Validation section.

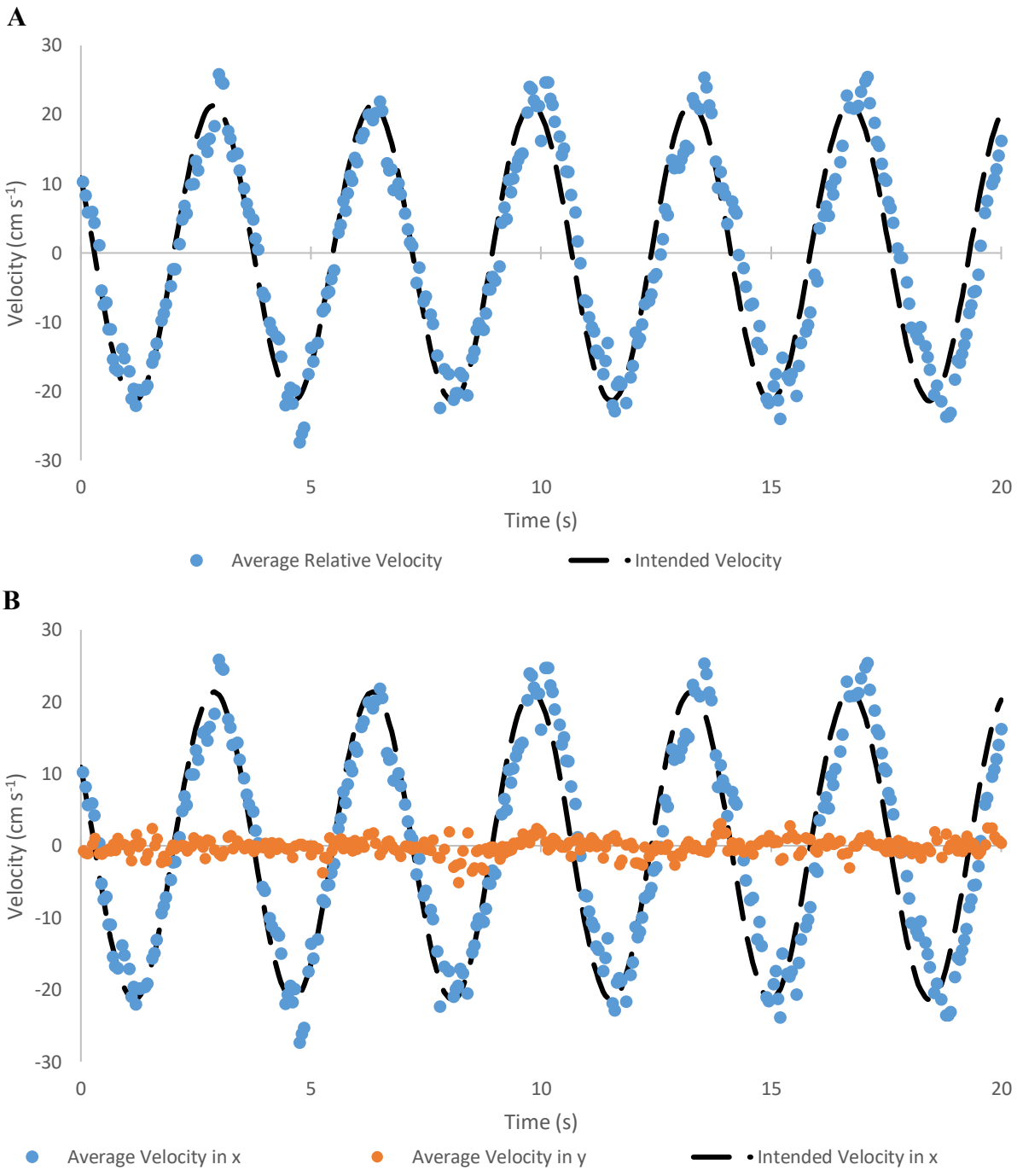

Figure A1.8. Average A.) relative velocity and B.) velocity in the x and y direction over a 20 second period of movement within the Simulated Wave Motion Respirometer (SWMR) at an amplitude of 11.3 cm and 0.3 Hz frequency. Velocities were calculated using particle tracking software (MTrackJ) where individual particles were manually tracked over a period of at least three frames. Each point represents the average velocity of a particle tracked over at least two particle tracking runs at the same amplitude and frequency. Intended velocities were calculated using the formula described in further detail in the previous SWMR Validation section.

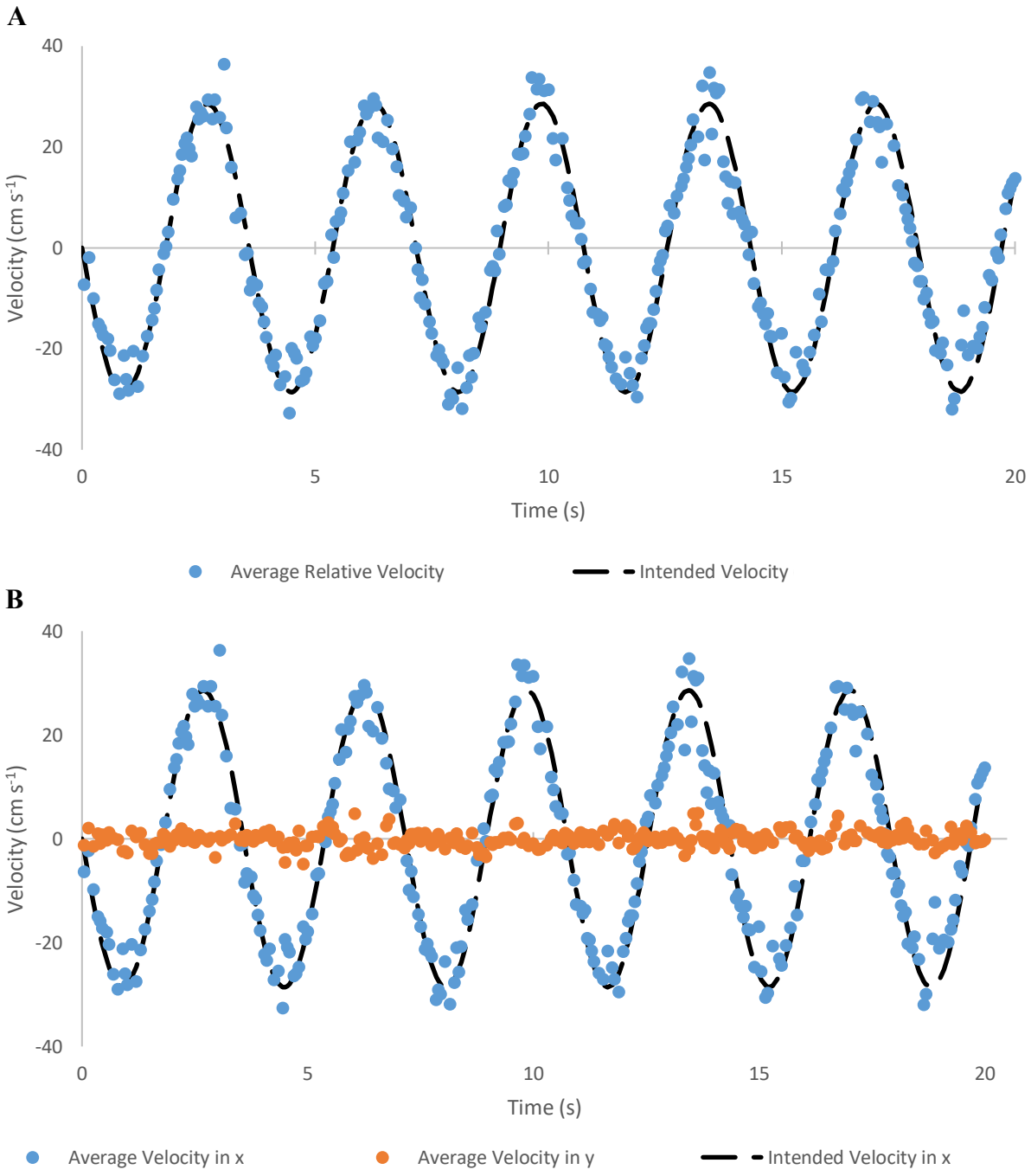

Figure A1.9. Average A.) relative velocity and B.) velocity in the x and y direction over a 20 second period of movement within the Simulated Wave Motion Respirometer (SWMR) at an amplitude of 15 cm and 0.3 Hz frequency. Velocities were calculated using particle tracking software (MTrackJ) where individual particles were manually tracked over a period of at least three frames. Each point represents the average velocity of a particle tracked over at least two particle tracking runs at the same amplitude and frequency. Intended velocities were calculated using the formula described in further detail in the previous SWMR Validation section.

Appendix 2

SWMR–Flume Respirometer Comparison

In order to further examine metabolic rates and swimming kinematics of fishes swum in the simulated wave motion respirometer (SWMR), a comparison test was run using the same individual fish in both the SWMR and in a Steffensen-type recirculating flume respirometer with bi-directional flow. The individual used was a labriform swimmer, the Goldring Surgeonfish, *Ctenochaetus strigosus* (TL= 8.2 cm, mass= 10.1 g). The individual was first swum through the SWMR apparatus according to procedures described previously (Section *2.2.4*). After allowing the fish to recover for one week, the same individual was tested again using bi-directional flow through the Steffensen-type recirculating flume respirometer. The data from these tests were analyzed for metabolic rate, fin-beat frequency, and percent changing direction in similar fashion also described previously (Section *2.2.5*).

The 8.4 L Steffensen-type flume respirometer was composed of a 9x26x10 cm (width x length x depth) swimming section with baffle screens, deflectors, and honey-comb flow straighteners both in front and behind the swimming section to create rectilinear, microturbulent flow in the working section (modified from Roche et al. 2014). A 45 L, flow-through sump tank (27-28° C) outside of the respirometer was used to moderate temperature fluctuations and to pump clean, aerated seawater into the water bath containing the flume, and water returned by a gravity fed overflow. Intermittent respirometry was used to flush out deoxygenated water from the respirometer via a computer-actuated pump and replace it with water from the surrounding bath. This flushing cycle occurred for a period of 4 minutes, followed by a one minute mixing period, then a 7 minute recording period where the decline in oxygen content of the water was recorded and relayed to a computer. Water oxygen content was measured by a fiberoptic optical

oxygen probe (PreSens Fibox 3, Regensburg, Germany) placed in the respirometer where seawater is continuously passed over the electrode. Data recording and activation of the flushing periods were controlled via AquaResp program (Loligo Systems, Cogenhagen, Denmark).

Flow within the respirometer was induced by a motor-driven propeller, controlled via computer using LabVIEW 2014 (National Instruments Inc., Austin, TX) to adjust voltage to the motor in a sinusoidal fashion. This created bi-directional, oscillatory flow where halfway through the cycle, the propeller, stopped and changed direction, altering the flow direction. Flow velocity calibrations were measured using particle tracking (see Appendix 1) and used to calculate adjusted voltages to cause the motor to reach the desired water velocities. Particle tracking was conducted for forward water flow (Fig. A2.1-A2.4), backwards water flow (Fig. A2.5-A2.9), and bidirectional water flow (Fig. A2.10-A2.21). Because the propeller was moving a large volume of water over short frequencies, there was a time offset of water changing direction, causing water to not reach maximum intended velocities according to voltage calibrations made in unidirectional flow. Using the oscillatory flow particle tracking data, voltage offsets were calculated to adjust for this effect, allowing the water to reach maximum intended velocities during oscillatory flow experiments.

The fish was placed in the flume respirometer the day before testing to acclimate to its environment overnight. During this time period, low unidirectional water flow (0.5 BL s^{-1}) was generated in the flume at a speed sufficient to keep the water mixed, but not high enough to induce swimming. Oxygen consumption was recorded overnight in order to calculate standard metabolic rate. The following day, the fish was run through the same procedure as described for the SWMR apparatus (Section *2.2.4*) in the flume respirometer using the calibrated offsets to generate similar water intensity parameters (amplitude, frequency, average/max velocity).

Oxygen consumption levels were measured before and after experimental procedure in the empty respirometer to calculate background levels of microbial respiration that were used to adjust oxygen consumption rates during experimental testing.

A2.1 Oxygen Consumption

In the SWMR apparatus, total metabolic rate of the fish ranged from 230-380 $mgO_2\ kg^{-1}\ h^{-1}$ (NCOS, 0-160 $mgO_2\ kg^{-1}\ h^{-1}$), nearly $1/4^{th}$ lower than the mean total metabolic rate and nearly half the mean NCOS measured for the other five *C. strigosus* (300-450 $mgO_2\ kg^{-1}\ h^{-1}$; NCOS, 0-280 $mgO_2\ kg^{-1}\ h^{-1}$, Fig. A2.22). Metabolic rate data from the fish swimming in the Steffensen-type flume respirometer was inconclusive due to the small mass of the fish (10.1 g) in a large respirometer (8.4 L) masking the effect of oxygen decline in the respirometer. Though no direct comparisons could be made between the metabolic rates of the fish, swimming kinematics were measured and examined to assess differences in swimming performance between the two apparatuses.

A2.2 Percent Turning

Similar to the other *C. strigosus* in the SWMR, the individual did not swim well (erratic swimming, biting glass, attempting to escape) at the lower amplitudes of the lowest frequency (0.1 Hz) in both the SWMR and the flume respirometer (Fig. A2.23). In the flume respirometer, as amplitude increased within the 0.2 Hz and 0.3 Hz frequency, percent turning decreased with each increase in amplitude, showing that as the distance the fish needed to travel each cycle increased, the more likely the fish was to swim in reverse. In the SWMR, however, at the highest

and lowest amplitudes within both the 0.2 Hz and 0.3 Hz frequency, percent turning remained under 6%, but at the middle amplitude (1.5 BL) at both frequencies, percent turning increased to just under 20%. While the comparison of percent turning is inconclusive at the lower frequency, as frequency and amplitude increased, the individual performed a majority of swimming in reverse, keeping the percent turning under 30% in both the SWMR and the flume respirometer. This relationship suggests that as frequency and amplitude increase, *C. strigosus* prefers to swim in reverse to cope with increased energy expenditure of changing direction every time the flow reverses, regardless of apparatus and physical space constraints.

A2.3 Fin-Beat Frequency

In both the SWMR and the flume respirometer, similar patterns of fin-beat frequency were seen, regardless of the fish swimming in reverse or swimming forward. In general, while the fish were swimming forward, fin-beat frequency remained relatively stable, with variation within each time point and also between points, with little discerning trend of increasing or decreasing fin-beat frequency (Fig. A2.24 and Fig. A2.25). A common characteristic of swimming forward seen in both the SWMR and the flume respirometer is an increase in fin-beat frequency at the end of the cycle (seen in the last one or two time points, especially at the higher frequencies and amplitudes). This may be due to the increase in fin-beats used for deceleration and/or increased activity due to turning around. While swimming in reverse, fin-beat frequencies were much more similar between apparatuses, with less variation between time points (Fig. A2.24 and Fig. A2.26). Swimming in reverse, appeared to begin at an elevated fin-beat frequency and decline throughout the cycle until nearing the end of the cycle where fin-beat frequency slightly increased, and this was especially pronounced at the higher frequency at all

amplitudes. This pattern may be indicative of a burst-and-coast strategy where the fish increases fin-beat frequency to accelerate following a change in water flow direction, then coast, decreasing fin-beat frequency, until the fins are again needed to decelerate similar to swimming the in the forward direction. This trend was seen in both the SWMR and the flume respirometer.

Though similar trends were seen between the two apparatuses, fin-beat frequency seemed to be slightly lower in the flume respirometer compared with the SWMR (Fig. A2.24-26). Observed both in the forward and reverse direction, fin-beat frequency was lower in the flume than it was in the SWMR, though more distinct in reverse swimming. This pattern may have emerged due to the increased physical space in which the fish was allowed to drift in the flume vs. the SWMR. While the increased volume may not have had a large impact on percent changing direction of this fish, the fish was observed to drift with the water flow much more than what was seen in the SWMR, reducing the fin-beat frequency by not forcing the fish to remain stationary in reference to a certain point in the respirometer.

A2.4 SWMR-Flume Respirometer

Both the simulated wave motion respirometer and the Steffensen-type flume respirometer provide unique ways to investigate the effects of bi-directional, oscillatory flow on the metabolic demands of fishes, similar to conditions seen in the wild. The larger ratio of fish mass to respirometer volume in the SWMR allows that system to better measure oxygen consumption rates, however, comparisons of swimming kinematics highlight the similarities of fish behavior between the two systems, and possible advantages of one system over another. While the flume respirometer may represent more realistic environmental conditions for smaller fish (larger

space, i.e. more room to maneuver similar to what is seen on the reef), this size flume can only be used for larger fish than what was examined in this study. The SWMR, however, is more accurate in examining the metabolic rate of smaller fishes and provides more control for examining swimming kinematics as a function of their environmental conditions.

A2.5 Figures

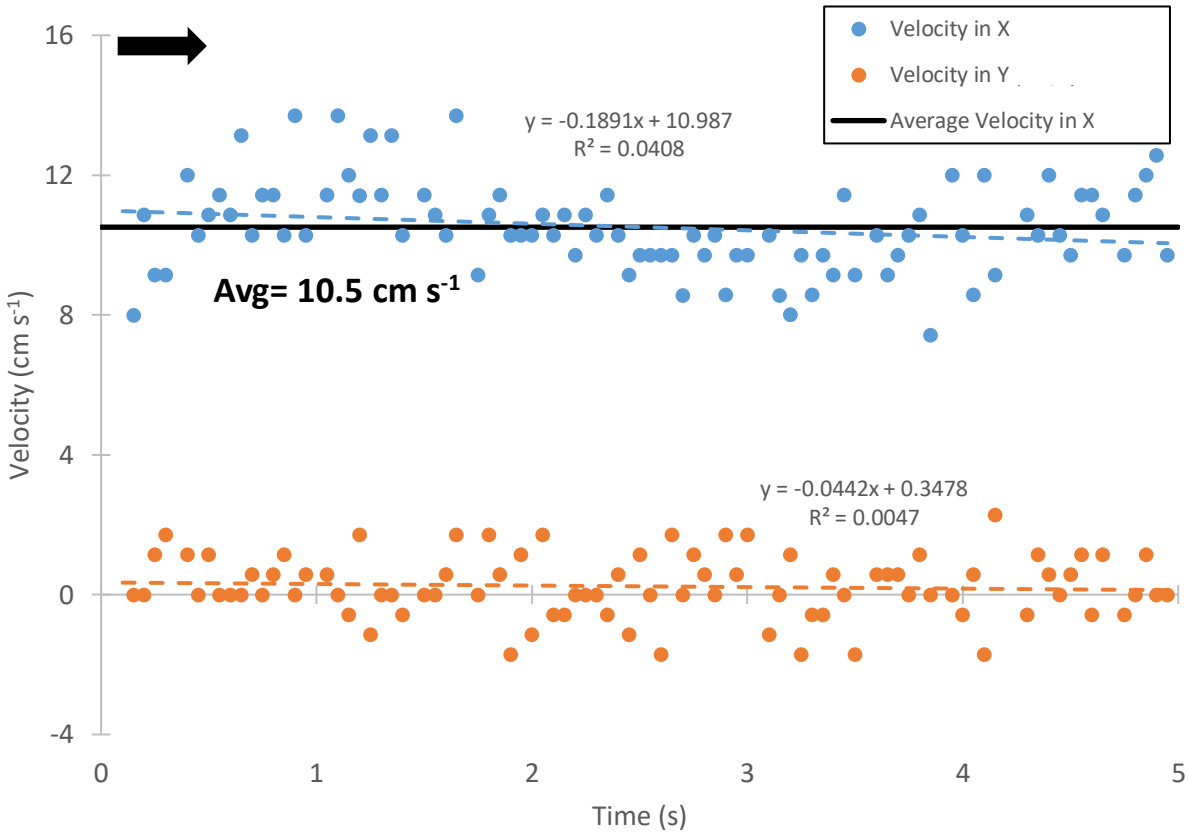

Figure A2.1. Average water velocity in the x and y direction over a 5 second time period of forward water circulation at an intended velocity of 9.0 cm s^{-1} within the flume respirometer. Velocities were calculated using particle tracking software (MTrackJ) where individual particles were manually tracked over a period of at least three frames. Each point represents the instantaneous velocity of a single particle moving in the respirometer. The average water velocity for the measurement time was 10.5 cm s^{-1}.

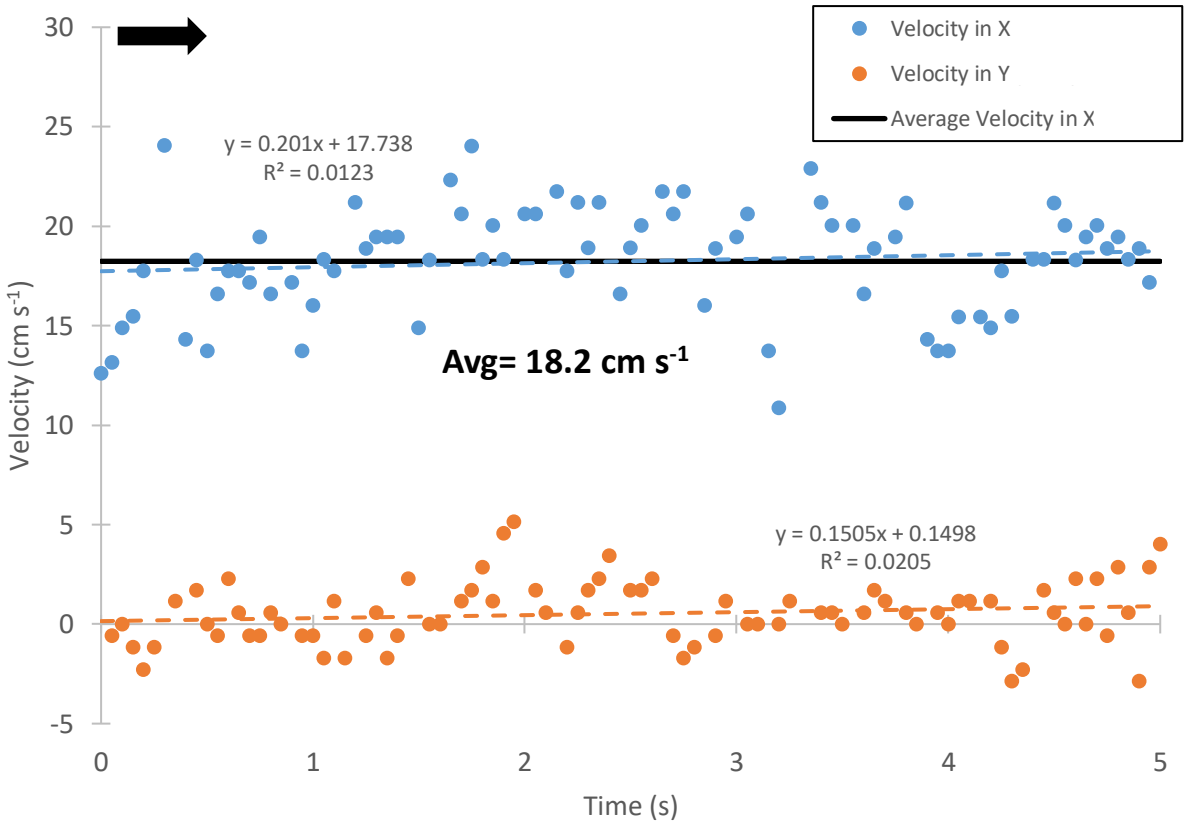

Figure A2.2. Average water velocity in the x and y direction over a 5 second time period of forward water circulation at an intended velocity of 17.0 cm s^{-1} within the flume respirometer. Velocities were calculated using particle tracking software (MTrackJ) where individual particles were manually tracked over a period of at least three frames. Each point represents the instantaneous velocity of a single particle moving in the respirometer. The average water velocity for the measurement time was 18.2 cm s^{-1}.

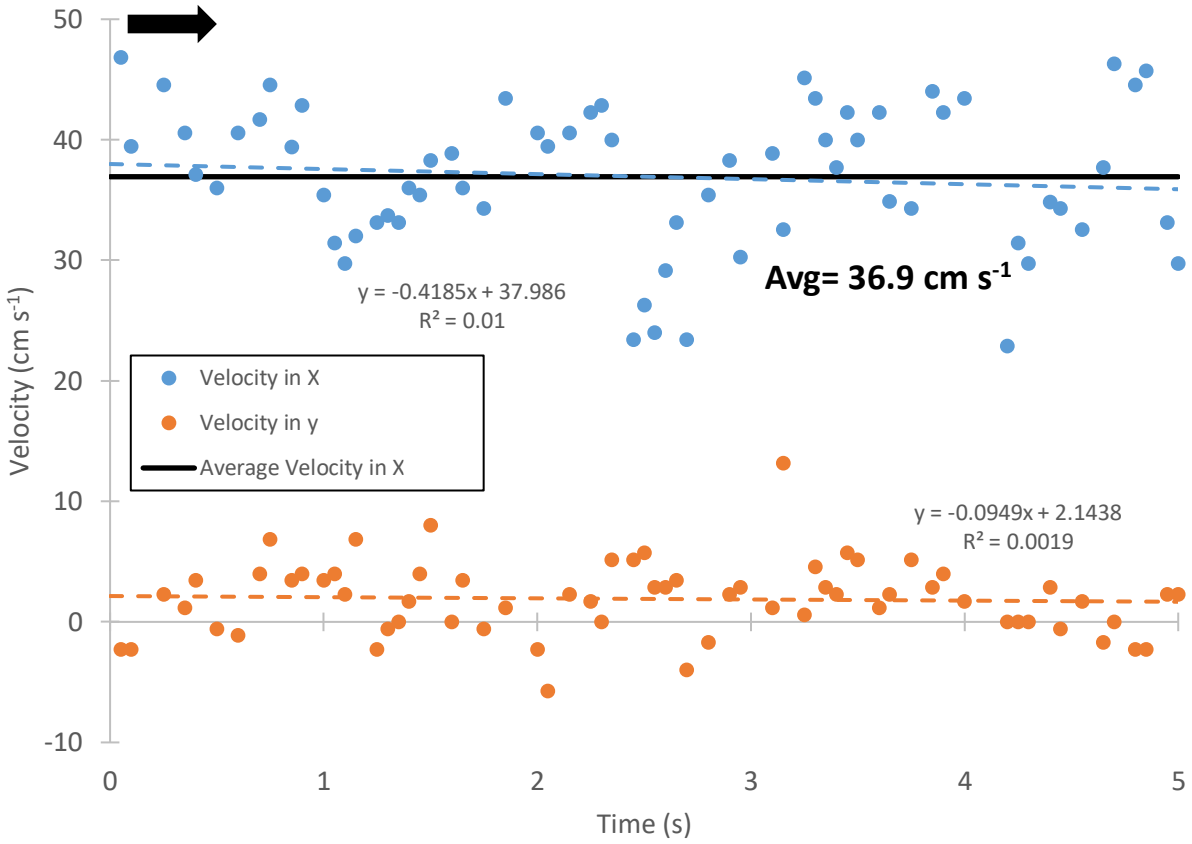

Figure A2.3. Average water velocity in the x and y direction over a 5 second time period of forward water circulation at an intended velocity of 36.0 cm s^{-1} within the flume respirometer. Velocities were calculated using particle tracking software (MTrackJ) where individual particles were manually tracked over a period of at least three frames. Each point represents the instantaneous velocity of a single particle moving in the respirometer. The average water velocity for the measurement time was 36.9 cm s^{-1}.

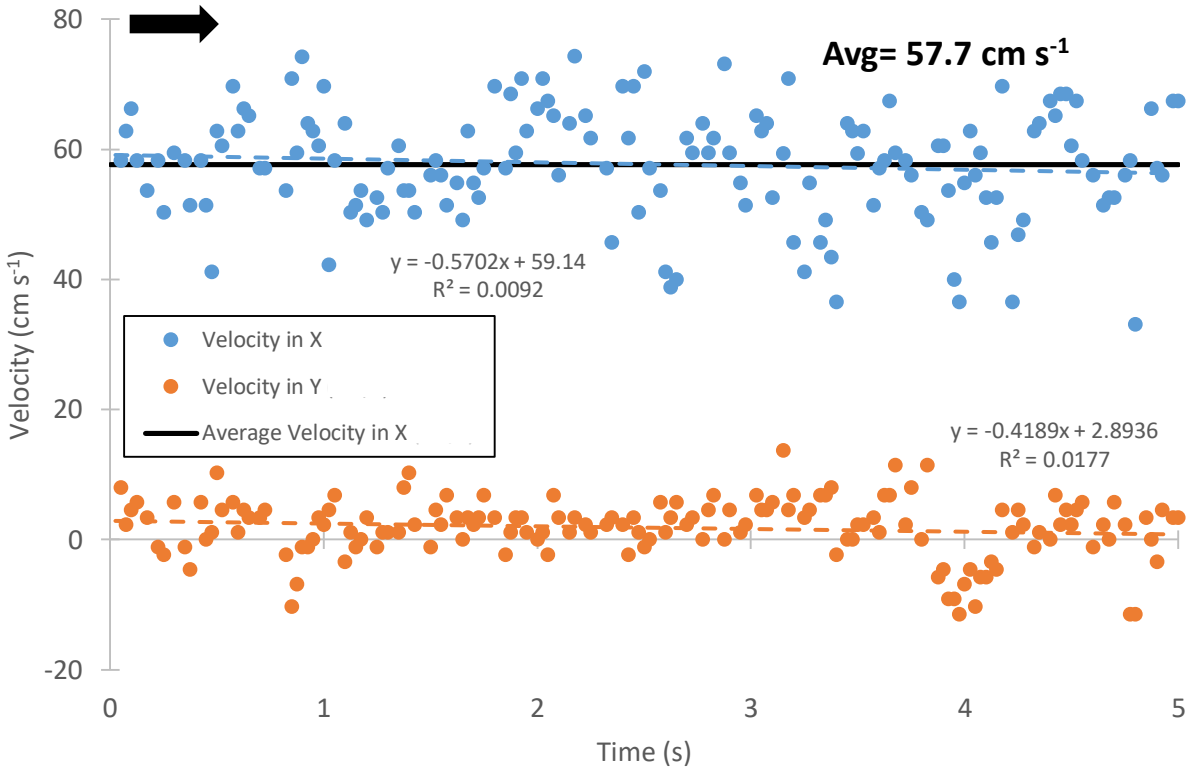

Figure A2.4. Average water velocity in the x and y direction over a 5 second time period of forward water circulation at an intended velocity of 55.0 cm s^{-1} within the flume respirometer. Velocities were calculated using particle tracking software (MTrackJ) where individual particles were manually tracked over a period of at least three frames. Each point represents the instantaneous velocity of a single particle moving in the respirometer. The average water velocity for the measurement time was 57.7 cm s^{-1}.

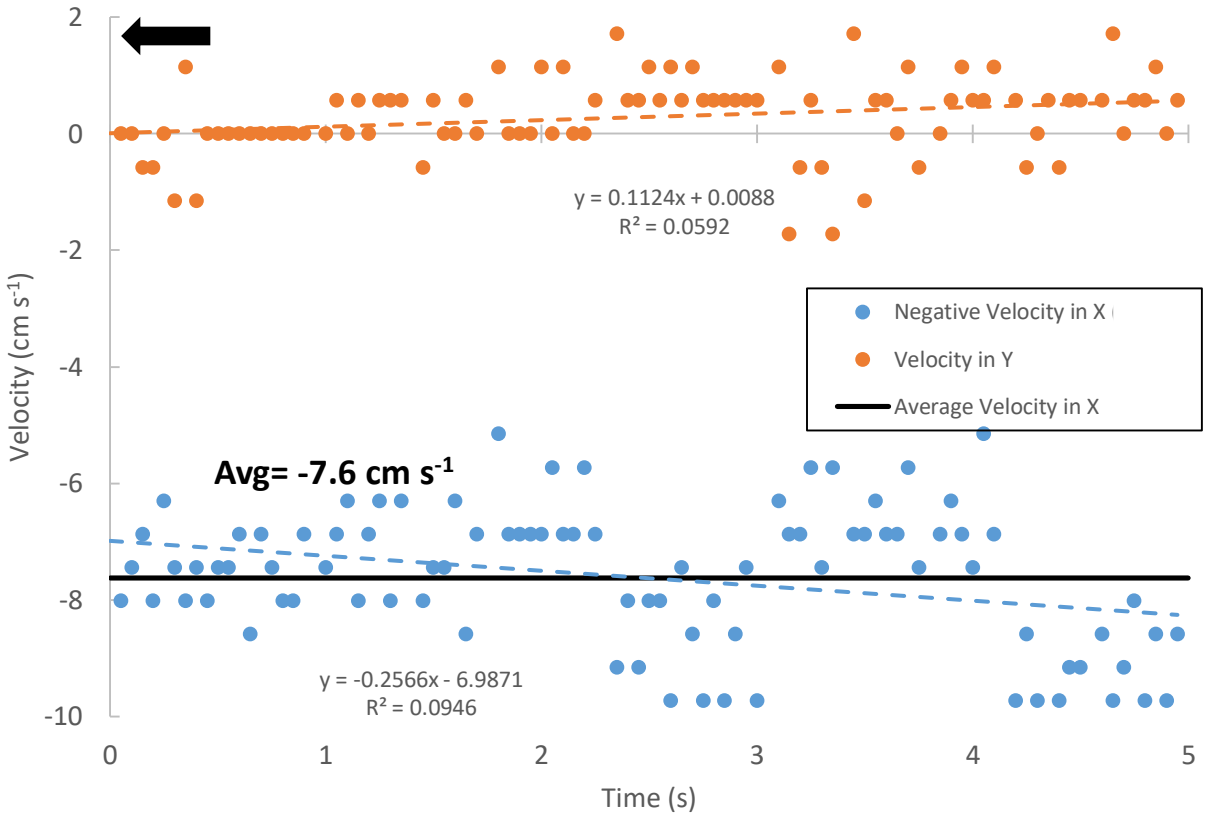

Figure A2.5. Average water velocity in the x and y direction over a 5 second time period of backward water circulation at an intended velocity of -7.0 cm s^{-1} within the flume respirometer. Velocities were calculated using particle tracking software (MTrackJ) where individual particles were manually tracked over a period of at least three frames. Each point represents the instantaneous velocity of a single particle moving in the respirometer. The average water velocity for the measurement time was -7.6 cm s^{-1}.

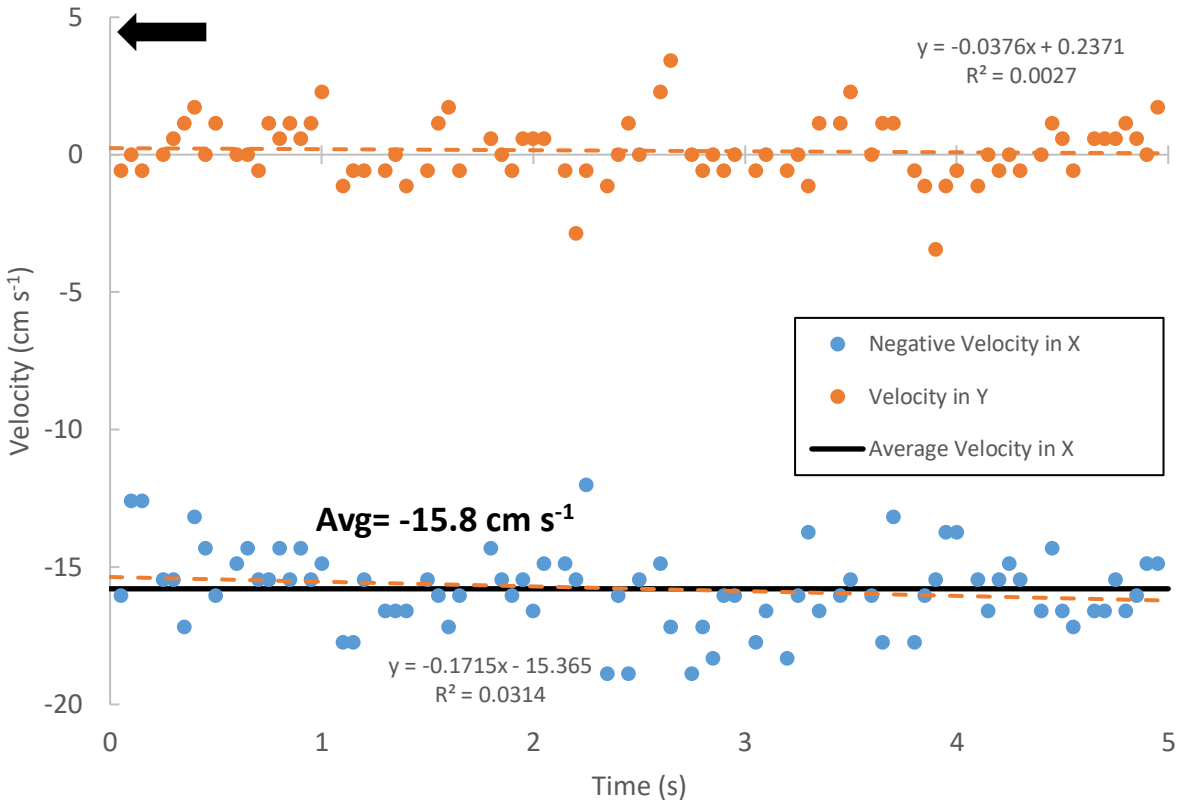

Figure A2.6. Average water velocity in the x and y direction over a 5 second time period of backward water circulation at an intended velocity of -14.5 cm s^{-1} within the flume respirometer. Velocities were calculated using particle tracking software (MTrackJ) where individual particles were manually tracked over a period of at least three frames. Each point represents the instantaneous velocity of a single particle moving in the respirometer. The average water velocity for the measurement time was -15.8 cm s^{-1}.

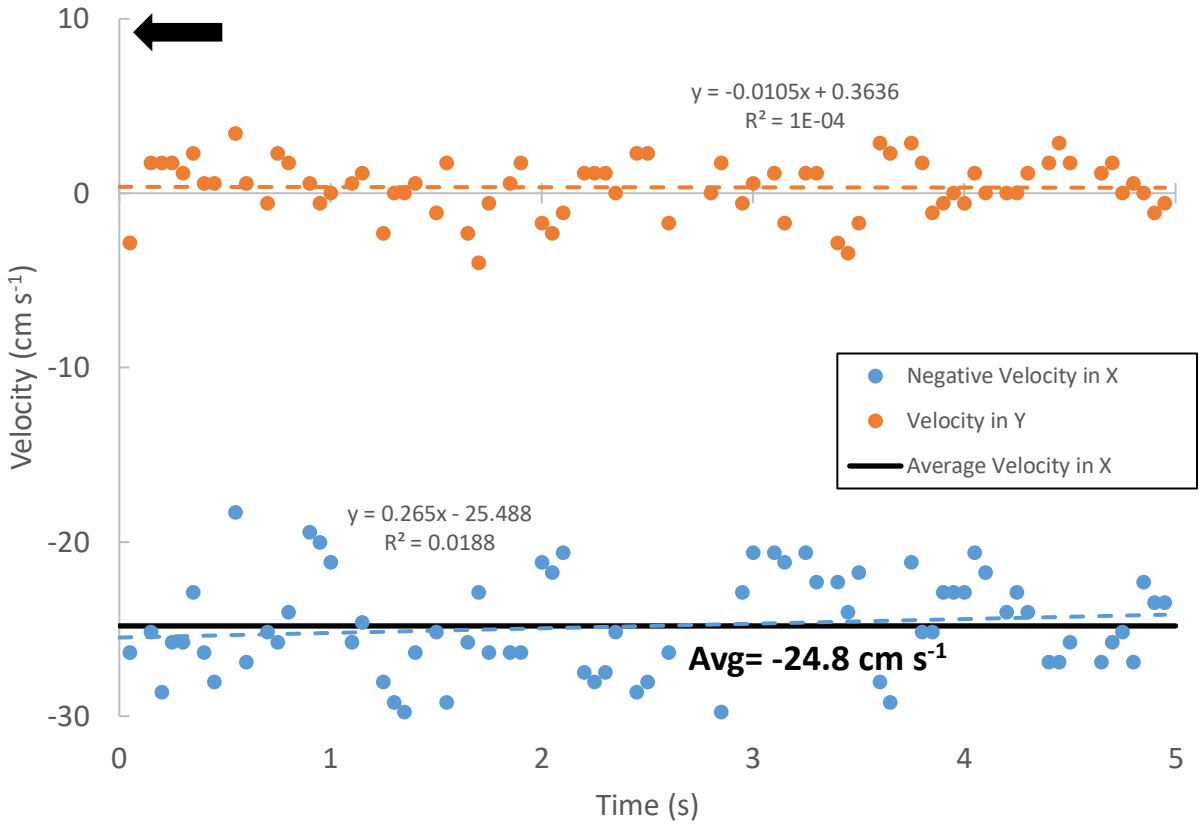

Figure A2.7. Average water velocity in the x and y direction over a 5 second time period of backward water circulation at an intended velocity of -25.0 cm s^{-1} within the flume respirometer. Velocities were calculated using particle tracking software (MTrackJ) where individual particles were manually tracked over a period of at least three frames. Each point represents the instantaneous velocity of a single particle moving in the respirometer. The average water velocity for the measurement time was -24.8 cm s^{-1}.

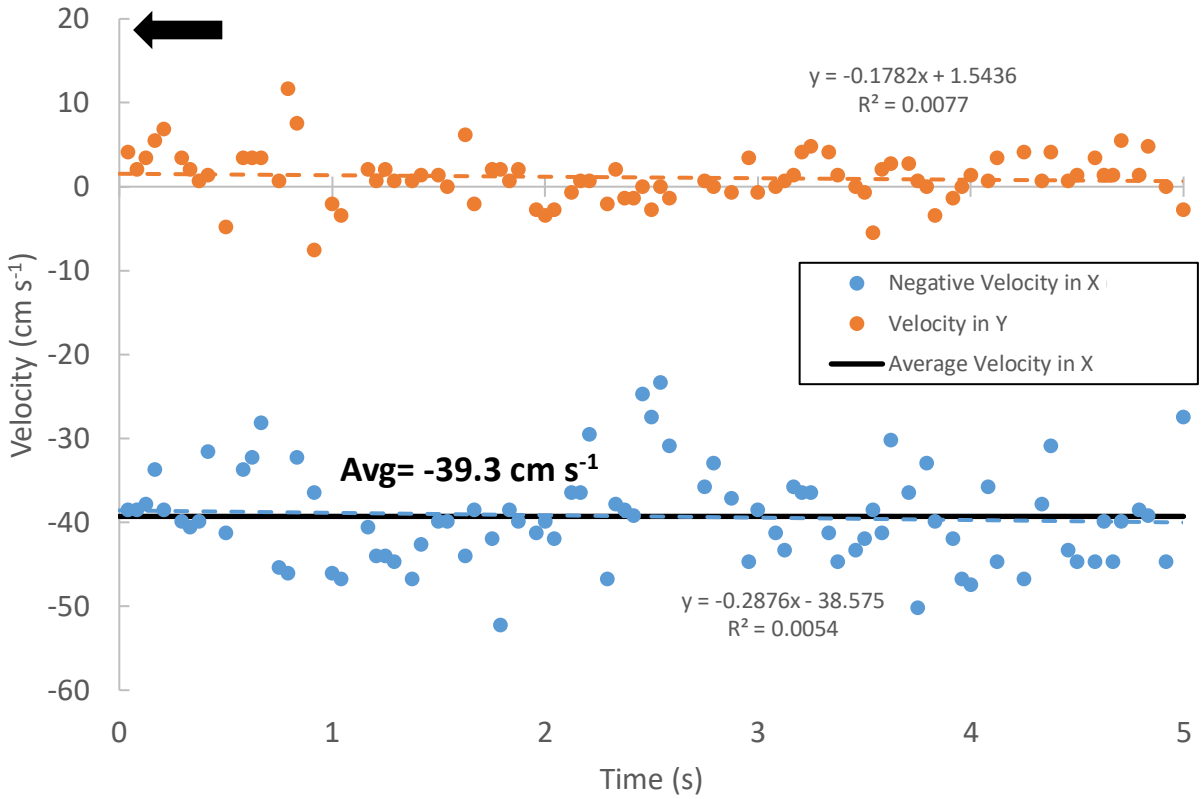

Figure A2.8. Average water velocity in the x and y direction over a 5 second time period of backward water circulation at an intended velocity of -40.0 cm s^{-1} within the flume respirometer. Velocities were calculated using particle tracking software (MTrackJ) where individual particles were manually tracked over a period of at least three frames. Each point represents the instantaneous velocity of a single particle moving in the respirometer. The average water velocity for the measurement time was -39.3 cm s^{-1}.

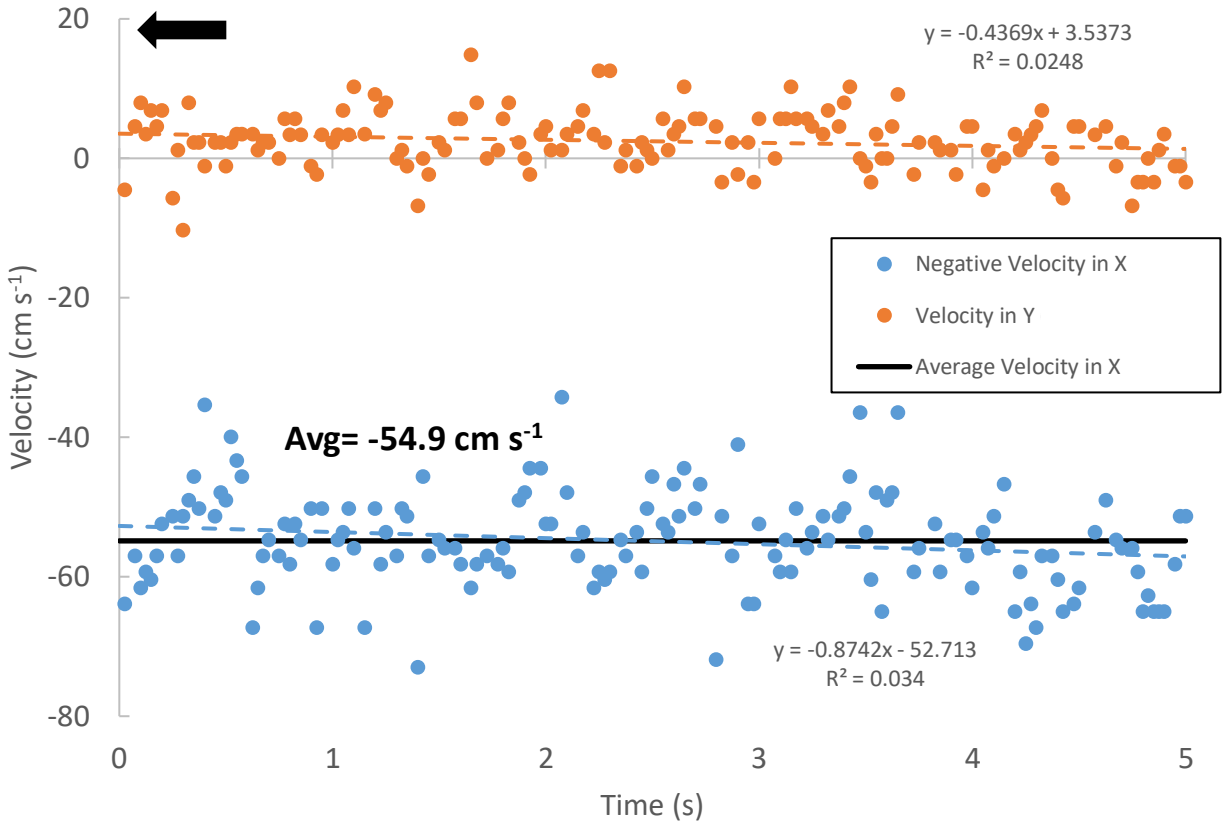

Figure A2.9. Average water velocity in the x and y direction over a 5 second time period of backward water circulation at an intended velocity of -54.0 cm s^{-1} within the flume respirometer. Velocities were calculated using particle tracking software (MTrackJ) where individual particles were manually tracked over a period of at least three frames. Each point represents the instantaneous velocity of a single particle moving in the respirometer. The average water velocity for the measurement time was -54.9 cm s^{-1}.

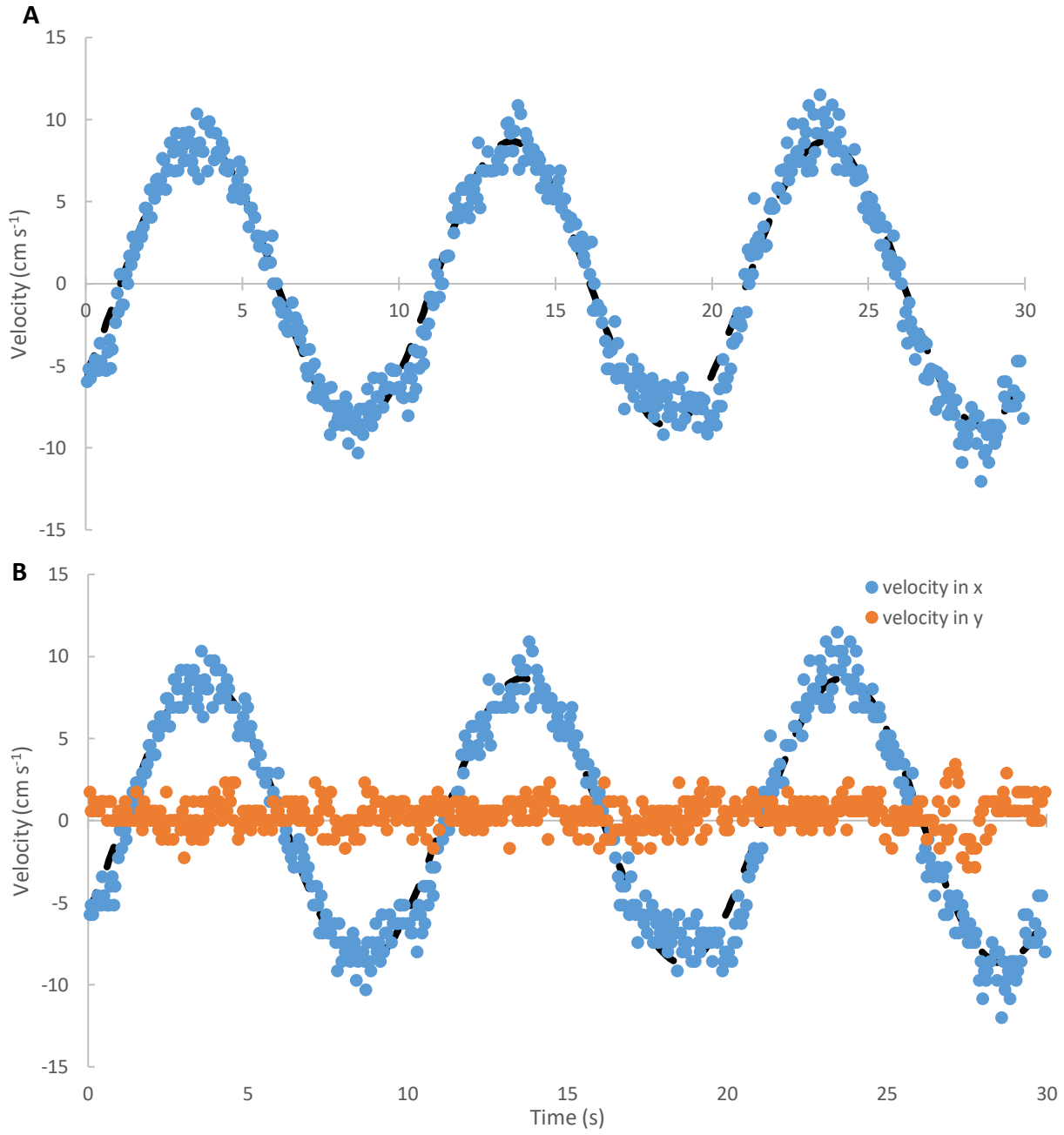

Figure A2.10. Average A.) relative velocity and B.) velocity in the x and y direction over three full oscillations at 0.1 Hz frequency with an intended velocity of 10 cm s^{-1} for a 9.4 cm TL fish in the Steffensen type flume respirometer. Black dashed lines underlying the points represent a sine wave function fit to the data using the measured amplitude. Velocities were calculated using particle tracking software (MTrackJ) where individual particles were manually tracked over a period of at least three frames. Each point represents the instantaneous velocity of a single particle moving in the respirometer. Correction factors were calculated to correct motor voltage up to the intended velocity in the swimming section of the flume.

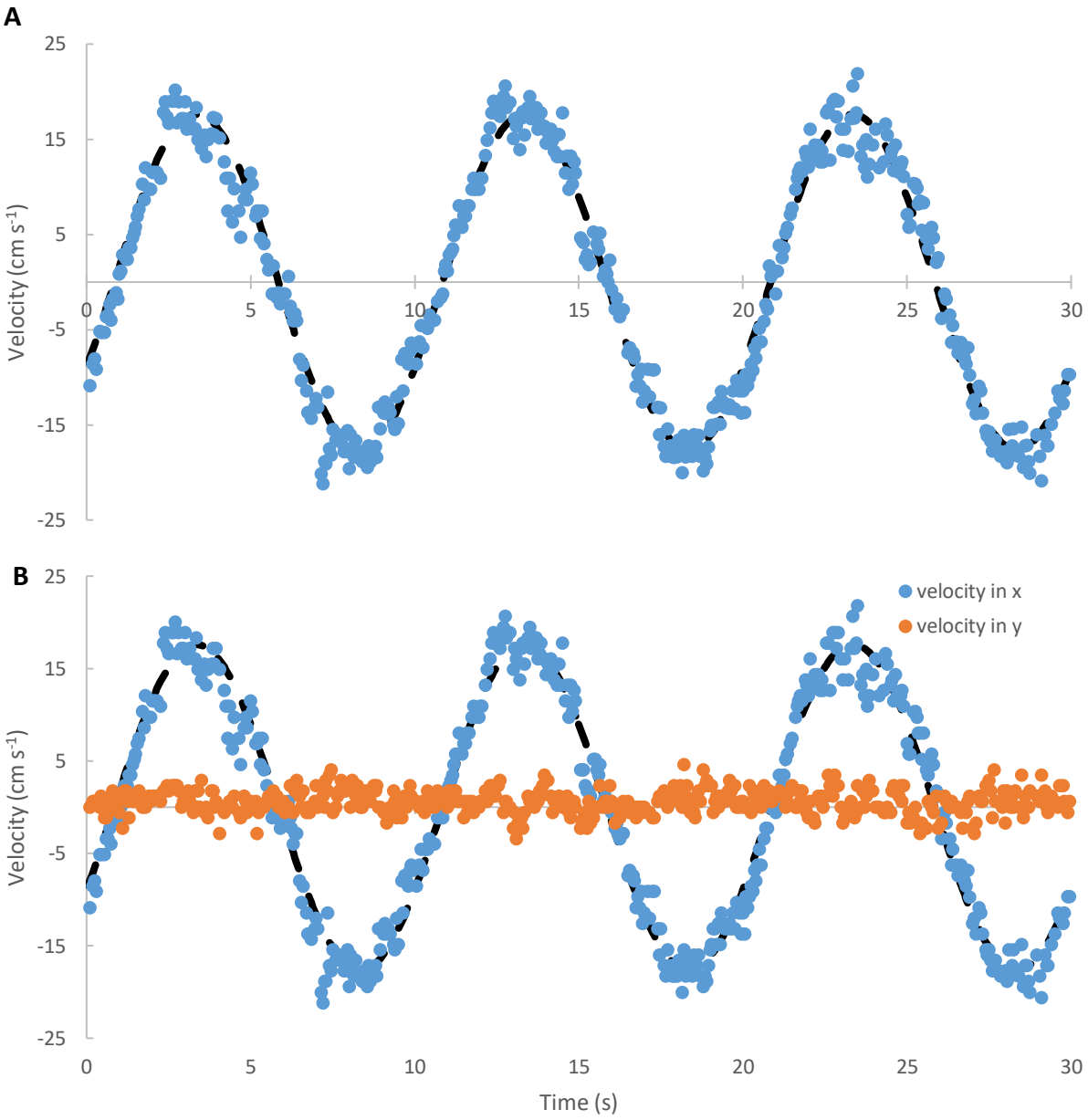

Figure A2.11. Average A.) relative velocity and B.) velocity in the x and y direction over three full oscillations at 0.1 Hz frequency with an intended velocity of 20 cm s^{-1} for a 9.4 cm TL fish in the Steffensen type flume respirometer. Black dashed lines underlying the points represent a sine wave function fit to the data using the measured amplitude. Velocities were calculated using particle tracking software (MTrackJ) where individual particles were manually tracked over a period of at least three frames. Each point represents the instantaneous velocity of a single particle moving in the respirometer. Correction factors were calculated to correct motor voltage up to the intended velocity in the swimming section of the flume.

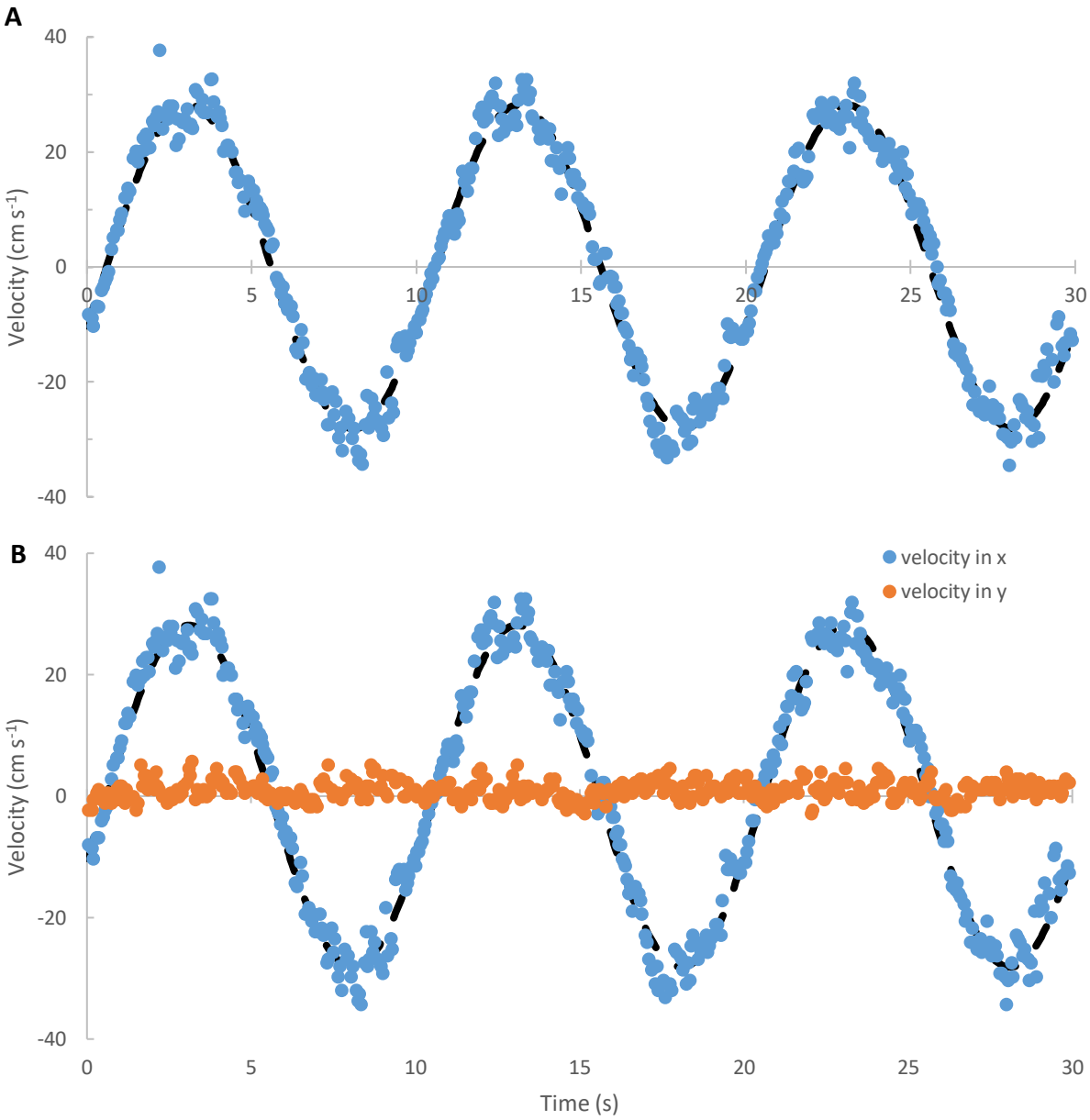

Figure A2.12. Average A.) relative velocity and B.) velocity in the x and y direction over three full oscillations at 0.1 Hz frequency with an intended velocity of 30 cm s^{-1} for a 9.4 cm TL fish in the Steffensen type flume respirometer. Black dashed lines underlying the points represent a sine wave function fit to the data using the measured amplitude. Velocities were calculated using particle tracking software (MTrackJ) where individual particles were manually tracked over a period of at least three frames. Each point represents the instantaneous velocity of a single particle moving in the respirometer. Correction factors were calculated to correct motor voltage up to the intended velocity in the swimming section of the flume.

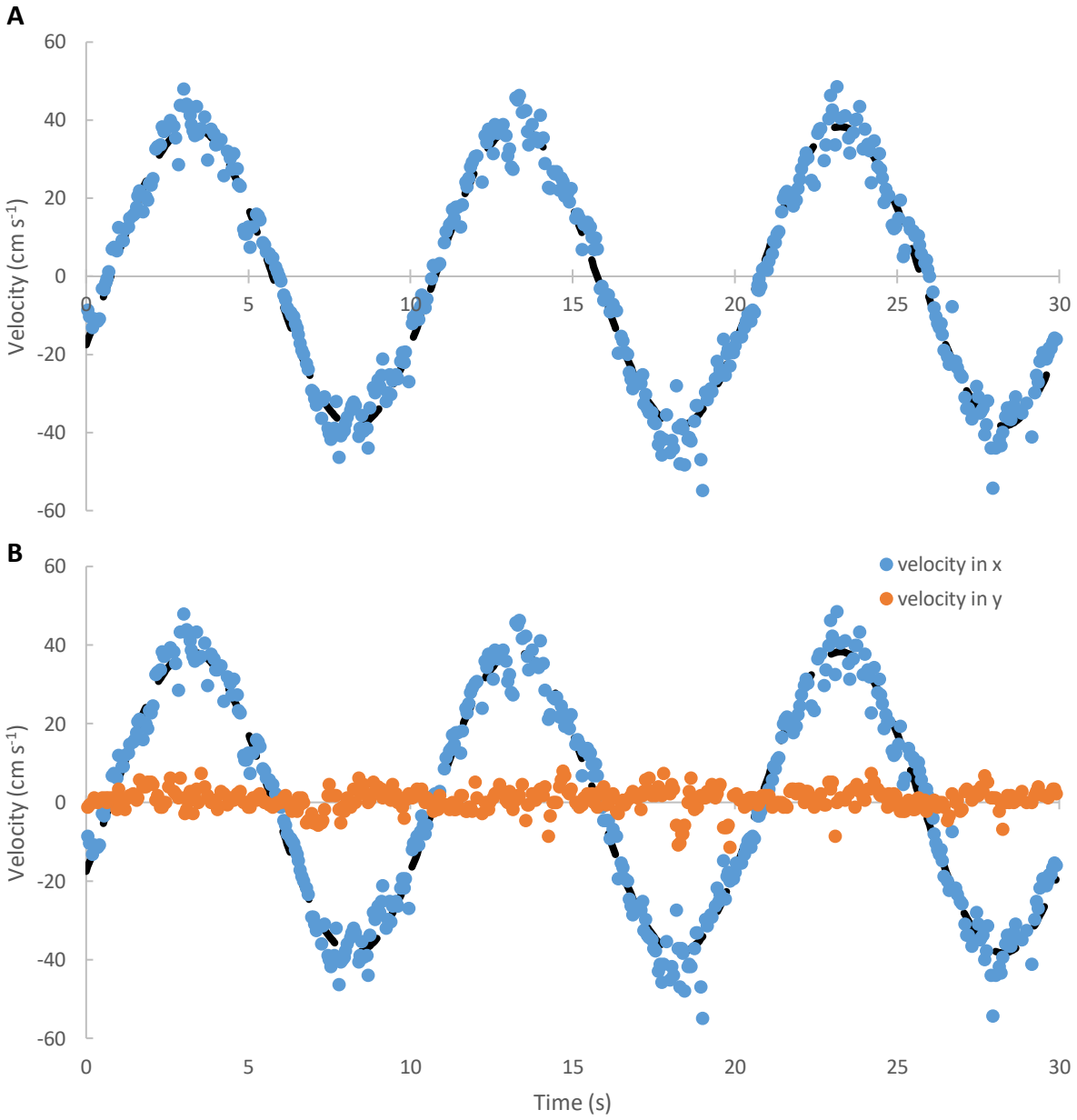

Figure A2.13. Average A.) relative velocity and B.) velocity in the x and y direction over three full oscillations at 0.1 Hz frequency with an intended velocity of 40 cm s^{-1} for a 9.4 cm TL fish in the Steffensen type flume respirometer. Black dashed lines underlying the points represent a sine wave function fit to the data using the measured amplitude. Velocities were calculated using particle tracking software (MTrackJ) where individual particles were manually tracked over a period of at least three frames. Each point represents the instantaneous velocity of a single particle moving in the respirometer. Correction factors were calculated to correct motor voltage up to the intended velocity in the swimming section of the flume.

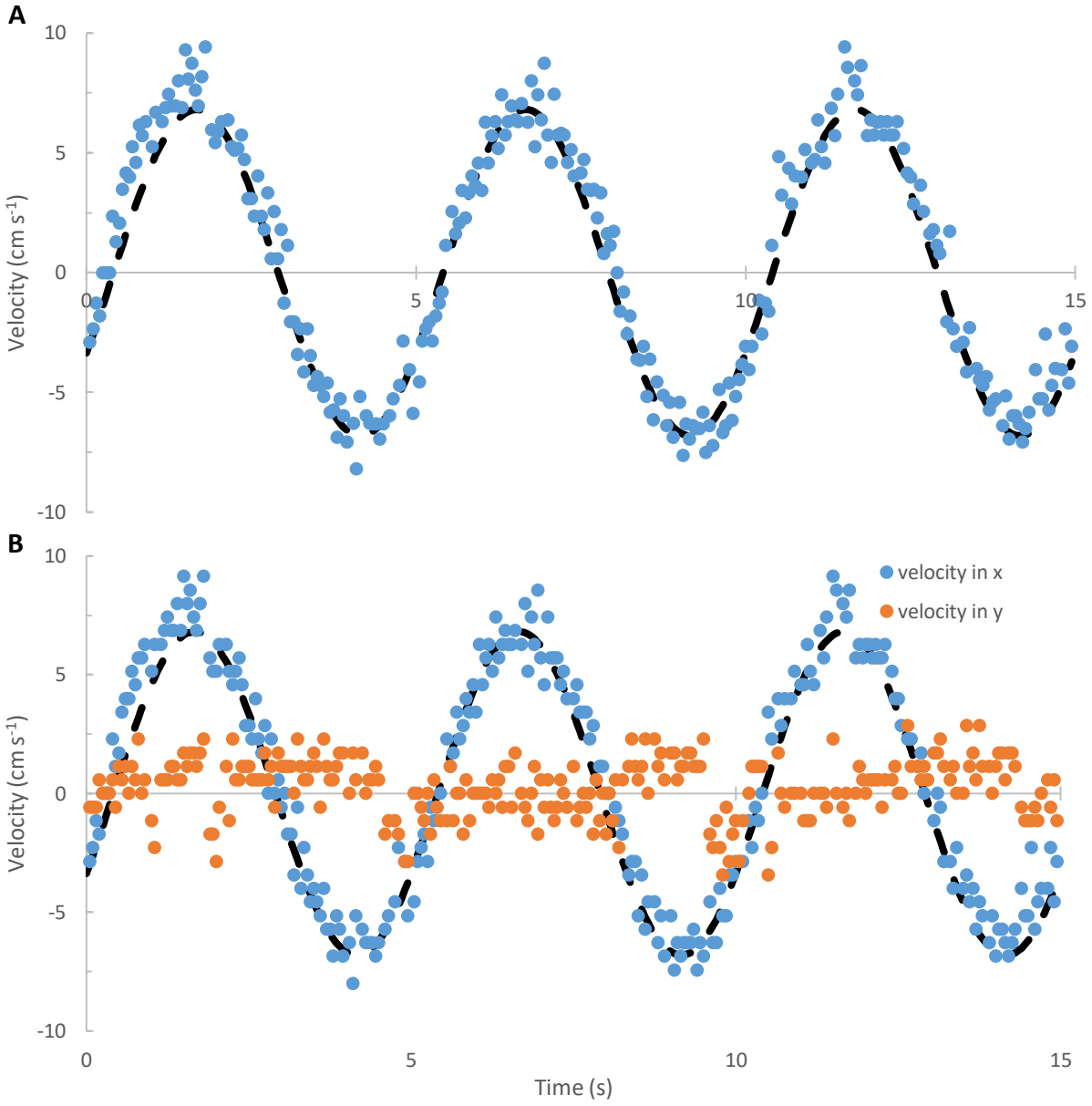

Figure A2.14. Average A.) relative velocity and B.) velocity in the x and y direction over three full oscillations at 0.2 Hz frequency with an intended velocity of 10 cm s^{-1} for a 9.4 cm TL fish in the Steffensen type flume respirometer. Black dashed lines underlying the points represent a sine wave function fit to the data using the measured amplitude. Velocities were calculated using particle tracking software (MTrackJ) where individual particles were manually tracked over a period of at least three frames. Each point represents the instantaneous velocity of a single particle moving in the respirometer. Correction factors were calculated to correct motor voltage up to the intended velocity in the swimming section of the flume.

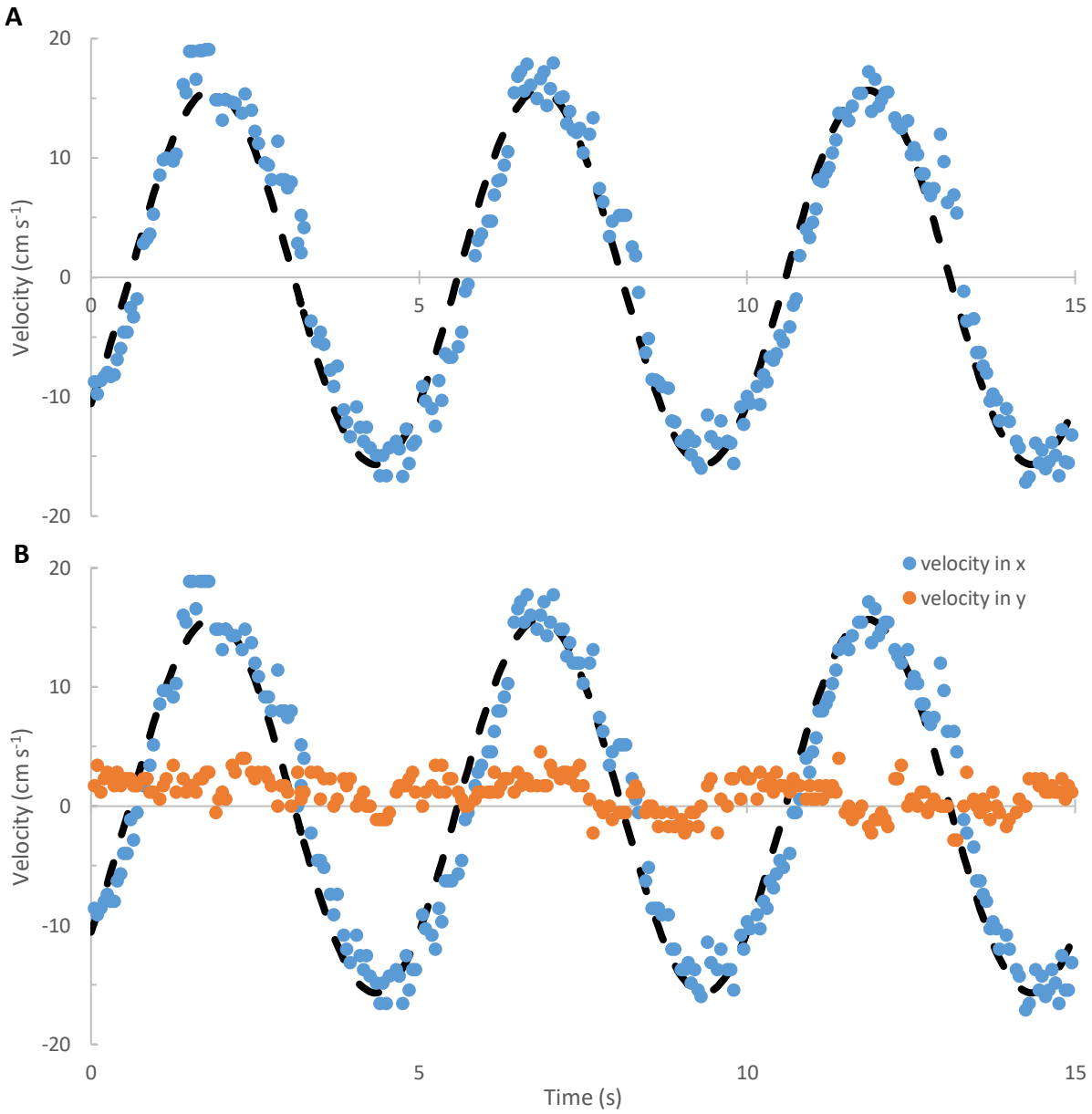

Figure A2.15. Average A.) relative velocity and B.) velocity in the x and y direction over three full oscillations at 0.2 Hz frequency with an intended velocity of 20 cm s^{-1} for a 9.4 cm TL fish in the Steffensen type flume respirometer. Black dashed lines underlying the points represent a sine wave function fit to the data using the measured amplitude. Velocities were calculated using particle tracking software (MTrackJ) where individual particles were manually tracked over a period of at least three frames. Each point represents the instantaneous velocity of a single particle moving in the respirometer. Correction factors were calculated to correct motor voltage up to the intended velocity in the swimming section of the flume.

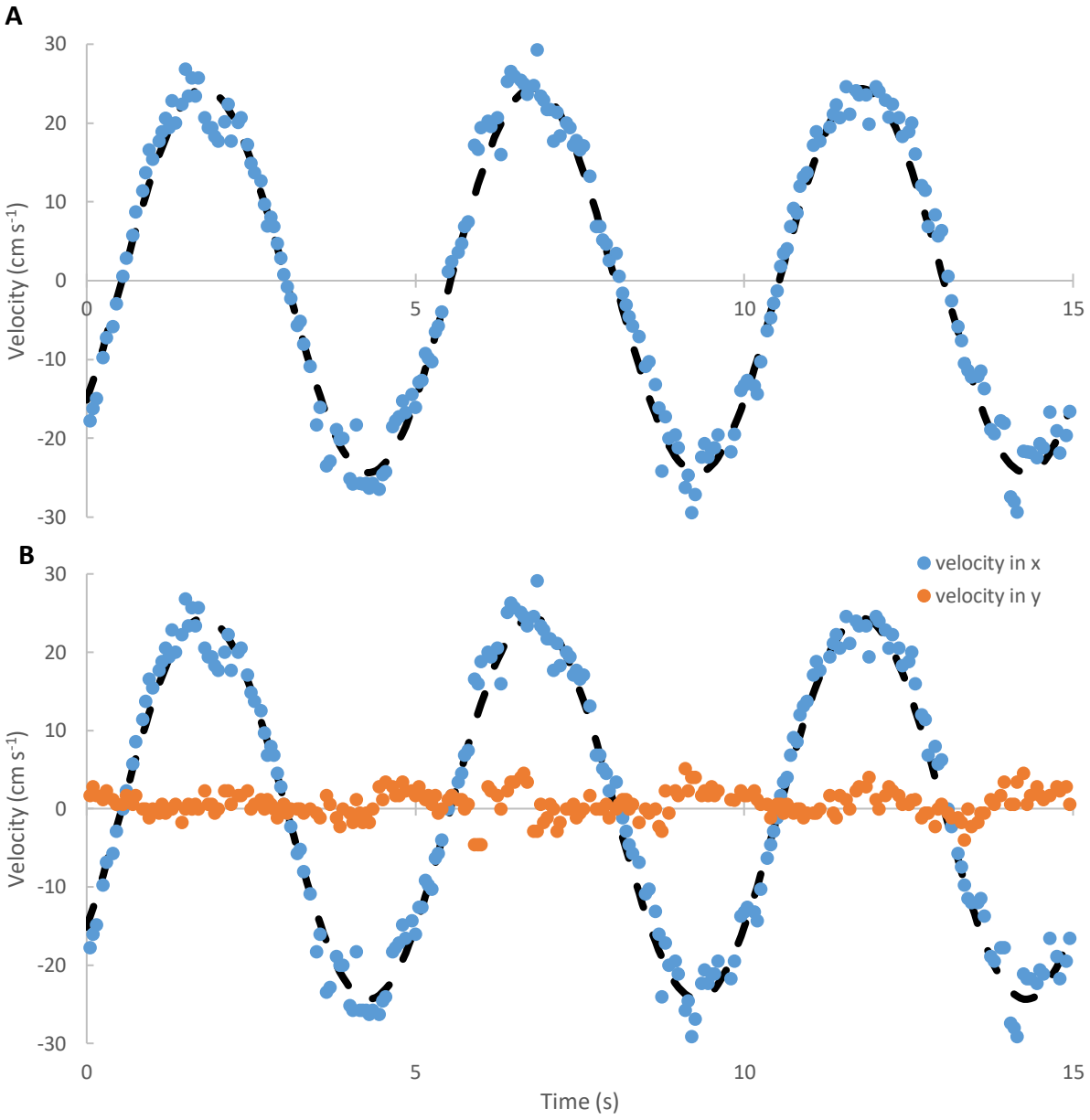

Figure A2.16. Average A.) relative velocity and B.) velocity in the x and y direction over three full oscillations at 0.2 Hz frequency with an intended velocity of 30 cm s^{-1} for a 9.4 cm TL fish in the Steffensen type flume respirometer. Black dashed lines underlying the points represent a sine wave function fit to the data using the measured amplitude. Velocities were calculated using particle tracking software (MTrackJ) where individual particles were manually tracked over a period of at least three frames. Each point represents the instantaneous velocity of a single particle moving in the respirometer. Correction factors were calculated to correct motor voltage up to the intended velocity in the swimming section of the flume.

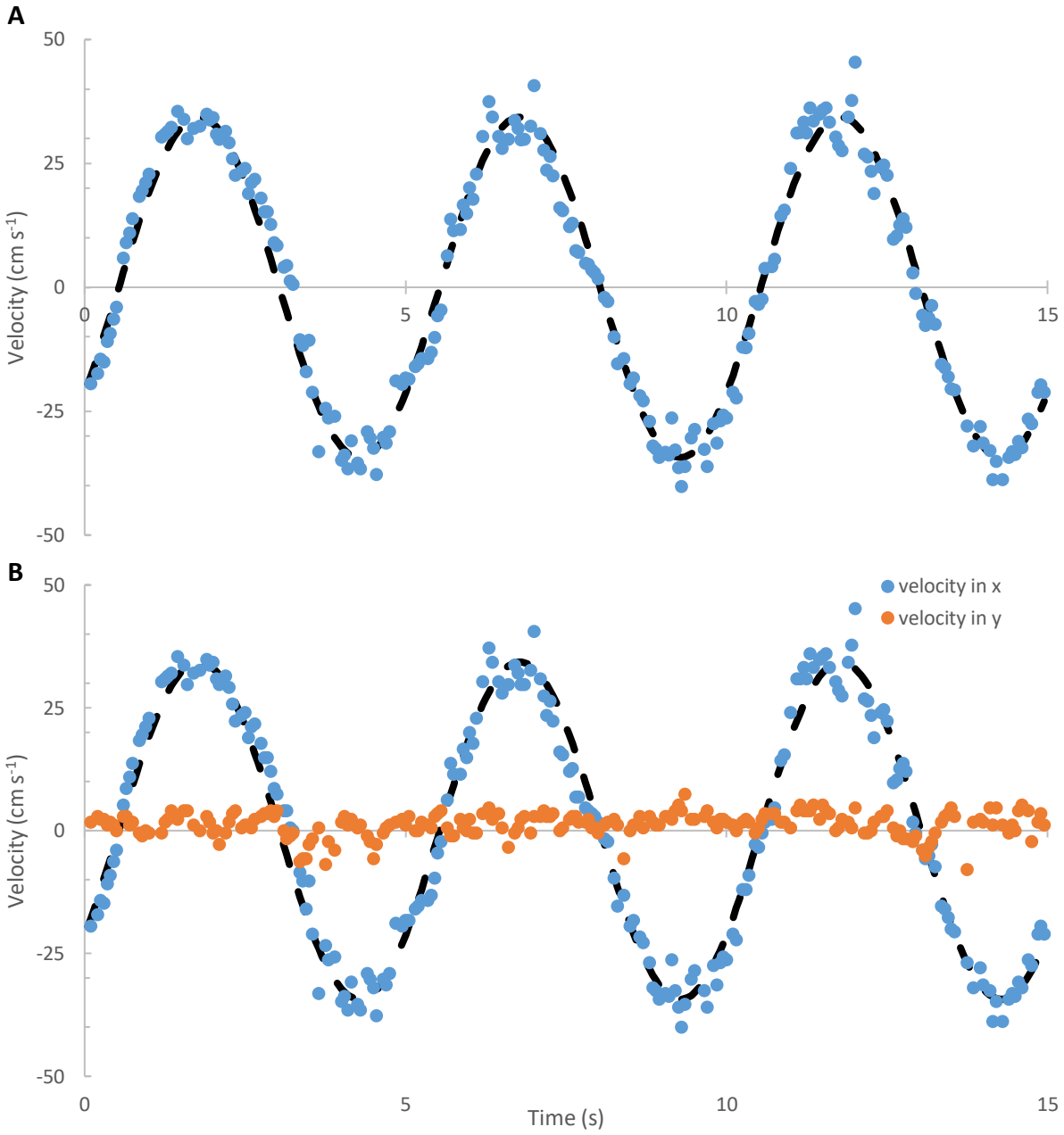

Figure A2.17. Average A.) relative velocity and B.) velocity in the x and y direction over three full oscillations at 0.2 Hz frequency with an intended velocity of 40 cm s^{-1} for a 9.4 cm TL fish in the Steffensen type flume respirometer. Black dashed lines underlying the points represent a sine wave function fit to the data using the measured amplitude. Velocities were calculated using particle tracking software (MTrackJ) where individual particles were manually tracked over a period of at least three frames. Each point represents the instantaneous velocity of a single particle moving in the respirometer. Correction factors were calculated to correct motor voltage up to the intended velocity in the swimming section of the flume.

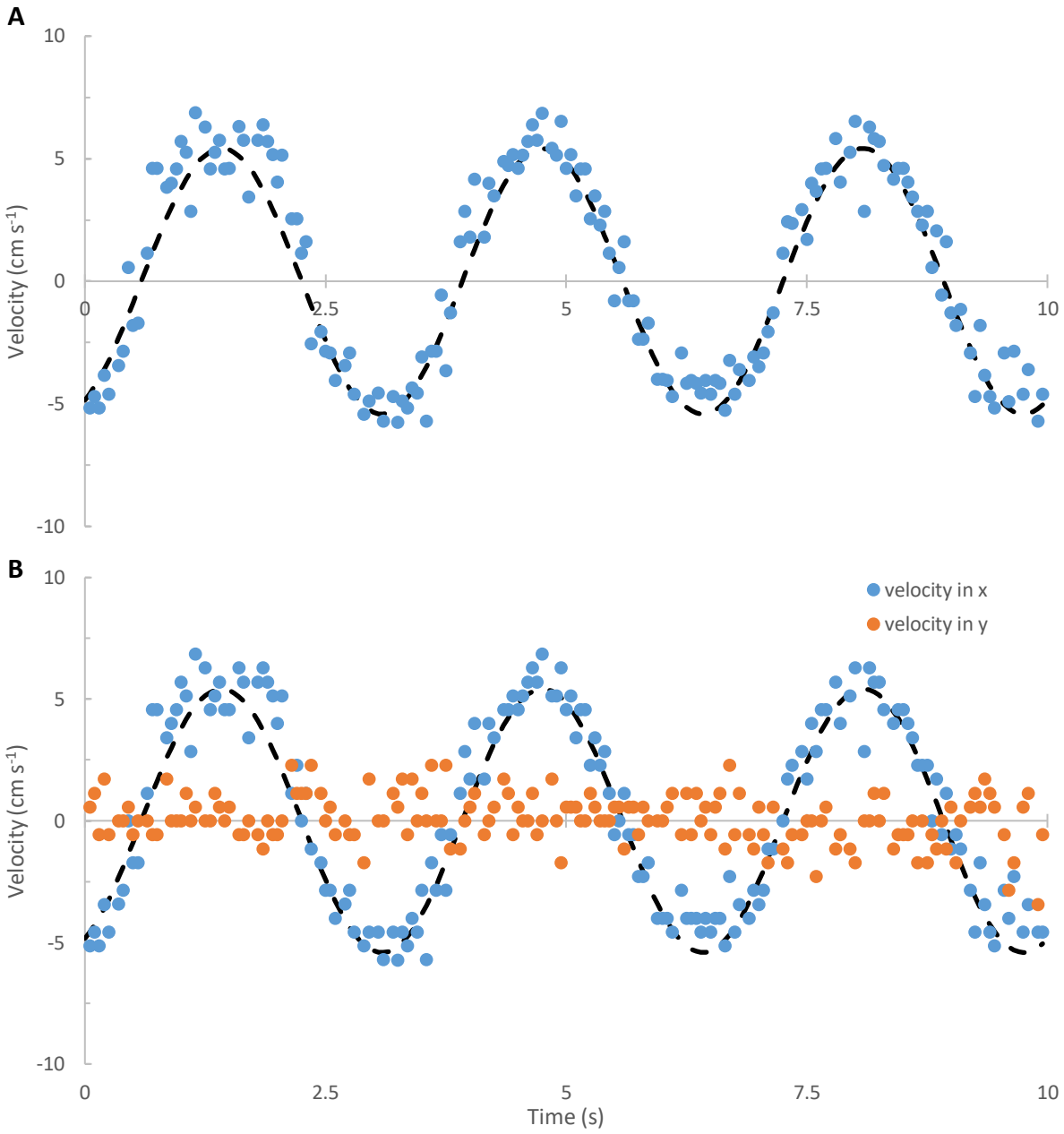

Figure A2.18. Average A.) relative velocity and B.) velocity in the x and y direction over three full oscillations at 0.3 Hz frequency with an intended velocity of 10 cm s^{-1} for a 9.4 cm TL fish in the Steffensen type flume respirometer. Black dashed lines underlying the points represent a sine wave function fit to the data using the measured amplitude. Velocities were calculated using particle tracking software (MTrackJ) where individual particles were manually tracked over a period of at least three frames. Each point represents the instantaneous velocity of a single particle moving in the respirometer. Correction factors were calculated to correct motor voltage up to the intended velocity in the swimming section of the flume.

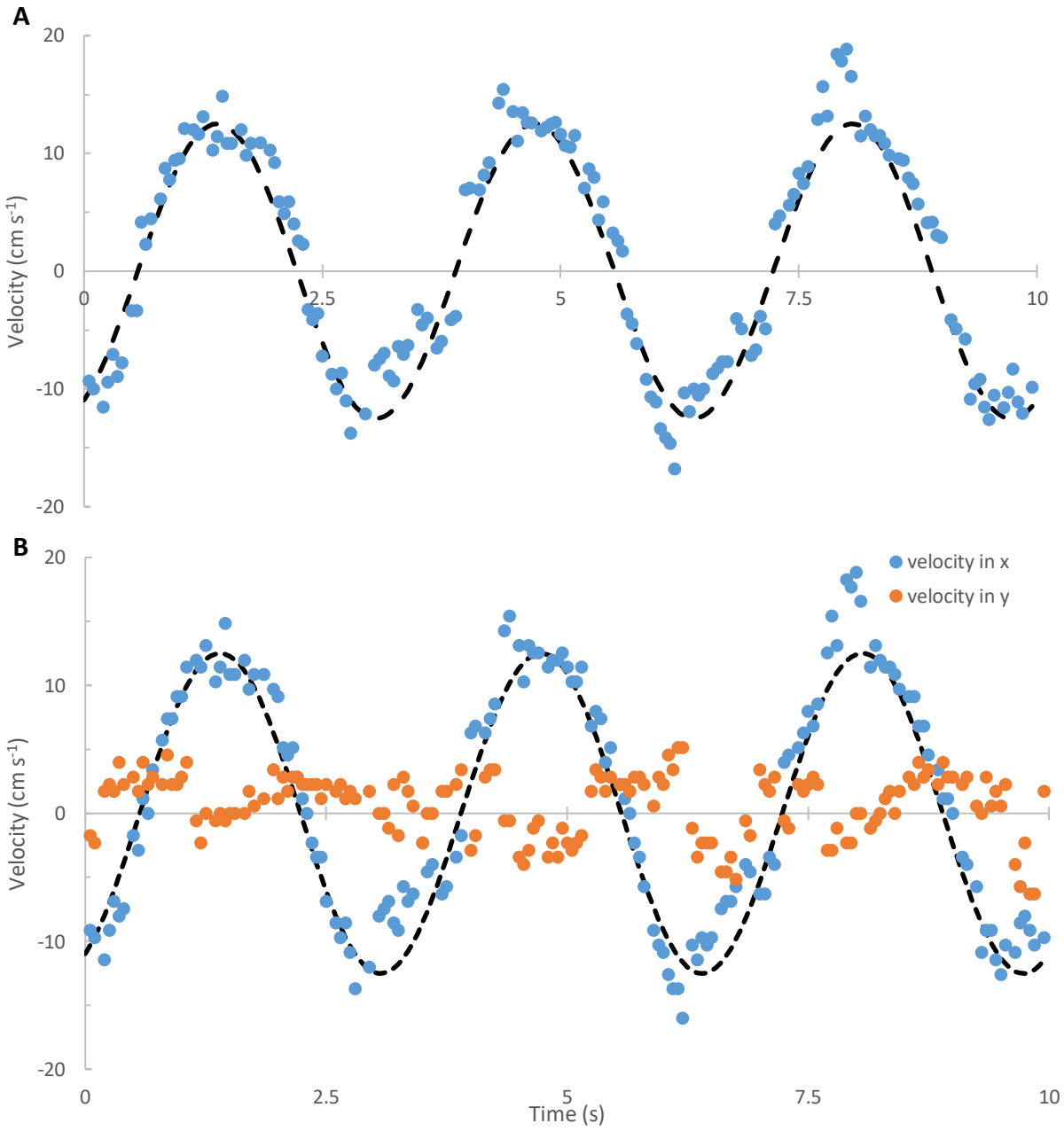

Figure A2.19. Average A.) relative velocity and B.) velocity in the x and y direction over three full oscillations at 0.3 Hz frequency with an intended velocity of 20 cm s^{-1} for a 9.4 cm TL fish in the Steffensen type flume respirometer. Black dashed lines underlying the points represent a sine wave function fit to the data using the measured amplitude. Velocities were calculated using particle tracking software (MTrackJ) where individual particles were manually tracked over a period of at least three frames. Each point represents the instantaneous velocity of a single particle moving in the respirometer. Correction factors were calculated to correct motor voltage up to the intended velocity in the swimming section of the flume.

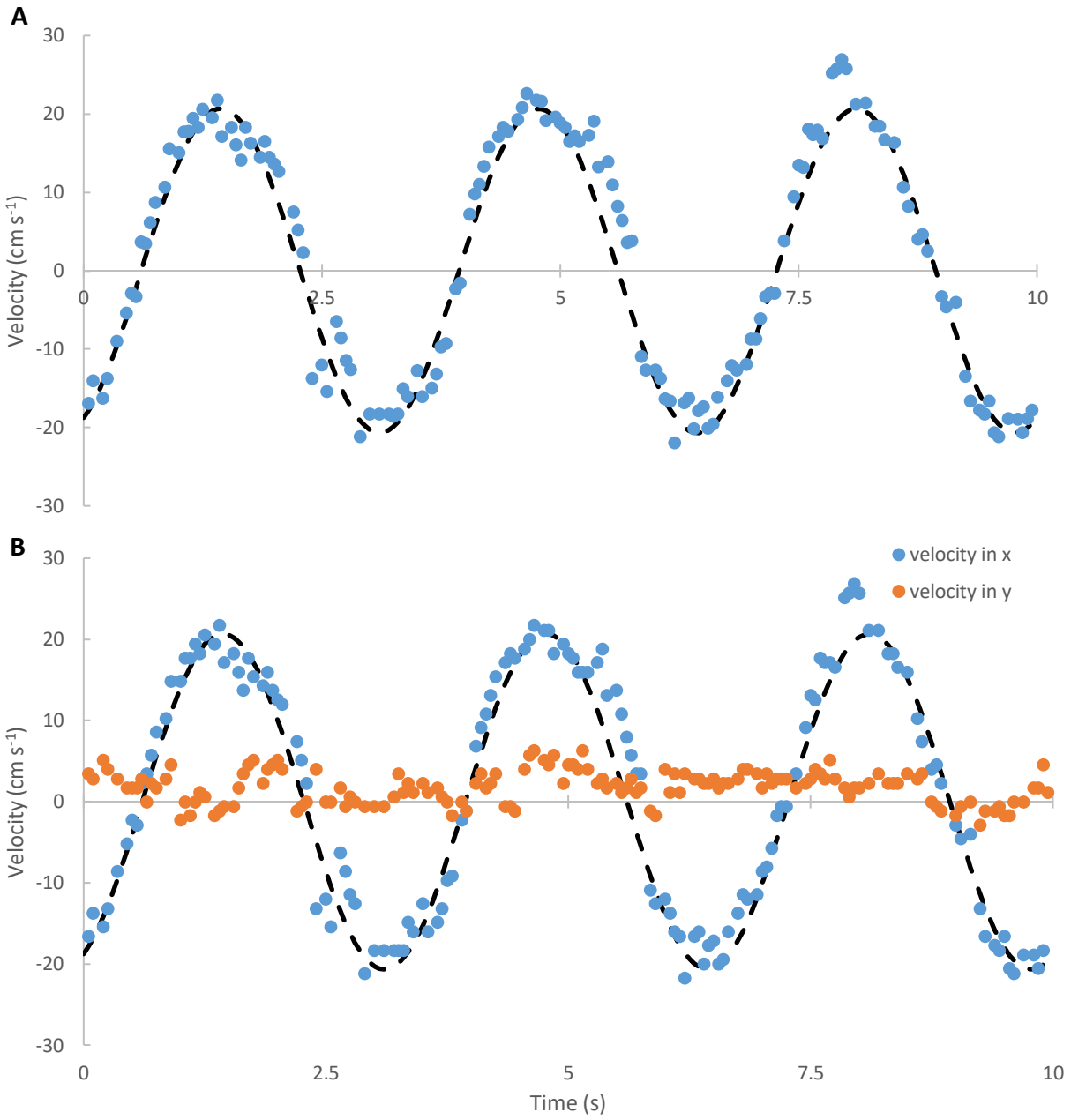

Figure A2.20. Average A.) relative velocity and B.) velocity in the x and y direction over three full oscillations at 0.3 Hz frequency with an intended velocity of 30 cm s^{-1} for a 9.4 cm TL fish in the Steffensen type flume respirometer. Black dashed lines underlying the points represent a sine wave function fit to the data using the measured amplitude. Velocities were calculated using particle tracking software (MTrackJ) where individual particles were manually tracked over a period of at least three frames. Each point represents the instantaneous velocity of a single particle moving in the respirometer. Correction factors were calculated to correct motor voltage up to the intended velocity in the swimming section of the flume.

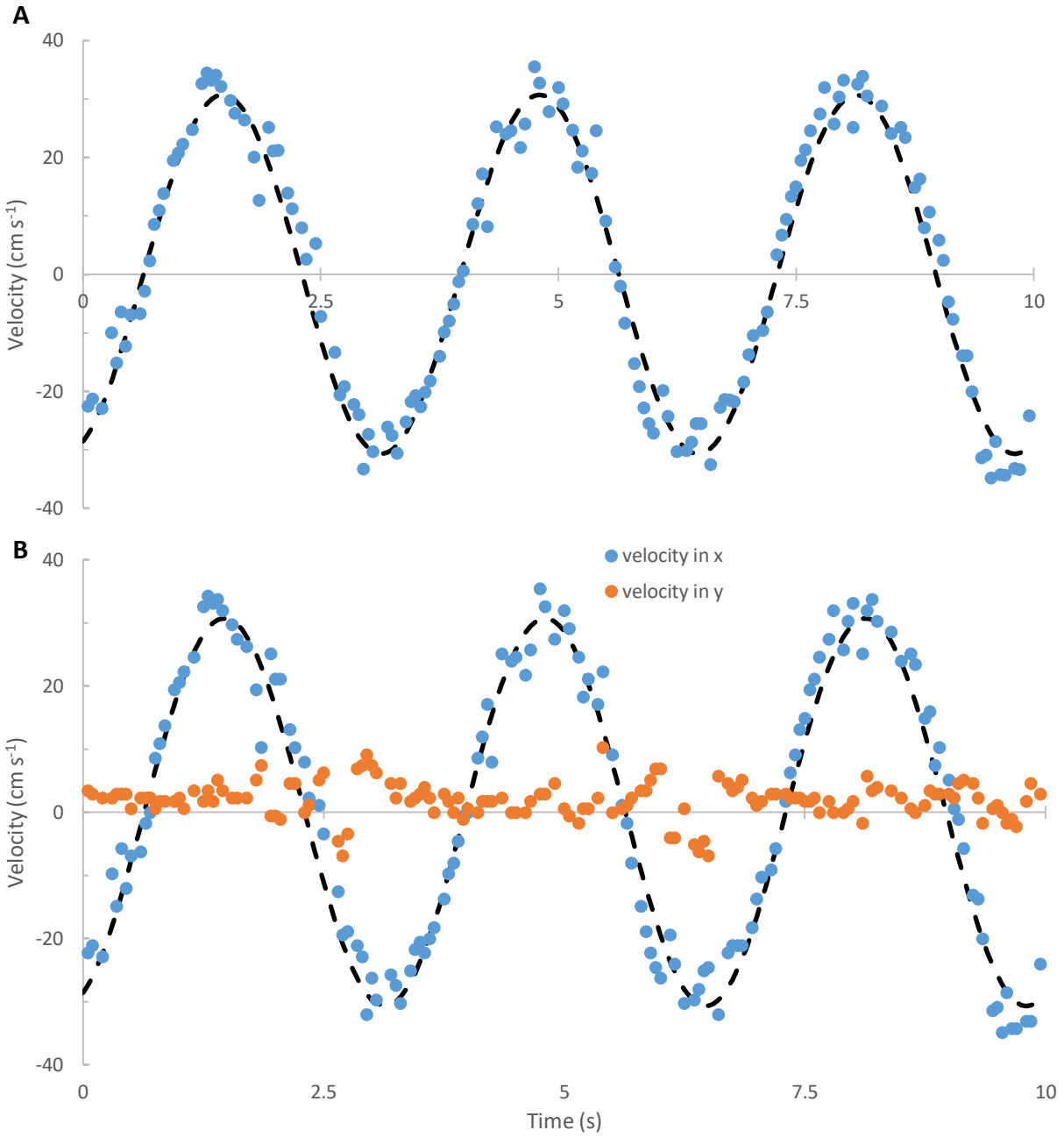

Figure A2.21. Average A.) relative velocity and B.) velocity in the x and y direction over three full oscillations at 0.3 Hz frequency with an intended velocity of 40 cm s^{-1} for a 9.4 cm TL fish in the Steffensen type flume respirometer. Black dashed lines underlying the points represent a sine wave function fit to the data using the measured amplitude. Velocities were calculated using particle tracking software (MTrackJ) where individual particles were manually tracked over a period of at least three frames. Each point represents the instantaneous velocity of a single particle moving in the respirometer. Correction factors were calculated to correct motor voltage up to the intended velocity in the swimming section of the flume.

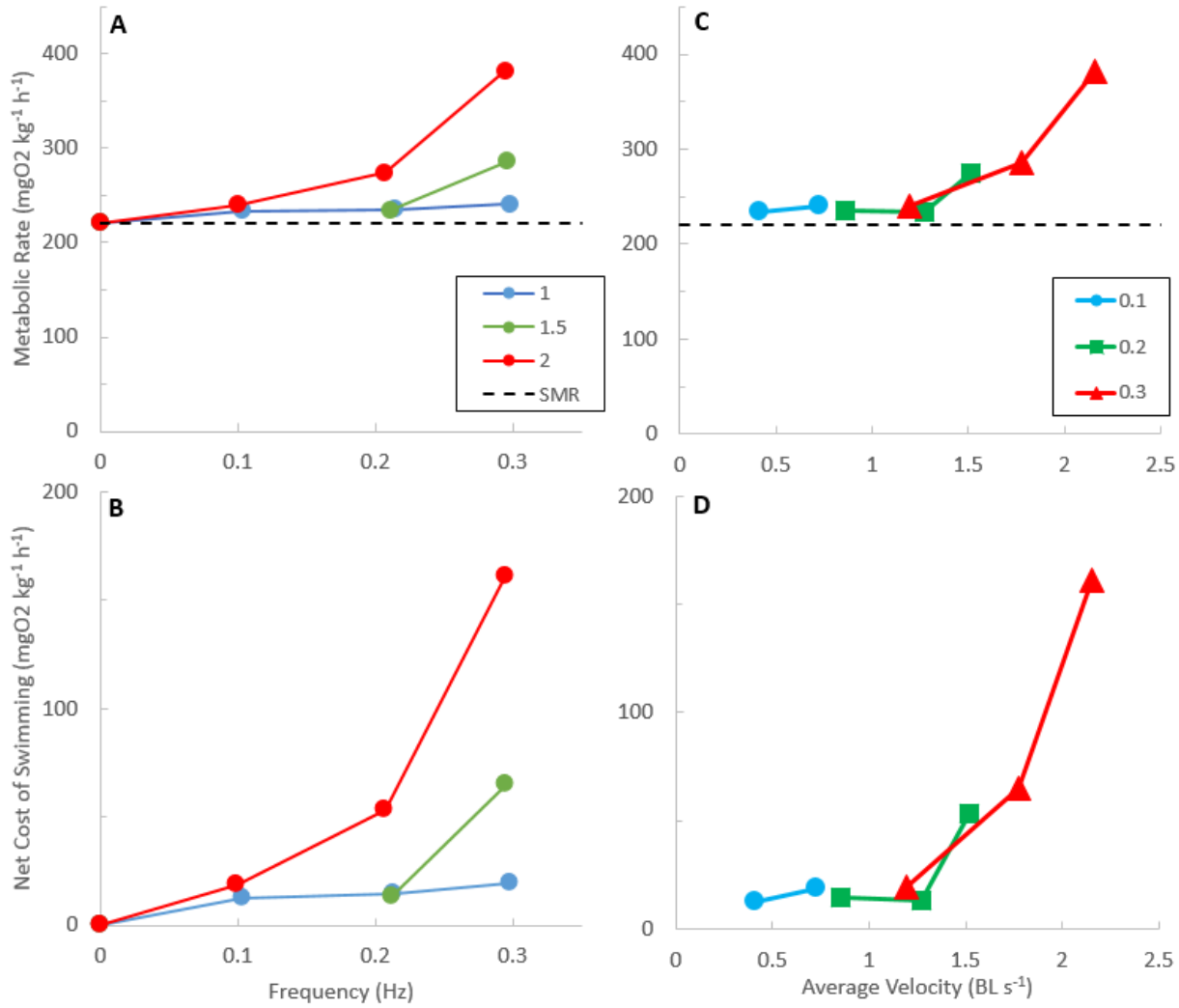

Figure A2.22. Total metabolic rate as a function of wave frequency (Hz) at 3 different wave amplitudes (reported relative to fish body length, BL) (**A**), and average swimming velocity (BL s^{-1}) at the three frequencies, during oscillatory swimming (**C**). Mean and standard error for net cost of swimming (NCOS, mgO_2 kg^{-1} h^{-1}) as a function of wave frequency (Hz) at 3 different wave amplitudes (reported relative to fish body length, BL) (**B**), and average swimming velocity (BL s^{-1}) at the three frequencies, during oscillatory swimming (**D**). NCOS was calculated by subtracting standard metabolic rate from total oxygen consumption rate. Average swimming velocity was calculated as the average absolute velocity over one wave cycle.

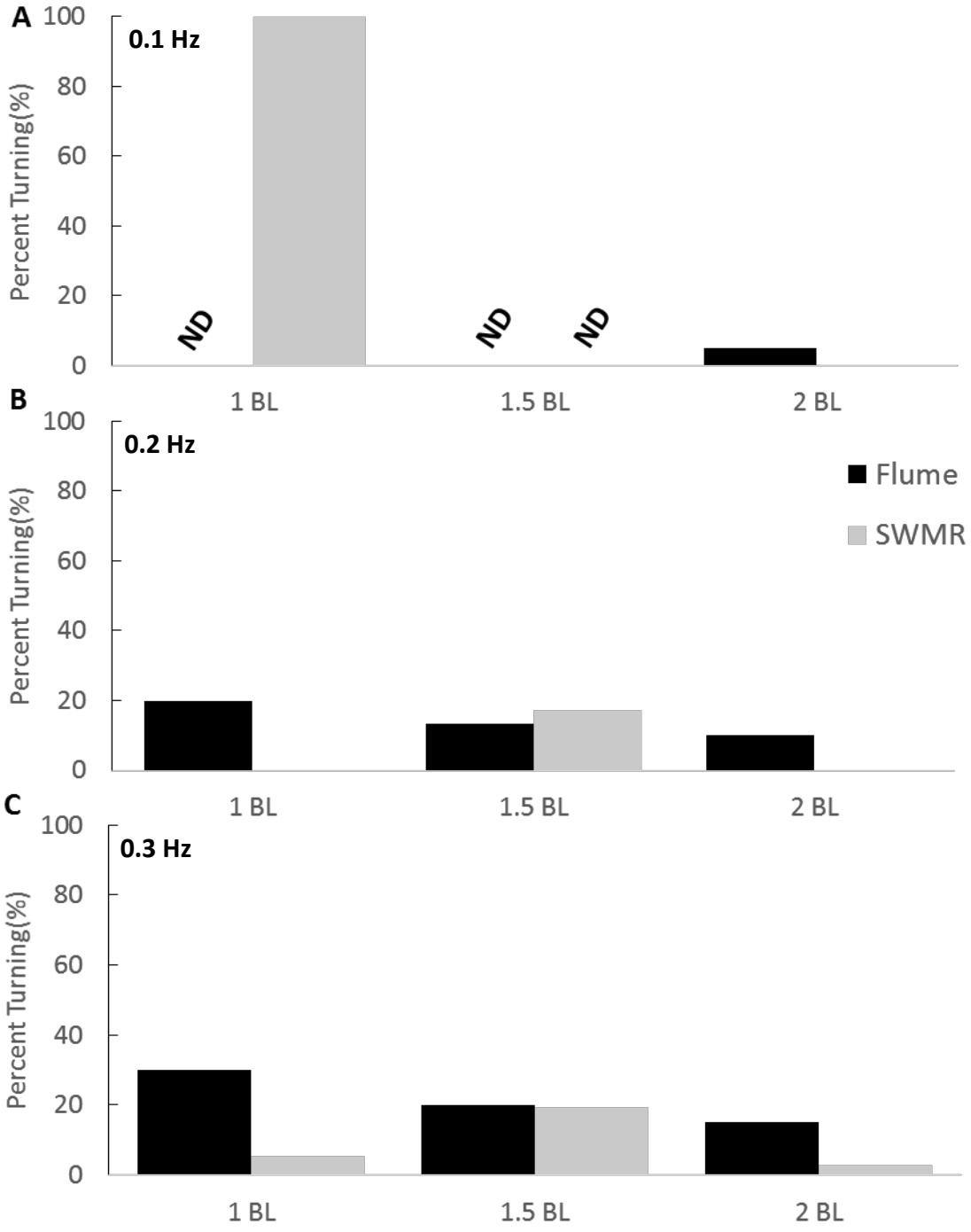

Figure A2.23. Percent turning as a function of amplitude (reported relative to fish body length, BL) at three different frequencies; 0.1 Hz (**A**), 0.2 Hz (**A**), and 0.3 Hz (**A**), for the same individual (*Ctenochaetus strigosus*) in the flume respirometer and the simulated wave motion respirometer (SWMR). Percent turning was quantified as the number of times the individual turned around relative to the total number of changes in direction in a randomly chosen one

minute video clip and shown as a percentage. **ND** represents data points for which no data exists due to erratic swimming.

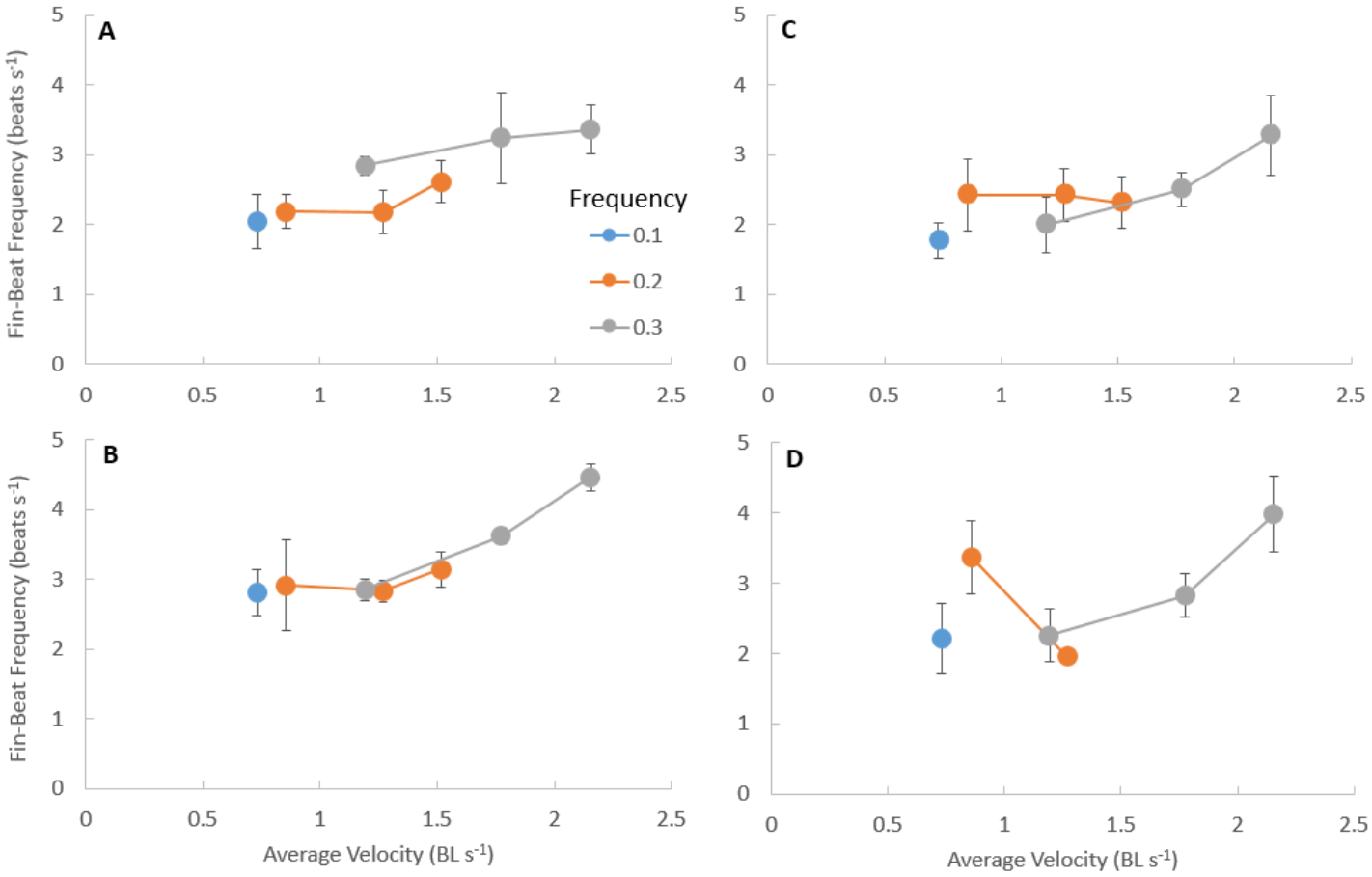

Figure A2.24. Pectoral fin-beat frequency (mean ± S.D.) as a function of average velocity (reported relative to fish body length per second, BL s^{-1}) at three frequencies of oscillation for *C. strigosus* swimming forward (**A**) and reverse (**B**) in the SWMR, and forward (**C**) and reverse (**D**) in the flume respirometer. No data exists at the two lowest average velocities for the 0.1 Hz frequency due to erratic swimming of all individuals at these intensities. Only two data points exist while swimming in reverse in the flume respirometer (**D**) due to the fish only swimming forward during that intensity.

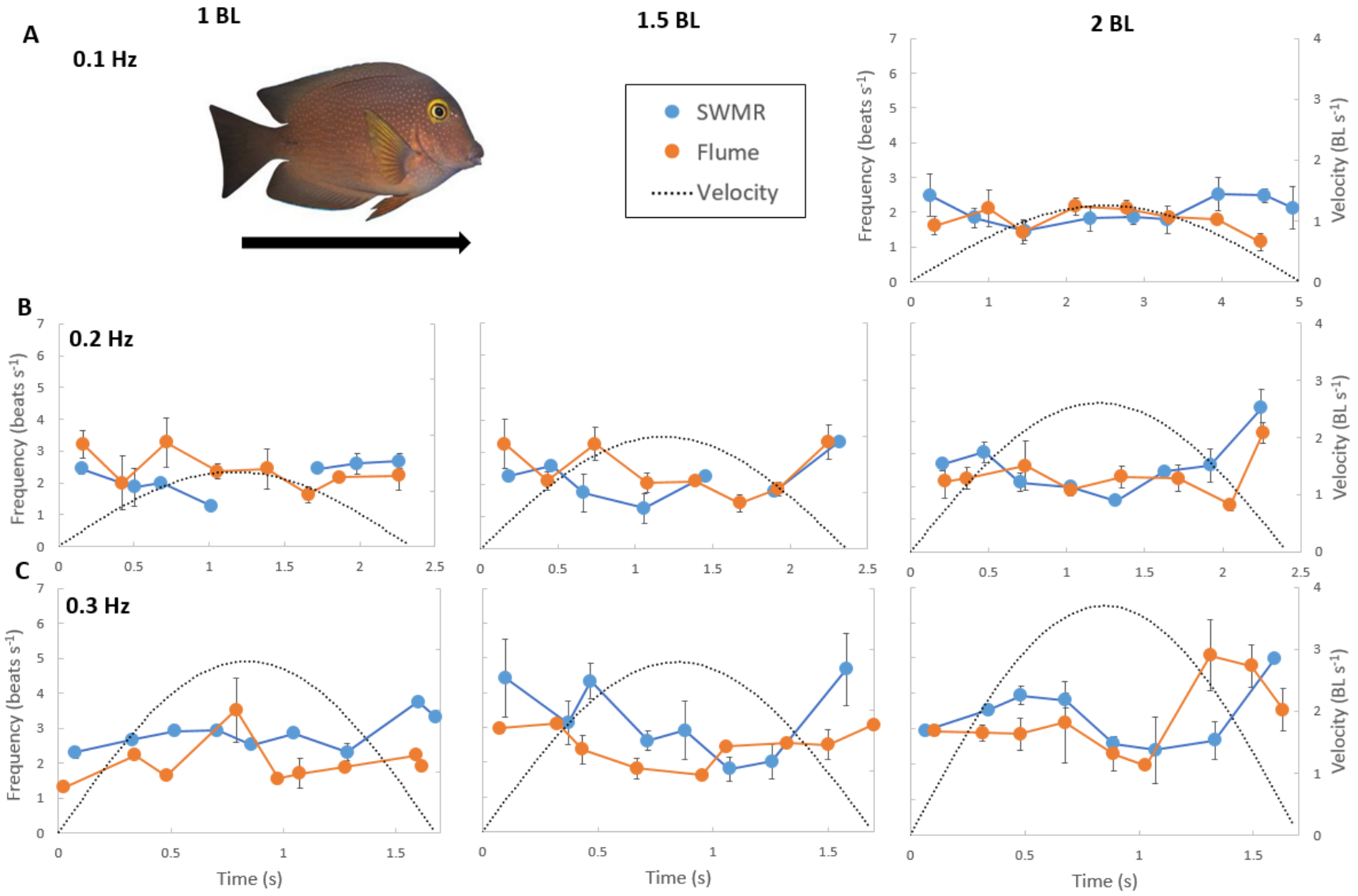
A
1 BL
1.5 BL
2 BL
0.1 Hz
SWMR
Flume
Velocity
B
0.2 Hz
C
0.3 Hz
Frequency (beats s-1)
Velocity (BL s-1)
Time (s)

Figure A2.25. Fin-beat frequency (mean ± S.E.) in the forward direction as a function of time during one half cycle of oscillatory swimming for *Ctenochaetus strigosus* in both the SWMR and the Steffensen-type flume respirometer. Amplitude of displacement (reported relative to fish body length, BL) increases from 1.0 BL (**left column**), to 1.5 BL (**center column**), to 2.0 BL displacement (mean maximum displacement= 1.98 BL) (**right column**). Wave frequency increases from **A**.) 0.1 Hz, to **B**.) 0.2 Hz, to **C**.) 0.3 Hz. The dotted line indicated the instantaneous velocity (BL s^{-1}) of the shuttle moving in the SWMR apparatus.

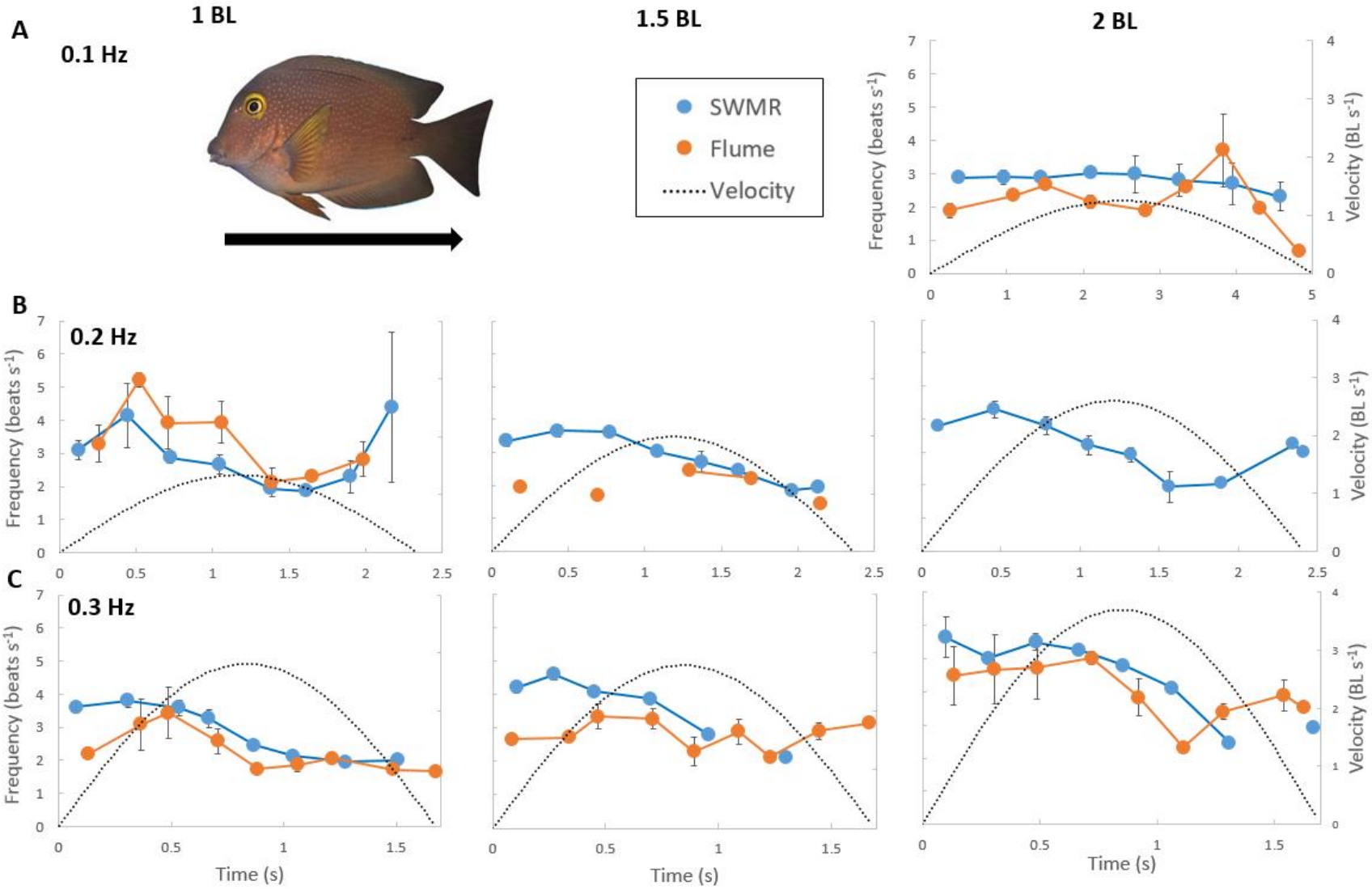
A
1 BL
1.5 BL
2 BL
0.1 Hz
SWMR
Flume
Velocity
B
0.2 Hz
C
0.3 Hz
Frequency (beats s-1)
Velocity (BL s-1)
Time (s)

Figure A2.26. Fin-beat frequency (mean ± S.E.) in the reverse direction as a function of time during one half cycle of oscillatory swimming for *Ctenochaetus strigosus* in both the SWMR and the Steffensen-type flume respirometer. Amplitude of displacement (reported relative to fish body length, BL) increases from 1.0 BL (**left column**), to 1.5 BL (**center column**), to 2.0 BL displacement (mean maximum displacement= 1.98 BL) (**right column**). Wave frequency increases from **A**.) 0.1 Hz, to **B**.) 0.2 Hz, to **C**.) 0.3 Hz. The dotted line indicated the instantaneous velocity (BL s^{-1}) of the shuttle moving in the SWMR apparatus.

Appendix 3

Fin Aspect Ratio and Body Morphology

To determine fin aspect ratio and body morphometrics, subjects were anesthetized using 100 mg L^{-1} of Tricaine Methanesulfonate (MS-222, Finquel, Tricaine-S) in seawater, buffered with an equal amount of Seachem Marine Buffer or Sodium Bicarbonate in seawater. Subjects were then measured for mass, total length, width, and depth. From the total length, width and depth, the body fineness ratio (measure of the body length relative to the cross-section diameter) was calculated:

$$\text{Body fineness ratio} = \frac{\text{length}}{\sqrt{\text{depth} + \text{width}}}$$

The subjects were then removed and placed on top of waterproof grid paper and photographed (Canon DSLR) with all of its swimming fins gently extended onto the graph paper. Subjects were then returned to untreated seawater to recover, and then placed back in their individual tanks.

The photographs were analyzed using the program ImageJ (V 1.49m; http://imagej.nih.gov/ij) to measure the leading edge and surface area of the swimming fins and height and surface area of the caudal fin. Swimming fin aspect ratio was calculated by:

$$\text{AR} = \frac{(\text{fin leading edge})^2}{\text{surface area of fin}}$$

Caudal fin aspect ratio was calculated by:

$$\text{AR} = \frac{(\text{height of the caudal fin})^2}{(\text{surface area of the fin})}$$

Table A3.1. *Summary of fin aspect ratio (AR) and body fineness ratio (mean ± S.D.) for individuals used in study.*

Swimming Mode and Species	Common Name	Pectoral AR	Dorsal/Anal AR	Caudal AR	Body Fineness Ratio
Labriform Swimmers					
Abudefduf sordidus	Black-Spot Sergeant	ND	ND	ND	4.11
Amphiprion ocellaris	Clown Anemonefish	0.82 ± 0.09	N/A	1.50 ± 0.10	4.24 ± 0.22
Ctenochaetus strigosus	Goldring Surgeonfish	1.90 ± 0.08	N/A	2.93 ± 0.52	4.27 ± 0.17
Balistiform Swimmers					
Rhinecanthus aculeatus	Lagoon Triggerfish	ND	0.46 ± 0.20	2.59 ± 0.12	3.50 ± 0.08
Sufflamen bursa	Lei Triggerfish	ND	0.47 ± 0.29	2.63 ± 0.05	3.91 ± 0.24
Body-and-Caudal Fin Swimmers					
Kuhlia spp.	Hawaiian Flagtail	3.64 ± 0.46	N/D	2.12 ± 0.54	4.71 ± 0.17
Mugil cephalus	Flathead Grey Mullet	2.63 ± 0.57	N/D	2.22 ± 0.36	6.07 ± 0.18
Osctraciiform Swimmers					
Ostracion meleagris	Spotted Boxfish	ND	1.97 ± 0.38	2.38 ± 0.97	3.50 ± 0.22